Synthesis and Redox Reactivity of Phosphine-Substituted Ruthenium(II) Polypyridine Complexes

Go Nakamura

Department of Structural Molecular Science
School of Physical Sciences
The Graduate University for Advanced Studies

Contents

General Introduction

Ruthenium(II) Polypyridine Complex

Ruthenium (Ru) is one of the most extensively studied transition metal ion due to its high redox stability and unique photochemical properties.[1] In particular, ruthenium(II) complexes with polypyridine ligands have been of great interest for over 40 years because this class of complexes exhibits several attractive physical properties such as (1) high chemical stability arising from the chelate effect of the multidentate ligands, (2) rich redox chemistry attributed to d orbitals of metal center and π orbitals of ligands, and (3) strong luminescent properties and excited state with long life time.[2] These unique features of the materials stimulated the growth of several branches in the field coordination chemistry and these complexes have played and are still playing a key role in the development of photochemistry, electrochemistry, photoelectrochemistry, chemi- and electrochemi-luminescence, and electron and energy transfer. Furthermore, the potential applications of the complexes for luminescent sensors,[3] electroluminescent displays,[4] oxidation and reduction catalysts[5] are also expected. (Figure 1)

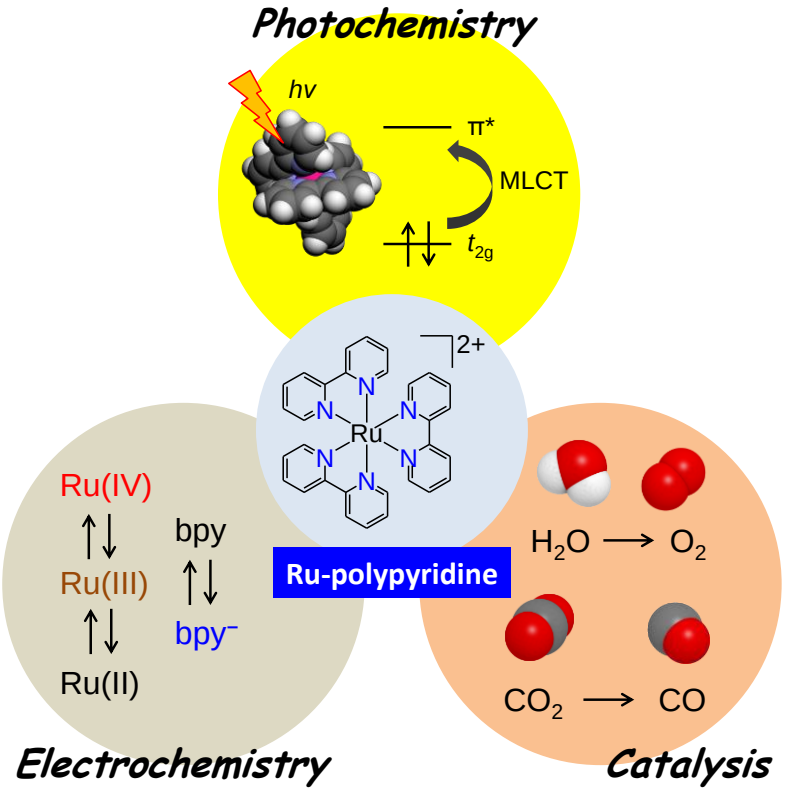

Figure 1. Attractive the possibilities of ruthenium(II) polypyridine complex

Ruthenium(II) Polypyridine Complex with a Labile Ligand

As described in the previous section, ruthenium(II) polypyridine complexes are considered as an attractive class of metal complexes that can be utilized not only for the fundamental studies but also for applied chemistry. Of particular interest are ruthenium(II) complexes which have a monodentate labile ligand because they can exhibit multiple electronic states and catalytic activity using a labile site as a reaction centre, and thus, these complexes have been also intensively investigated to date to accumulate knowledge of the conversion reactions involving multielectron transfer.[5] One typical example in this class of materials is a complex containing tridentate and bidentate polypyridine ligands and a monodentate labile ligand, $[Ru(N–N–N)(N–N)(L)]^{n+}$ (N–N–N = tridentate polypyridine ligand, *e.g.* trpy, N–N = bidentate polypyridine ligand, *e.g.* bpy, and L = monodentate labile ligand, Scheme 1). The several examples of ruthenium(II) polypyridine complexes with a labile ligand which is applied for water oxidation and CO_2 reduction will be described later in this chapter.

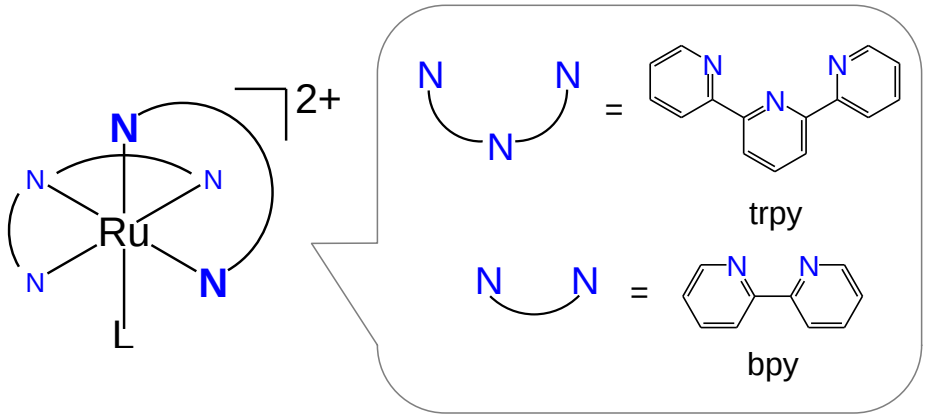

Scheme 1. Steric structure of $[Ru(N–N–N)(N–N)(L)]^{n+}$.

Multielectron Reduction and Oxidation

Modern society is maintained by consuming fossil fuels such as oil, coal, and natural gas, and it is facing the problem of inevitable resource exhaustion due to the increase in consumption. To solve environmental problems and convert from the consumer society to sustainable society, it is essential to generate artificial resources.[6] The need for high energy density batteries recently becomes increasingly important for the development of new and clean energy technologies, such as electric vehicles and electrical storage from wind and solar power.[7] However, such a stable energy supply depends on the weather. In order to overcome the disadvantage, the method of storing chemical energy obtained from natural energy is valuable.[8]

At the core of many important energy conversion processes in chemistry and biology are oxidation-reduction reactions in which both electrons and protons are transferred.[9] In the natural carbon cycle (Scheme 2a), nature uses energy of the sun to recycle carbon dioxide (CO_2) from natural sources through photosynthesis. It captures CO_2 from the atmosphere with vegetation, plankton, algae, etc. CO_2 and water as the hydrogen source are converted into glucose and oxygen (O_2) by the reaction $6CO_2 + 12H_2O = C_6H_{12}O_6 + 6H_2O + 6O_2$. This step named carbon-fixation reaction includes multielectron reduction. O_2 evolution and reduction are cyclical processes through carbon-fixation reaction in the ecosystem (Scheme 2b). Carbon in the atmosphere mainly presents in the CO_2 gas state. Although a small amount of CO_2 is approximately 0.04% among the total air, that plays an important role for life activities are maintained. The energy from the sun and green chlorophyll acting as the catalyst eventually can be converted to fossil fuels over millions of years.[10]

In the nitrogen case, even though dinitrogen (N_2) comprises approximately 78% among atmosphere of the earth, this abundant source is effectively inert and can be used for biosynthesis following conversion to a useable form like ammonia (NH_3). Reduced N_2 is an essential component of nucleic acids and proteins, and thus, all organisms require this nutrient for growth. In nature, this ability to fix N_2 ($N_2 + 8H^+ + 8e^- \rightarrow 2NH_3 + H_2$) is restricted to a small but diverse group of diazotrophic microorganisms that contain the enzyme nitrogenase.[11] Additionally, some bacteria and fungi under water and the soil conduct two multielectron processes, one is denitrification which is a reduction process to N_2 from NO_2^- or NO_3^-, the other is nitrification which is an oxidation process to NO_2^- or NO_3^- from NH_3.[12] The comprehensive nitrogen cycle is shown in Scheme 2c.

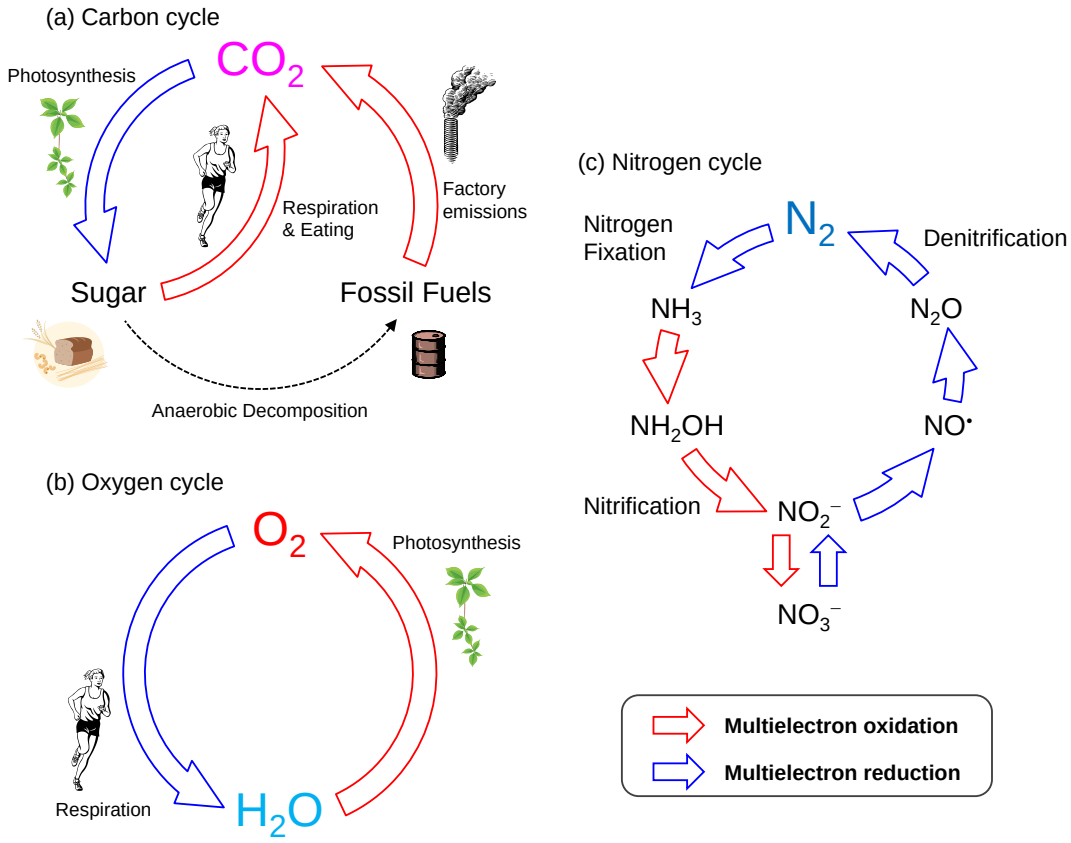

Scheme 2. (a) Carbon, (b) oxygen, and (c) nitrogen cycles.

Oxidation Reaction Catalyzed by Ruthenium(II) Polypyridine Complex

A summary of oxidation reactions catalyzed by ruthenium(II) polypyridine complex is shown in Scheme 3 and the oxidation reactions provides several kinds of pathway as described below.[13] A notable reaction is with hydroquinone which occurs by proton-coupled electron transfer (PCET).[14] In this case, the electron comes from a molecular orbital delocalized over the aromatic ring and the proton from the O−H bond. On the other hand, phenol oxidation to hydroquinone proceeds through electrophilic ring attack.[15] Oxygen-atom transfer to dimethyl sulfide (SMe_2)[16] and triphenylphosphine (PPh_3)[17] to give sulfoxide ($S(O)Me_2$) and triphenylphosphate ($P(O)Ph_3$) are also notable reactions. In the oxidation of cyclohexene, a ruthenium(III) intermediate is observed and a C−H insertion mechanism has been proposed.[18] The final product is the four-electron-oxidized ketone rather than the two-electron-oxidized alcohol. In this case, oxidation occurs by initial C−H insertion to give a bound alcohol intermediate which undergoes further rapid oxidation by $[Ru^{IV}=O]^{2+}$ oxidant.[18] Lastly, oxidation of benzyl alcohol occurs by hydride transfer.[19]

Oxidation of water into molecular oxygen (eq. 1) is one of the most important chemical processes in nature and fundamental reactions in the energy cycle.[20] However, development of artificial oxygen-evolving molecular catalysts remains a challenging target. Such catalysts will play a significant role in artificial solar energy-conversion systems based on visible light-driven water-splitting reactions (eq. 2). It was apparent from the earliest studies that polypyridine Ru-oxo reactivity would be extraordinary. The simplest net reaction to study is the proportionate reaction $[Ru^{IV}=O]^{2+}$ and $[Ru^{II}\text{-}OH_2]^{2+}$ to give $[Ru^{III}\text{-}OH]^{2+}$.[20] Therefore, ruthenium is one of the most extensively studied transition metal ion in the research field of redox chemistry and catalysis.[13] The mononuclear polypyridine complex, $[Ru(trpy)(bpy)(OH_2)]^{2+}$, exhibits high catalytic activity for the evolution of oxygen from water in the presence of cerium(IV) (Ce^{IV}) as an oxidant (eq. 3).[21]

$$2H_2O \rightarrow O_2 + 4H^+ + 4e^- \qquad \text{(eq. 1)}$$

$$2H_2O + 4h\nu \rightarrow 2H_2 + O_2 \qquad \text{(eq. 2)}$$

$$2H_2O + 4Ce^{IV} \rightarrow O_2 + 4H^+ + 4Ce^{III} \qquad \text{(eq. 3)}$$

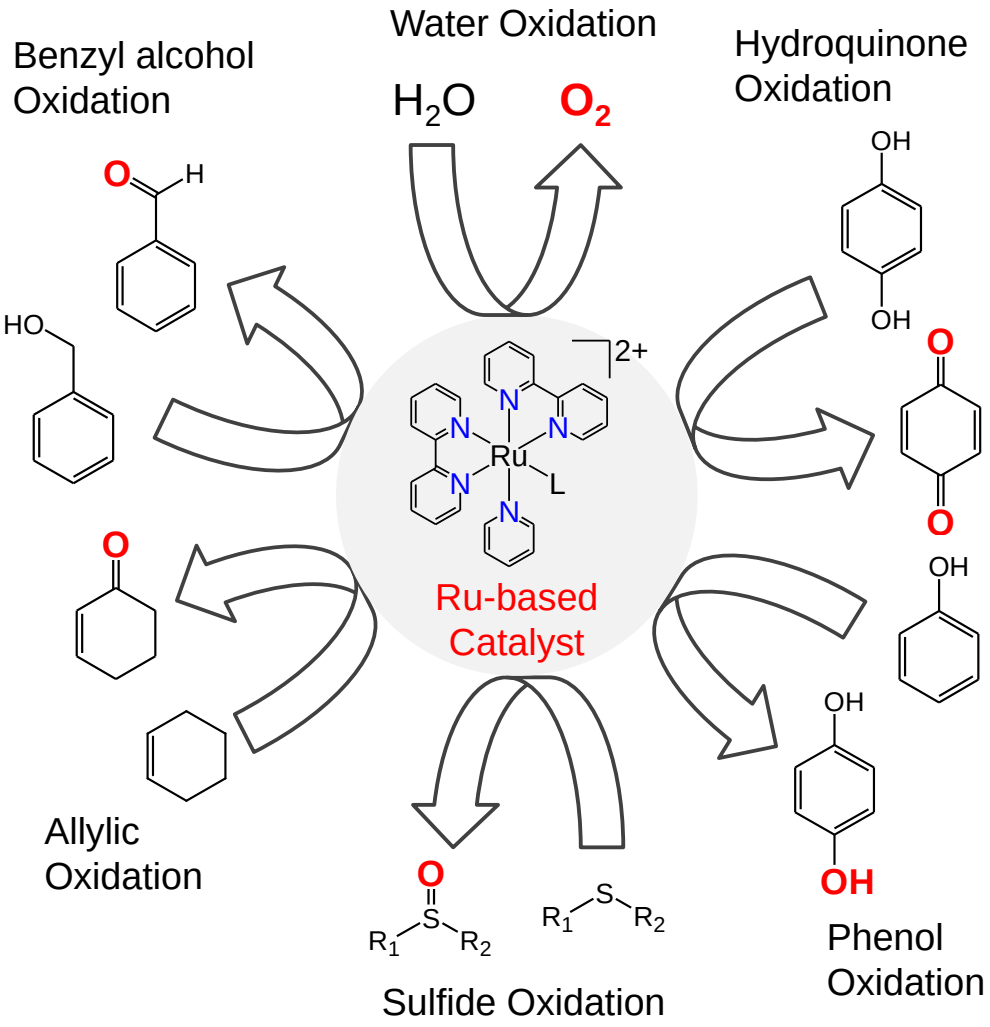

Scheme 3. Applications of ruthenium(II) polypyridine complexes as oxidation catalysts.

Reduction of Carbon Dioxide by Ruthenium(II) Polypyridine Complex

Two major energy-related problems confront the world. First, increased worldwide competition for gradually depleting fossil fuel reserves will lead to higher costs, both monetarily and politically. Second, atmospheric carbon dioxide (CO_2) levels are at their highest recorded level since records began. Therefore, the development of photocatalysts that capable of converting CO_2 to useful carbon resources is of paramount interest.[23]

Tanaka and co-workers discovered that the polypyridine complex, $[Ru(bpy)_2(CO)_2]^{2+}$, exhibits catalytic activity for the formation of carbon monoxide (CO) and formic acid (HCOOH) from CO_2 in the presence of water, however the electrochemical reduction products have been limited to two-electron reduction products such as CO and HCOOH so far, and four- and six-electron reduction products have not been generated such as formaldehyde (HCHO) and methanol (CH_3OH).[23] Several years later, they also reported $[Ru(trpy)(bpy)(CO)]^{2+}$ which exhibits the similar catalytic activity as $[Ru(bpy)_2(CO)_2]^{2+}$.[24] Since then, several researchers also have studied that the mononuclear ruthenium analogous systems ($[Ru(N–N)_2(L)_2]^{n+}$ and $[Ru(N–N–N)(N–N)(L)]^{n+}$) carried out similar catalytic activity toward carbon dioxide by electrolysis (Scheme 4).[25,26] Although the mechanisms of homogeneous redox and chemical catalysis of CO_2 are reasonably well understood, the details are still lacking. The relationships between catalytic efficiency and structure remain essentially empirical. As with other catalytic reactions, the factors that govern the durability of the catalyst have been so far rarely analyzed.[27] Meyer and co-workers have reported that CO_2 reduction occurs following rate limiting substitution of MeCN by CO_2 in $[Ru(trpy)(bpy)(MeCN)]^{2+}$ to give $[Ru(trpy)(bpy)(CO_2)]^{0}$ followed by further $2e^-$ reduction. There is no kinetic information but $[Ru(trpy)(bpy)(CO_2)]^{2-}$ might give CO_3^{2-} under CO_2 and form the CO complex as an intermediate. The two-electron reduced CO intermediate, $[Ru(trpy)(bpy)(CO)]^{0}$, is known to undergo rapid loss of CO (Scheme 5).[28] Eq. 4 shows total reaction for this electrochemical reduction.

$$2CO_2 + 2e^- \rightarrow CO + CO_3^{2-} \qquad \text{(eq. 4)}$$

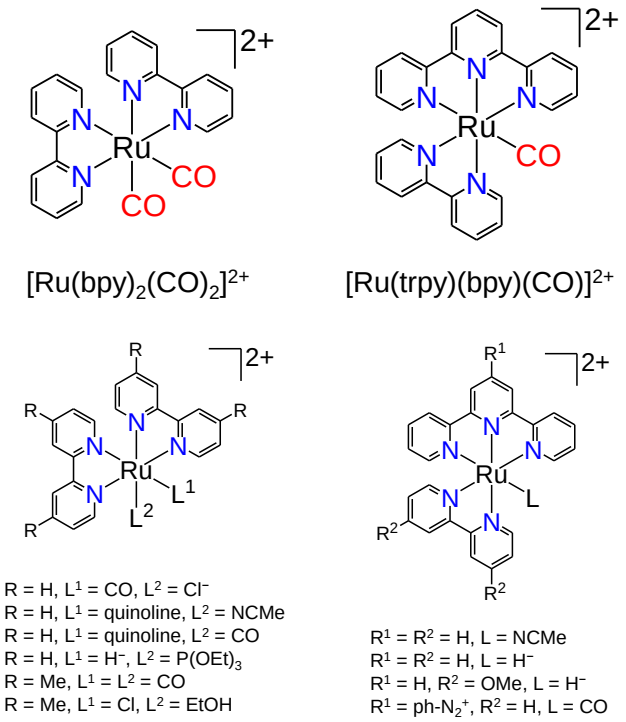

Scheme. 4. Structures of mononuclear carbon dioxide reduction catalysts.

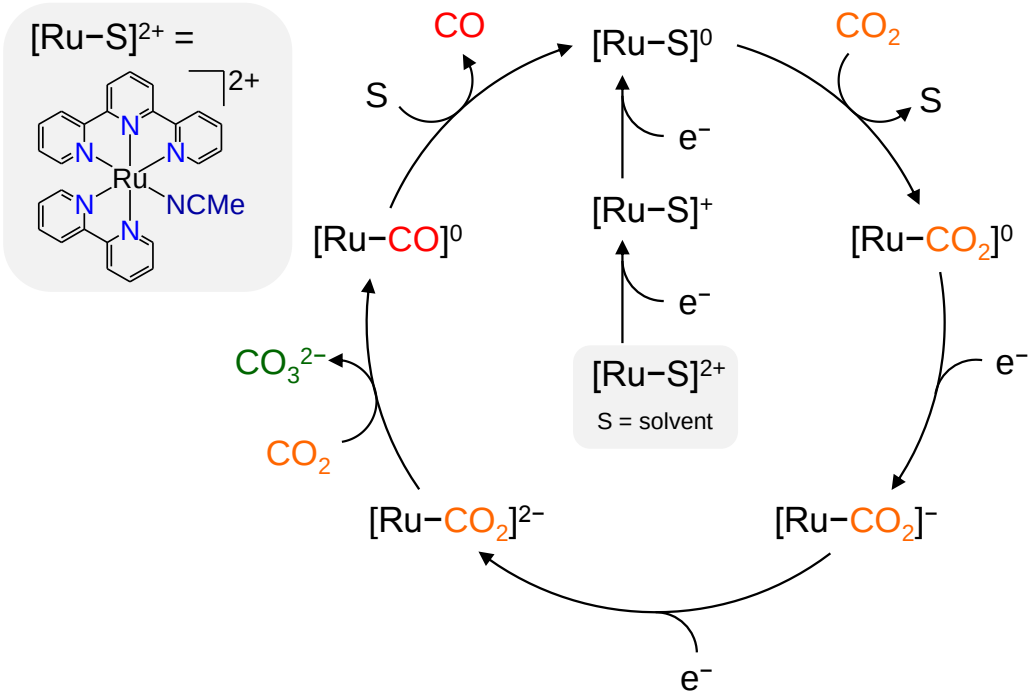

Scheme. 5. Suggested catalytic mechanism for the carbon dioxide reduction.

Control of catalytic activity by isomerization

When designing ruthenium(II) polypyridine complexes with a labile site, the formation of structural isomers should be considered. In particular, combinations of *mer*-type tridentate ligand (*e.g.* trpy) and asymmetric bidentate ligands are considered a form of *cis-trans* isomers (Scheme 6).

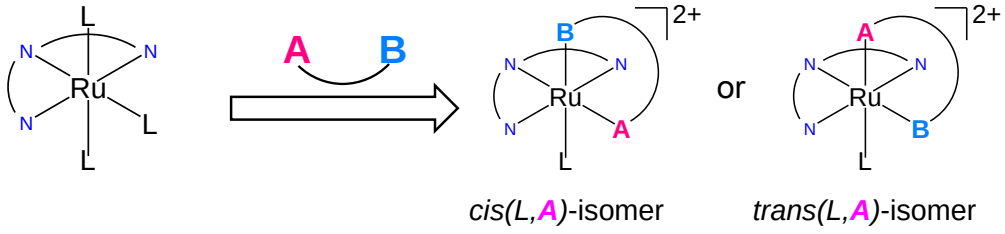

combination with a *mer*-type tridentate ligand → **two kinds of isomers**

Scheme 6. Steric structure of $[Ru(N–N–N)(N–N)(L)]^{n+}$ with asymmetric bidentate ligands.

Several examples of both of isolated *cis-trans* isomers which are ruthenium(II) polypyridine complexes with a labile site have been reported.[29-31] The complexes including a 2-(2-pyridyl)-1,8-naphthyridine (pynp)[30] reported by Yagi et al. and a 2-(2-pyridyl-1,8-naphthyridine) (PAD)[31] reported by Tanaka et al. were known as the different catalytic activity for water oxidation between *cis-trans* isomers (Scheme 7). The activity of pre-photoisomerized species is higher than that of photoisomerized species. However, the geometric design guide for control of activity still has not been provided. Therefore it is important to investigate the differences of the catalytic activity and isomerization phenomena between isomers.

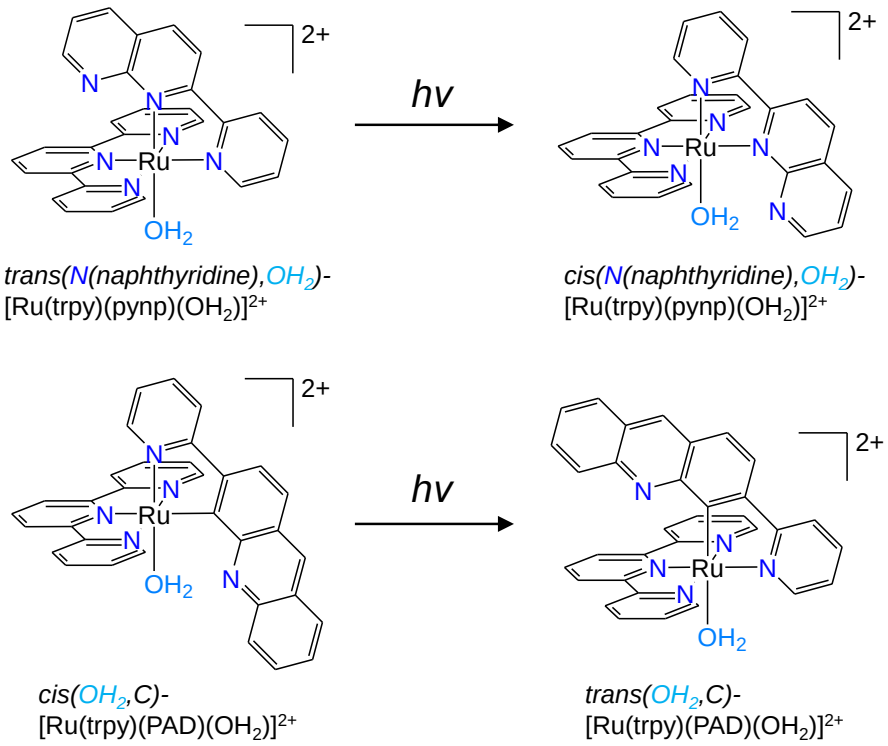

Scheme 7. Examples of photoisomerization reactions between *cis-trans* isomers.

Ruthenium(II) Phosphine Complexes

Phosphines coordinate to transition metals, not only as σ-donor ligands but also as π-acceptor ligands. In typical octahedral complexes, σ-donation is the interaction between empty dσ(M) and filled n(P) orbitals, and π-back donation occurs between filled dπ(M) and empty σ*(P–C) orbitals.[32] These characteristics influence the structures and properties of metal complexes. Phosphine derivatives influence coordination character by electronic and steric effects of substituents on the phosphorus atoms. Therefore, ruthenium(II) phosphine complexes are also attractive targets for potential applications to olefin metathesis,[33] asymmetric hydrogenation,[34] and photosensitizer,[35] (Figure 2) because the introduction of phosphine ligands can control electronic structures of the ruthenium center due to σ-donating and π-accepting abilities. In other words, the introduction of phosphine ligands to ruthenium(II) polypyridine complexes should be one of the key strategies to develop the metal complexes with novel properties and reactivities.

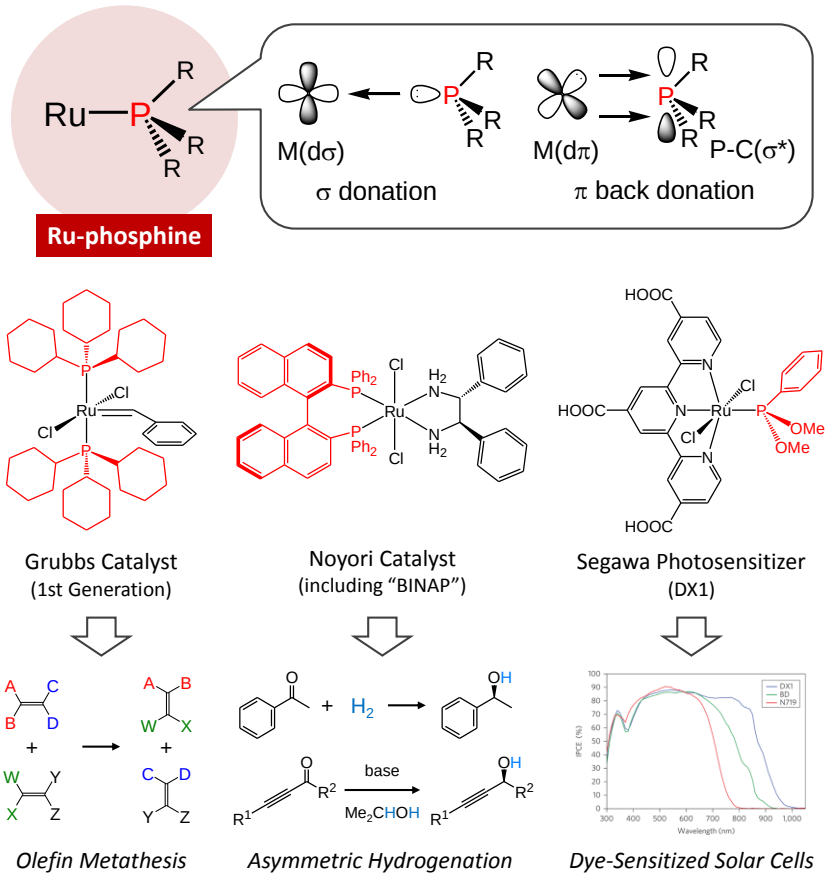

Figure 2. Applications of ruthenium(II) phosphine complexes.

The Aim of This Thesis

Ruthenium(II) polypyridine complexes with phosphine ligands are considered to be one of attractive targets for investigating properties and reactivities because the introduction of phosphine ligands can control electronic structures of the ruthenium center due to σ-donation and π-back donation abilities. However, it is surprising that there are only few studies examining substitution of phosphine for pyridine moiety in such ruthenium(II) polypyridine complexes with a monodentate labile ligand.

This study describes the effects of the substitution of phosphines for pyridine in a series of ruthenium(II) polypyridine complexes with a monodentate labile ligand. 8-(diphenylphosphanyl)quinoline (Pqn, P−N type ligand) and 1,2-bis(diphenyl-phosphanyl)benezene (dppbz, P−P type ligand) were used as bidentate ligands as shown in Scheme 8 and involves comparison with the complex with N−N type ligand, bpy. Control over the spectroscopic and electrochemical properties is expected to be achieved by changing the number and position of phosphine donors in $[Ru(N{-}N{-}N)(N{-}N)(L)]^{n+}$-type complexes.

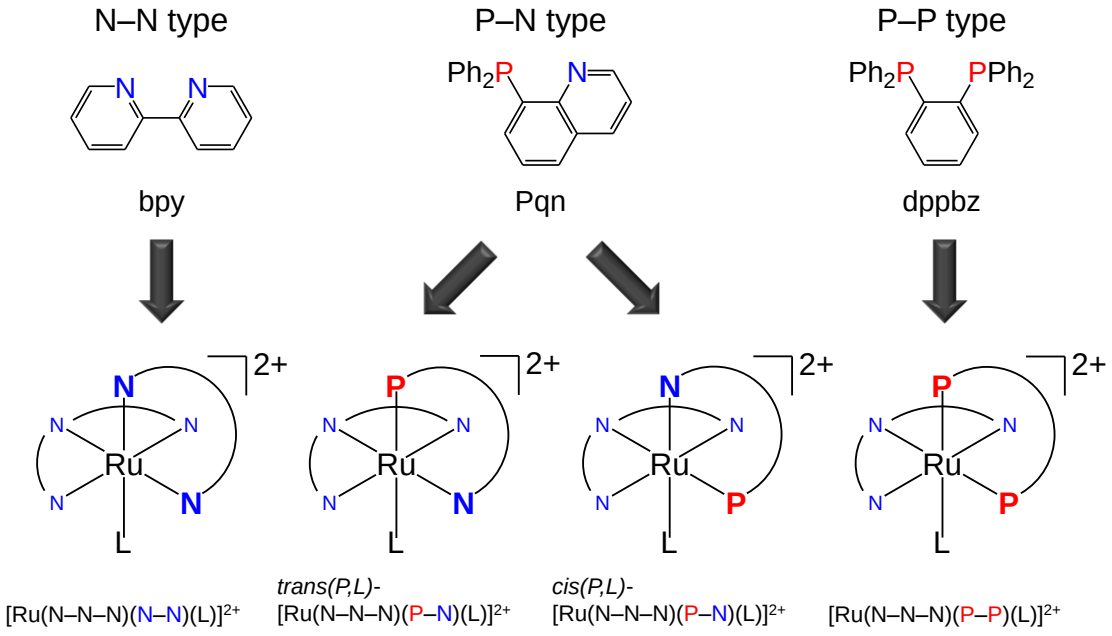

Scheme 8. Structures of ligands and complexes used in this study.

Survey of this thesis

Chapter 1 describes the electrochemical behavior of phosphine-substituted ruthenium(II) polypyridine complexes with a single labile ligand. A series of phosphine-substituted ruthenium polypyridine complexes, *cis(P,Cl)*-[Ru(trpy)(Pqn)Cl]-PF_6 (***cis*-Cl**), *trans(P,MeCN)*-[Ru(trpy)(Pqn)(MeCN)]$(PF_6)_2$ (***trans*-PN**), *cis(P,MeCN)*-[Ru(trpy)(Pqn)(MeCN)]$(PF_6)_2$ (***cis*-PN**), and [Ru(trpy)(dppbz)(MeCN)]$(PF_6)_2$ (**PP**) were synthesized and crystallographically characterized (trpy = 2,2':6',2"-terpyridine, Pqn = 8-(diphenylphosphanyl)quinoline and dppbz = 1,2-bis(diphenylphosphanyl)-benzene). In electrochemical measurements for ***cis*-PN** and **PP**, the reduction of ***cis*-PN** resulted in the formation of ***trans*-PN** *via cis-trans* isomerization, and that of **PP** proceeded *via* a two-electron transfer reaction. The mechanism of the electrochemical behaviors is discussed through consideration of five-coordinated species, $[Ru(trpy)(Pqn)]^{n+}$ or $[Ru(trpy)(dppbz)]^{n+}$ (n = 0, 1 or 2), formed by liberation of a monodentate labile ligand.

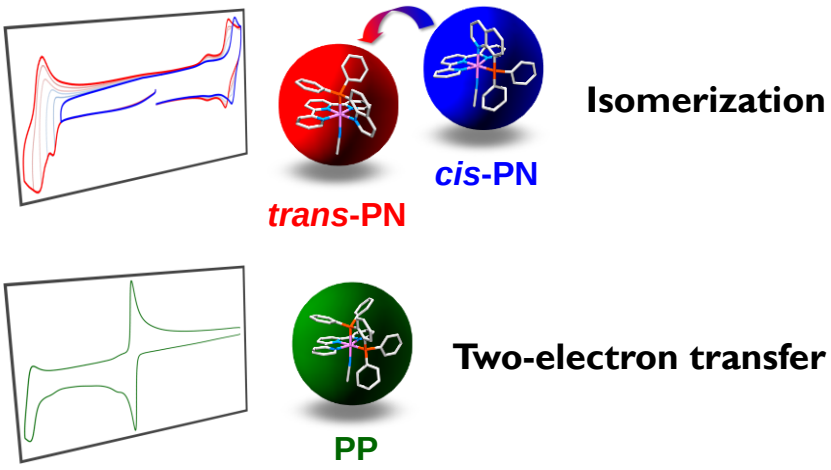

Chapter 2 describes the syntheses and properties of phosphine-substituted ruthenium(II) polypyridine complexes with nitrogen oxide. A series of phosphine-substituted ruthenium polypyridine nitrito complexes, *trans(P,NO$_2$)*-[Ru(trpy)(Pqn)(NO$_2$)]PF$_6$ (***trans*-NO$_2$**), *cis(P,NO$_2$)*-[Ru(trpy)(Pqn)(NO$_2$)]PF$_6$ (***cis*-NO$_2$**), and [Ru(trpy)(dppbz)-(NO$_2$)]PF$_6$ (**PP-NO$_2$**) were synthesized and crystallographically characterized. In electrochemical measurements for ***trans*-NO$_2$** and **PP-NO$_2$**, the both of oxidation and reduction of ***trans*-NO$_2$** and **PP-NO$_2$** resulted in the irreversible formation of ***trans*-MeCN** and **PP-MeCN** with ligand substitution. Only ***cis*-NO$_2$** can form the nitrosyl complex, *cis(P,NO)*-[Ru(trpy)(Pqn)(NO)](PF$_6$)$_3$ (***cis*-NO**) and ***trans*-NO$_2$** and **PP-NO$_2$** were not successful in formation of the nitrosyl complexes due to strong σ-donation of *trans*-position phosphine moiety.

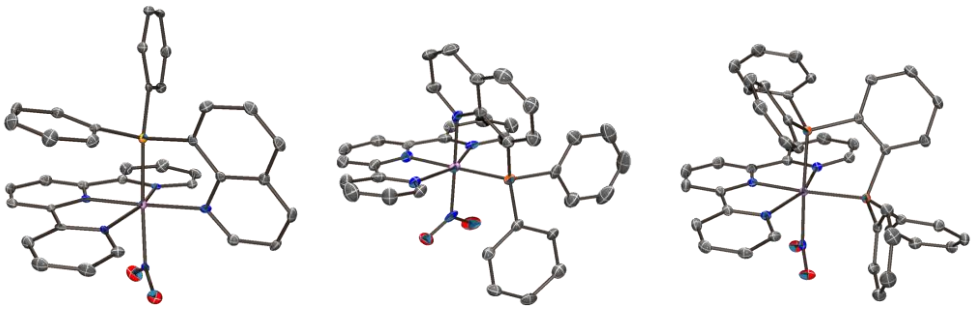

***trans*-NO$_2$** ***cis*-NO$_2$** **PP-NO$_2$**

Chapter 3 describes the electrochemical behavior of phosphine-substituted ruthenium(II) polypyridine complexes with a single labile ligand under carbon dioxide (CO_2). *trans(P,MeCN)*-[Ru(trpy)(Pqn)(MeCN)]$(PF_6)_2$ (***trans*-MeCN**) undergoes an $1e^-$ ligand-based reduction to form $[Ru(trpy^-)(Pqn)(MeCN)]^+$ Next, $[Ru(trpy^-)(Pqn)(MeCN)]^+$ undergoes an $1e^-$ reduction followed by substitution of CO_2 for MeCN. In this reaction, internal electron transfer occurs to give the metallocarboxylate intermediate, $[Ru(trpy)(Pqn)(CO_2^{2-})]^0$ (***trans*-CO_2**). A phosphine moiety of Pqn achieved to release of acetonitrile ligand to form ***trans*-CO_2** and it gives CO and CO_3^{2-} as final products with further ligand-based reduction under CO_2 continuously.

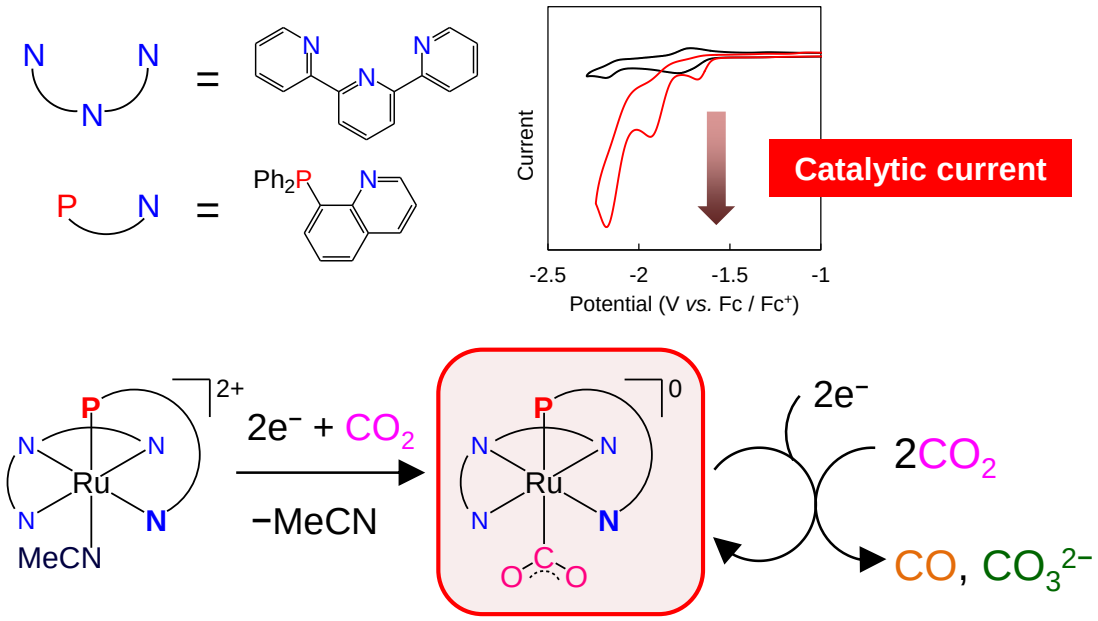

References

1 B. K. Ghosh, A. Chakravorty, *Coord. Chem. Rev.* **1989**, *95*, 239–294.

2 (a) K. Kalyanasundaram, *Coord. Chem. Rev.* **1982**, *46*, 159–244, (b) A. Juris, V. Balzani, F. Barigelletti, S. Campagna, P. Belser, A. von Zelewsky, *Coord. Chem. Rev.* **1988**, *84*, 85–277, (c) V. Balzani, A. Juris, *Coord. Chem. Rev.* **2001**, 211, 97–115, (d) S. Campagna, F. Puntoriero, F. Nastasi, G. Bergamini, V. Balzani, *Top. Curr. Chem.* **2007** *280*, 117–214, (e) T. P. Yoon, M. A. Ischay, J. Du, *Nat. Chem.* **2010**, *2*, 527–532, (f) Q. Sun, S. Mosquera-Vazquez, Y. Suffren, J. Hankache, N. Amstutz, L. M. L. Daku, E. Vauthey, A. Hauser, *Coord. Chem. Rev.* **2015**, *282–283*, 87–99.

3 (a) A. Lavie-Cambot, C. Lincheneau, M. Cantuel, Y. Leydet, N. D. McClenaghan, *Chem. Soc. Rev.* **2010**, *39*, 506–515, (b) O. Filevich, B. García-Acosta, R. Etchenique, *Photochem. Photobiol. Sci.* **2012**, *11*, 843–847.

4 (a) N. Haddour, J. Chauvin, C. Gondran, S. Cosnier, *J. Am. Chem. Soc.* **2006**, *128*, 9693–9698, (b) H. Wei, E. Wang, *Trends Anal. Chem.* **2008**, *27*, 447–459, (c) J. L. Delaney, C. F. Hogan, J. Tian, W. Shen, *Anal. Chem.* **2011**, *83*, 1300–1306.

5 (a) K. Tanaka, D. Ooyama, *Coord. Chem. Rev.* **2002**, *226*, 211–218, (b) J.-M. Savéant, *Chem. Rev.* **2008**, *108*, 2348–2378. (c) M. D. Kärkäs, O. Verho, E. V. Johnston, B. Åkermark, *Chem. Rev.* **2014**, in press.

6 (a) T. J. Meyer, *Acc. Chem. Res.* **1989**, *22*, 163–170. (b) V. Balzani, A. Credi, M. Venturi, *ChemSusChem* **2008**, *1*, 26–58. (c) S. Berardi, S. Drouet, L. Francàs, C. Gimbert-Suriñach, M. Guttentag, C. Richmond, T. Stoll, A. Llobet, *Chem. Soc. Rev.* **2014**, *43*, 7501–7519.

7 X.-P. Gao, H.-X. Yang, *Energy Environ. Sci.* **2010**, *3*, 174–189.

8 (a) S. P. Fletcher, F. Dumur, M. M. Pollard, B. L. Feringa, *Science* **2005**, *310*, 80–82. (c) S. Linic, P. Christopher, D. B. Ingram, *Nature Materials* **2011**, *10*, 911–921.

9 M. H. V. Huynh, T. J. Meyer, *Chem. Rev.* **2007**, *107*, 5004–5064.

10 G. A. Olah, G. K. S. Prakash, A. Goeppert, *J. Am. Chem. Soc.* **2011**, *133*, 12881–12898.

11 (a) J. B. Howard, D. C. Rees, *Chem. Rev.* **1996**, *96*, 2965–2982. (b) B. K. Burgess, D. J. Lowe, *Chem. Rev.* **1996**, *96*, 2983–3011.

12 J. C. Gaby, D. H. Buckley, *Environ. Microbiol.* **2011**, *13*, 1790–1799.

13 T. J. Meyer, M. H. V. Huynh, *Inorg. Chem.* **2003**, *42*, 8140−8160.

14 R. A. Binstead, M. E. McGuire, A. Dovletoglou, W. K. Seok, L. E. Roecker, T. J. Meyer, *J. Am. Chem. Soc.* **1992**, *114*, 173−186.

15 W. K. Seok, J. C. Dobson, T. J. Meyer, *Inorg. Chem.* **1988**, *27*, 3−5.

16 L. Roecker, J. C. Dobson, W. J. Vining, T. J. Meyer, *Inorg. Chem.* **1987**, *26*,

779−781.

17 B. A. Moyer, B. K. Sipe, T. J. Meyer, *Inorg. Chem.* **1981**, *20*, 1475−1480.

18 L. K. Stultz, M. H. V. Huynh, R. A. Binstead, M. Curry, T. J. Meyer, *J. Am. Chem. Soc.* **2000**, 122, 5984–5996.

19 L. Roecker, T. J. Meyer, *J. Am. Chem. Soc.* **1987**, *109*, 746–754.

20 B. A. Moyer, T. J. Meyer, *J. Am. Chem. Soc.* **1978**, *100*, 3601–3603. (b) B. A. Moyer, T. J. Meyer, *Inorg. Chem.* **1981**, *20*, 436–444. (c) R. A. Binstead, B. A. Moyer, G. J. Samuels, T. J. Meyer, *J. Am. Chem. Soc.* **1981**, *103*, 2897–2899.

21 (a) S. Masaoka, K. Sakai, The 88th Annual Meeting of Chemical Sciety of Japan, Tokyo, 26th March, **2008**, Paper No. 1E6-39. (b) S. Masaoka, K. Sakai, *Chem. Lett.* **2009**, *38*, 182–183.

22 (a) K. Tanaka, *Chem. Rec.* **2009**, *9*, 169–186. A. M. Appel, J. E. Bercaw, A. B. Bocarsly, H. Dobbek, D. L. DuBois, M. Dupuis, J. G. Ferry,. E. Fujita, R. Hille, P. J. A. Kenis, C. A. Kerfeld, R. H. Morris, C. H. F. Peden, A. R.Portis, S. W. Ragsdale, T. B. Rauchfuss, J. N. H. Reek, L. C. Seefeldt, R. K. Thauer, G. L. Waldrop, *Chem. Rev.* **2013**, *113*, 6621−6658.

23 (a) H. Ishida, H. Tanaka, K. Tanaka, *J. Chem. Soc. Chem. Commun.* **1987**, 131–132. (b) H. Ishida, K. Tanaka, T. Tanaka, *Organometallics* **1987**, *6*, 181–186. (c) H. Ishida, H. Tanaka, K. Tanaka, T. Tanaka, *Chem. Lett.* **1987**, 597–600.

24 (a) Nagao, H.. Mizukawa, T.. Tanaka, K. *Chem. Lett.* **1993**, *22*, 955–958. (b) Tanaka, K.. Ooyama, D. *Coord. Chem. Rev.* **2002**, *226*, 211–218.

25 (a) Nakajima, H.. Kushi, Y.. Nagao, H.. Tanaka, K. *Organometallics*, **1995**, *14*, 5093–5098. (b) J. Chen, D. J. Szalda, E. Fujita, C. Creutz, *Inorg. Chem.* **2010**, *49*, 9380–9391. (c) Y. Tamaki, T. Morimoto, K. Koike, O. Ishitani, *Proc. Natl. Acad. Sci. USA* **2012**, *109*, 15673–15678. (d) P. Voyame, K. E. Toghill, M. A. Méndez, H. H. Girault, *Inorg. Chem.* **2013**, *52*, 10949–10957. (e) Yusuke Kuramochi, Masaya Kamiya, Hitoshi Ishida, *Inorg. Chem.* **2014**, *53*, 3326–3332. (f) F. H. Haghighi, H. Hadadzadeh, H. Farrokhpour, N. Serri, K. Abdi, H. A. Rudbari, *Dalton Trans.* **2014**, *43*, 11317–11332.

26 (a) H. Konno, A. Kobayashi, K. Sakamoto, F. Fagalde, N. E. Katz, H. Saitoh, O. Ishitani, *Inorg. Chim. Acta* **2000**, *299*, 155–163. (b) Y. Tsukahara, T. Wada, K. Tanaka, *Chem. Lett.* **2010**, *39*, 1134–1135. (c) Z. Chen, C. Chen, D. R. Weinberg, P. Kang, J. J. Concepcion, D. P. Harrison, M. S. Brookhart, T. J. Meyer, *Chem. Commun.* **2011**, *47*, 12607–12609. (d) S. Kern, R. van Eldik, *Inorg. Chem.* **2012**, *51*, 7340–7345.

27 J.-M. Savéant, *Chem. Rev.* **2008**, *108*, 2348–2378.

28 (a) Z. Chen, J. J. Concepcion, M. K. Brennaman, P. Kang, M. R. Norris, P. G. Hoertz, T. J. Meyer, *Proc. Natl. Acad. Sci. USA* **2012**, *109*, 15606–15611. (b) Z. Chen, P. Kang, M.-T. Zhang, T. J. Meyer, *Chem. Commun.* **2014**, *50*, 335–337. (c) P. Kang, Z. Chen, A. Nayak, S. Zhang, T. J. Meyer, *Energy Environ. Sci.* **2014**, *7*, 4007–4012.

29 (a) E. Masllorens, M. Rodriguez, I. Romero, A. Roglans, T. Parella, J. Benet-Buchholz, M. Poyatos, A. Llobet, *J. Am. Chem. Soc.* **2006**, *128*, 5306–5307. (b) L. Vaquer, P. Riente, X. Sala, S. Jansat, J. Benet-Buchholz, A. Llobet, M. A. Pericàs, *Catal. Sci. Technol.* **2013**, *3*, 706–714. (c) D. Oyama, K. Yuzuriya, R. Naoi, T. Hamada, T. Takase, *Bull. Chem. Soc. Jpn.* **2014**, *87*, 1107–1115. (d) B. A. Albani, C. B. Durr, B. Peña, K. R. Dunbar C. Turro, *Dalton Trans.* **2014**, *43*, 17828–17837.

30 (a) H. Yamazaki, T. Hakamata, M. Komi, M. Yagi, *J. Am. Chem. Soc.* **2011**, *133*, 8846−8849. (b) J. L. Boyer, D. E. Polyansky, D. J. Szalda, R. Zong, R. P. Thummel, E. Fujita, *Angew. Chem. Int. Ed.* **2011**, *50*, 12600−12604. (c) M. Hirahara, Z. M. Ertem, M. Komi, H. Yamazaki, C. J. Cramer, M. Yagi, *Inorg. Chem.* **2013**, *52*, 6354−6364.

31 S. K. Padhi, R. Fukuda, M. Ehara, K. Tanaka, *Inorg. Chem.* **2012**, *51*, 5386−5392.

32 (a) M. M. Rahman, H.-Y. Liu, K. Eriks, A. Prock, W. P. Giering, *Organomettalics* **1989**, *8*, 1–7. (b) D. G. Gilheany, *Chem. Rev.* **1994**, *94*, 1339–1374.

33 (a) P. Schwab, M. B. France, J. W. Ziller, R. H. Grubbs, *Angew. Chem. Int. Ed.* **1995**, *34*, 2039–2041. (b) H. Clavier, S. P. Nolan, *Chem. Eur. J.* **2007**, *13*, 8029–8036. (c) G. C. Vougioukalakis, R. H. Grubbs, *Chem. Rev.* **2010**, *110*, 1746–1787. (d) J. S. M. Samec, B. K. Keitz, R. H. Grubbs, *J. Organomet. Chem.* **2010**, *695*, 1831–1837. (e) S. P. Nolan, H. Clavier, *Chem. Soc. Rev.* **2010**, *39*, 3305–3316.

34 (a) R. Noyori, T. Ohkuma, *Angew. Chem. Int. Ed.* **2001**, *40*, 40–73. (b) R. Noyori, *Angew. Chem. Int. Ed.* **2002**, *41*, 2008–2022. (c) R. Noyori, *Adv. Synth. Catal.* **2003**, *345*, 15–32. (d) S. E. Clapham, A. Hadzovic, R. H. Morris, *Coord. Chem. Rev.* **2004**, *248*, 2201–2237. (e) A. F. Trindade, P. M. P. Gois, C. A. M. Afonso, *Chem. Rev.* **2009**, *109*, 418–514. (f) R. Noyori, *Angew. Chem. Int. Ed.* **2013**, *52*, 79–92.

35 (a) T. Kinoshita, J. T. Dy, S. Uchida, T. Kubo, H. Segawa, *Nat. Photonics* **2013**, *7*, 535–539. (b) R. Katoh, A. Furube, *J. Photochem. Photobiol. C* **2014**, 20, 1–16.

Chapter 1

Electrochemical Behavior of Phosphine-Substituted Ruthenium(II) Polypyridine Complexes with a Single Labile Ligand

Inorganic Chemistry, **2014**, *53*, 7214-7226.

Introduction

Ruthenium(II) polypyridine complexes have been studied to gain knowledge of fundamental coordination chemistry, electrochemistry, photochemistry, and photophysics,[1,2] and also to find potential applications to energy conversion, luminescent sensors, electroluminescence displays, and biotechnology.[3-6] Of particular interest are ruthenium(II) complexes containing tridentate and bidentate polypyridine ligands and a monodentate labile ligand, $[Ru(N–N–N)(N–N)(L)]^{n+}$ (N–N–N = tridentate polypyridine ligand, N–N = bidentate polypyridine ligand, and L = monodentate labile ligand), because these complexes can act as catalysts for chemical conversions such as oxidation,[7-10] reduction,[11-13] and photo-induced reactions.[14]

Ruthenium(II) phosphine complexes are also attractive targets for potential applications to photophysics[15] and catalysis[16-19] because the introduction of phosphine ligands can control electronic structures of the ruthenium center due to σ-donating and π-accepting abilities. Thus, the introduction of phosphine ligands to ruthenium(II) polypyridine complexes should be one of the key strategies to develop the metal complexes with novel properties and reactivities. In fact, there have been several examples of ruthenium (II) polypyridine complexes containing monodentate phosphine ligands.[20,21] However, surprisingly, few studies examining substitution of phosphine for pyridine moiety in $[Ru(N–N–N)(N–N)(L)]^{n+}$-type complexes have been reported; there have been only a few studies of diphosphine-coordinated ruthenium(II) polypyridine complexes, $[Ru(N–N–N)(P–P)(L)]^{2+}$ (P−P = diphosphine ligand), and no crystal structures have been reported.[22] In addition, no studies involving the introduction of only one phosphine moiety into $[Ru(N–N–N)(N–N)(L)]^{n+}$-type complexes, *e.g.*, $[Ru(P–N–N)(N–N)(L)]^{2+}$ or $[Ru(N–N–N)(P–N)(L)]^{2+}$, have been reported. Thus, investigation of phosphine-substituted $[Ru(N–N–N)(N–N)(L)]^{n+}$-type complexes is important not

only for the design and development of new catalysts but also for the understanding of their basic properties.

This report describes the syntheses, structural characterization, and electrochemical and spectroscopic properties of a series of ruthenium(II) polypyridine complexes containing 8-(diphenylphosphanyl)quinoline (Pqn), *cis(P,Cl)*-[Ru(trpy)(Pqn)Cl]PF_6 (***cis*-Cl**), *trans(P,MeCN)*-, and *cis(P,MeCN)*-[Ru(trpy)(Pqn)(MeCN)]$(PF_6)_2$ (***trans*-PN** and ***cis*-PN**, trpy = 2,2':6',2"-terpyridine) or 1,2-bis(diphenylphosphanyl)benzene (dppbz), [Ru(trpy)(dppbz)(MeCN)]$(PF_6)_2$ (**PP**) (Scheme 1). Effects of the number and position of phosphine donors on the structures and electronic properties also were investigated based on comparisons with [Ru(trpy)(bpy)(MeCN)]$(PF_6)_2$ (**NN**).[9,12,13,23,24] Control over the spectroscopic and electrochemical properties is expected to be achieved by changing the number and position of phosphine donors in $[Ru(N{-}N{-}N)(N{-}N)(L)]^{n+}$-type complexes. Indeed, characteristics of crystal structures and spectroscopic properties were simply explained through σ-donation and π-back donation of phosphine donors. However, the electrochemical measurements of these complexes showed distinct behavior in their reduction reactions; reduction of ***cis*-PN** resulted in *cis-trans* isomerization to ***trans*-PN**, and that of **PP** proceeded *via* a two-electron transfer reaction (Scheme 2). The mechanism of these electrochemical behaviors was explained in conjunction with the liberation of a monodentate labile ligand.

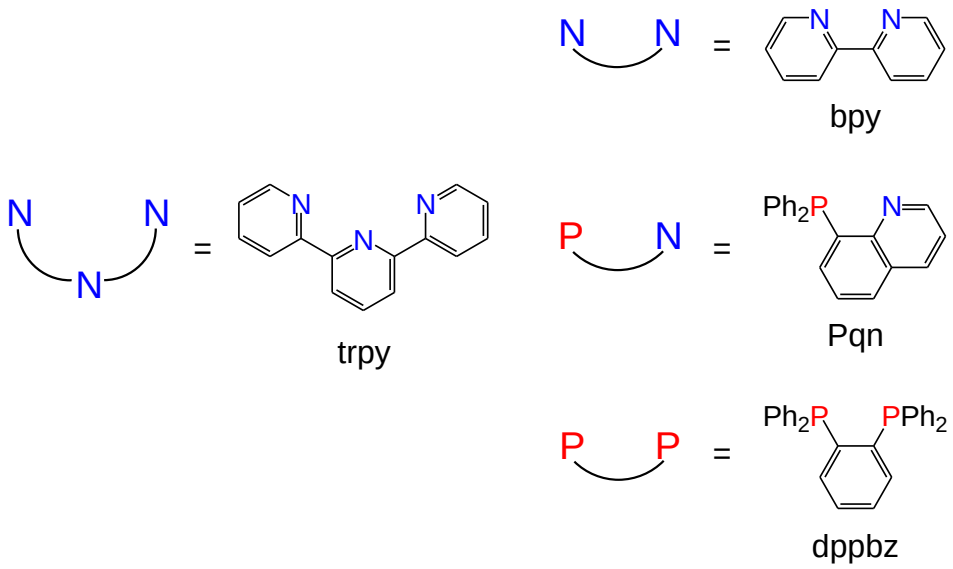

Scheme 1. Structures of a tridentate ligand (trpy) and bidentate ligands (bpy, Pqn, and dppbz) used in this study.

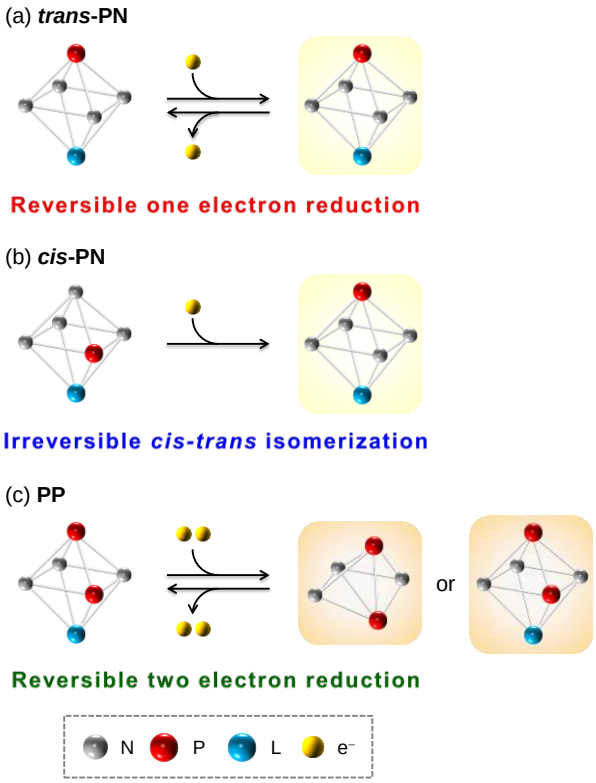

Scheme 2. Schematic illustration of electrochemical reduction reactions for (a) *trans*-**PN**, (b) *cis*-**PN**, and (c) **PP**. Each polyhedron represents a ruthenium polypyridine complex with a phosphine donor (P) and a monodentate labile ligand (L).

Results

Synthesis.

***trans*-PN**, ***cis*-PN**, and **PP** were synthesized according to the reactions shown in Scheme 3, while **NN** was prepared by a method reported previously.[25] The unsymmetrical bidentate Pqn ligand, which contains diphenylphosphanyl and quinolyl groups, was used for the syntheses of the two geometrical isomers, ***trans*-PN** and ***cis*-PN**, and can form a strain-free 5-membered chelate ring like 2,2'-bipyridine (bpy) or 1,10-phenanthroline (phen).[26]

cis*-Cl**, the PF_6^- salt of the chloro precursor for ***trans*-PN** and ***cis*-PN**, was synthesized by reaction of $[Ru(trpy)Cl_3]\cdot H_2O$[27] with Pqn, followed by the addition of an aqueous solution of $NaPF_6$. The $^{31}P\{^1H\}$ NMR spectrum of ***cis*-Cl** in CD_3CN showed a singlet at δ 51.16. ^1H and $^{31}P\{^1H\}$ NMR spectroscopies confirmed that isomerization and ligand substitution of ***cis*-Cl** does not occur in acetonitrile at room temperature. The preparation of single crystals of ***cis*-Cl** suitable for X-ray crystallography was not successful. Crystals suitable for the analysis were obtained as the BPh_4^- salt, *cis(P,Cl)*-$[Ru(trpy)(Pqn)Cl]BPh_4$ (cis*-Cl'**), prepared by ion-exchange reaction from PF_6^- to BPh_4^-. Note that complex with *trans* form was isolated not as Cl-coordinated form but as solvent coordinated form in the reaction of $[Ru(trpy)Cl_3]\cdot H_2O$ with Pqn. Although unidentified compound was detected in the ^1H NMR spectrum of the reaction mixture (Figure 1), further treatment of the mixture with acetonitrile afforded MeCN coordinated complex, ***trans*-PN**, as a by-product of the reaction and ***trans*-PN** was identified by ^1H and $^{31}P\{^1H\}$ NMR spectra. This may be due to easy dissociation of the chloride ligand at the *trans* position of the phosphino group in *trans(P,Cl)*-$[Ru(trpy)(Pqn)Cl]^+$ (***trans*-Cl**), that affords *trans(P,L)*-$[Ru(trpy)(Pqn)(L)]^{2+}$ (L = monodentate labile ligand, *e.g.*, solvent molecules) through the *trans* labilizing effect.[28]

Reaction of ***cis*-Cl** with an equimolar amount of $AgPF_6$ in 2:1 mixture of 2-butanone:water at 100 °C and further treatment with MeCN gave ***trans*-PN** as a major product, and the product was characterized by the ^1H NMR spectroscopy. The *cis*-isomers were not detected under these reaction conditions. The $^{31}P\{^1H\}$ NMR spectrum of ***trans*-PN** in CD_3CN showed a singlet at δ 58.80, similar to the signal reported for $[Ru(bpy)_2(Pqn)](PF_6)_2$ (δ 58.81 (s)).[29] Note that solvent with high boiling point is required to obtain ***trans*-PN** because the isomerization of ***cis*-Cl** or formed ***cis*-PN** to corresponding *trans* complex during the reaction is indespensible (For details

of heat induced isomerization behavior, see Solvent- and Photo-induced Isomerization section.)

In contrast, the reaction of ***cis*-Cl** with an equimolar amount of $AgPF_6$ in acetonitrile at 70 °C gave ***cis*-PN** as a major product, which was confirmed by the ^1H NMR spectroscopy. Recrystallization from diethyl ether/chloroform/acetonitrile yielded ***cis*-PN** as orange crystals. The $^{31}P\{^1H\}$ NMR spectrum of ***cis*-PN** in CD_3CN gave a singlet at δ 55.96, showing an upfield shift ($\Delta\delta$ = 2.84) compared to the signal in the spectrum of ***trans*-PN**.

It should be noted that there have been several reports on photolabile ruthenium polypyridyl complexes.[10,30] Therefore, syntheses of ***cis*-Cl**, ***trans*-PN**, and ***cis*-PN** were also performed in the dark. However, the effect of light shielding on the yields of products is negligible (Table 1), suggesting that photoisomerization of these complexes does not proceed in the synthetic condition.

The ruthenium-diphosphine complex, **PP**, was produced by the reaction of $[Ru(trpy)Cl_3]\cdot H_2O$ with one equivalent of dppbz. The reaction in ethanol afforded a mixture of $[Ru(trpy)(dppbz)Cl]^+$ and $[Ru(trpy)(dppbz)(EtOH)]^{2+}$. The resulting mixture was then refluxed in acetonitrile to afford **PP**. The $^{31}P\{^1H\}$ NMR spectrum of **PP** in CD_3CN afforded two doublets at δ 68.57 and 69.77 with coupling constants of 20.2 Hz. These peak positions are similar to those of $[Ru(bpy)_2(dppbz)](PF_6)_2$ (δ 69.51 (s)).[29]

Table 1. The yields of ***cis*-Cl**, ***trans*-PN**, and ***cis*-PN** with and without the shielding of light.

Species	with the shielding of light	without the shielding of light
***cis*-Cl**	41%	43%
***trans*-PN**	83%	82%
***cis*-PN**	82%	93%

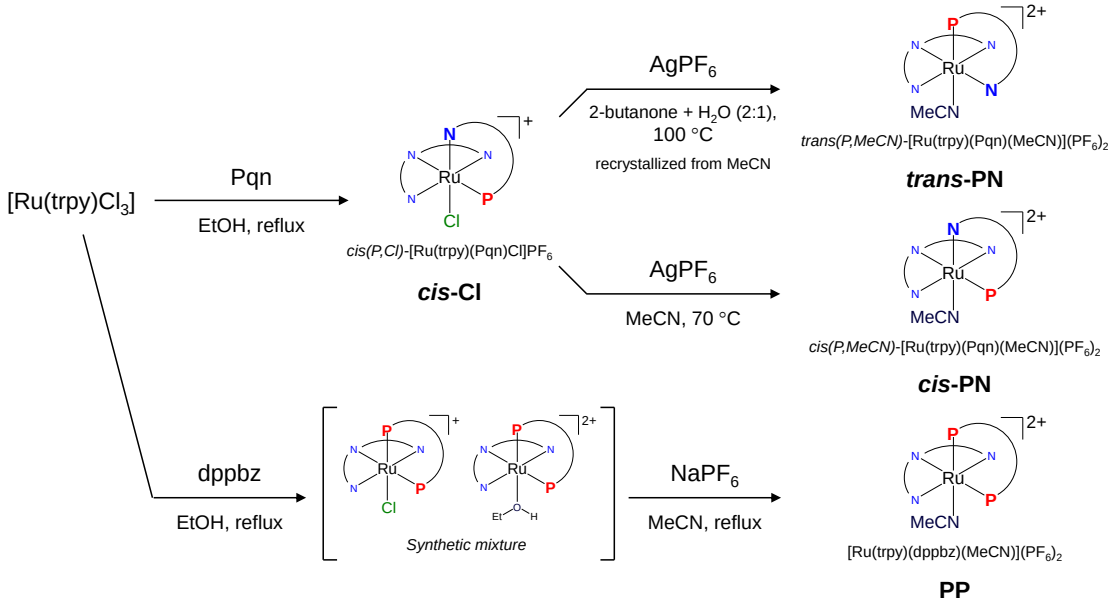

Scheme 3. Syntheses of ***cis*-Cl**, ***trans*-PN**, ***cis*-PN**, and **PP**

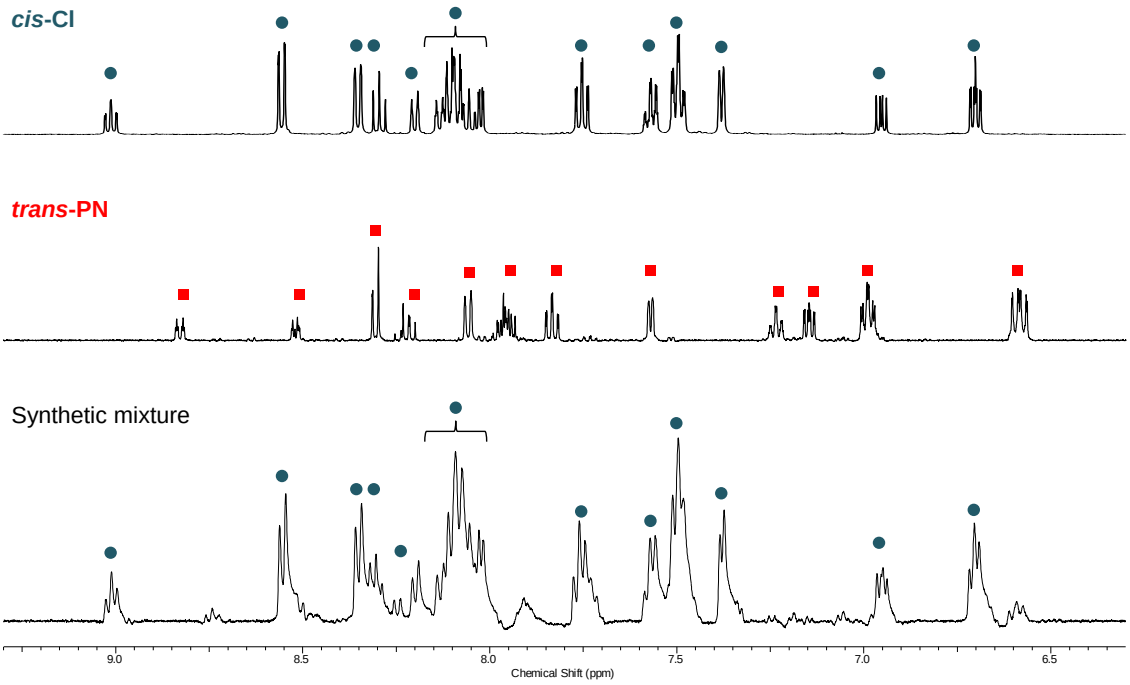

Figure 1. ^{1}H NMR spectra of ***cis*-Cl**, ***trans*-PN**, and the reaction mixture obtained after heating the solution of [Ru(trpy)Cl_3] and Pqn in the presence of ascorbic acid in CD_3CN at room temperature in aromatic region. ^{1}H NMR spectrum of the reaction mixture indicates that part of signals is attributed to ***cis*-Cl** but the remaining part of signals is attributed to unidentified compound.

Crystal Structures

The molecular structures of ***cis*-Cl'**, ***cis*-PN**, ***trans*-PN**, and **PP** were determined by single-crystal X-ray crystallography. The crystallographic data are shown in Table 2. The ***cis*-Cl'** crystallizes with two crystallographically independent ruthenium complexes, two BPh_4 anions, and one acetonitrile molecule as the crystal solvent in the asymmetric unit of the triclinic $P\bar{1}$ space group. No significant difference exists between the structures of the two independent ruthenium complexes. An ORTEP drawing of one of the cationic moieties of ***cis*-Cl'** is shown in Figure 2. Two chelate ligands, trpy and Pqn, coordinate to the metal ion in a perpendicular manner to form a distorted-octahedral geometry at the ruthenium atom, where the phosphorous donor of Pqn and the chloro ligand are located in *cis* positions of the octahedron. Bond distances between the ruthenium atom and middle nitrogen atom of trpy (Ru1−N2 and Ru2−N6) of ***cis*-Cl'** were 2.018(3) and 2.011(4) Å, respectively, and are significantly longer than that of the 2,2'-bipyridine analog (1.951(2) Å for [Ru(trpy)(bpy)Cl]PF_6). In contrast, the Ru−Cl distances (2.4049(11) and 2.4102(12) Å for Ru1−Cl1 and Ru2−Cl2, respectively) were similar to that of [Ru(trpy)(bpy)Cl]PF_6 (2.3969(7) Å).[31]

The asymmetric unit of the monoclinic $P2_1/c$ crystal of ***trans*-PN** contained one cationic ruthenium complex, two PF_6 anions, and one dichloromethane molecule. An ORTEP drawing of the cationic moiety is shown in Figure 4a and selected bond distances and angles are presented in Figure 3 and Table 3. Trpy and Pqn coordinate to the ruthenium center in a mutually perpendicular manner and create a distorted octahedral environment, where the phosphorous donor of Pqn and nitrogen atom of the acetonitrile ligand are located in *trans* position. Bond distance between the ruthenium atom and nitrogen atom of the acetonitrile ligand was 2.127(5) Å, which is longer than that found in **NN** (2.03(1) Å)[24] due to the stronger *trans* influence of the phosphorous atom of Pqn compared to that of the nitrogen atom of bpy.

The crystals of ***cis*-PN** showed a triclinic $P\bar{1}$ space group with one cationic ruthenium complex, two PF_6 anions, and one chloroform molecule as the asymmetric unit. The structure of the cationic moiety of ***cis*-PN** (Figure 4b was basically similar to that of ***cis*-Cl'**, except for coordination of an acetonitrile ligand instead of an anionic chloro ligand. Bond distance between the ruthenium atom and nitrogen atom of the acetonitrile ligand was 2.041(2) Å, which is much shorter than that of ***trans*-PN** (2.127(5) Å) but is similar to that of **NN** (2.03(1) Å). Bond distance between the ruthenium atom and middle nitrogen atom of trpy (Ru1−N2, 2.033(2) Å) in ***cis*-PN** was significantly longer than those of ***trans*-PN** (1.967(5) Å) and **NN** (1.953(8) Å) due to the *trans* influence of the phosphorous atom of Pqn. For the same reason, the average

value of the N-Ru-N bite angles of the [Ru(trpy)] moiety in ***cis*-PN** (77.9°) was much smaller than those in ***trans*-PN** (79.5°) and **NN** (79.9°).

PP crystallizes with one ruthenium complex, two PF_6 anions, and one dichloromethane molecule as the asymmetric unit in the orthorhombic *Pbca* space group. An ORTEP drawing of the cationic moiety is shown in Figure 4c, and selected bond distances and angles are shown in Table 3. Bond distance of Ru-N(acetonitrile) in **PP** was 2.110(3) Å, which is much longer than those in ***cis*-PN** and **NN**, and is close to that in ***trans*-PN**. The long Ru-N distance (Ru1−N2, 2.024(3) Å) and small N-Ru-N bite angles (av. 78.0°) of the [Ru(trpy)] moiety in **PP** were also affected significantly by the *trans* influence of the phosphorous atom of dppbz.

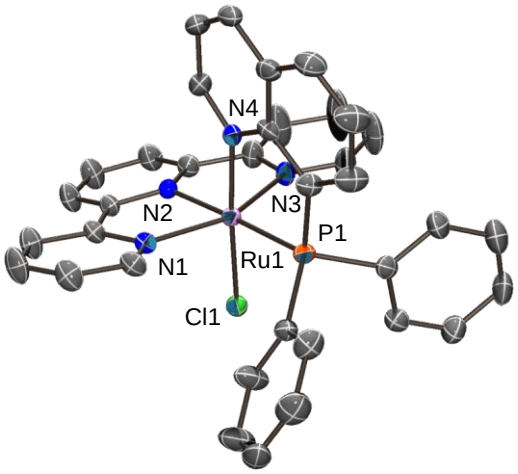

Figure 2. An ORTEP drawing (50% probability level) of one of the cationic complexes in ***cis*-Cl'**. Hydrogen atoms are omitted for clarity.

Table 2. Crystallographic Data for ***cis*-Cl'**, ***trans*-PN**, ***cis*-PN**, **PP**, ***trans*-PN^{DMF}**, ***trans*-PN^{H2O}**, and **trpyMeCN2Cl**.

Complex	***cis*-Cl'**·0.5CH_3CN	***trans*-PN**·CH_2Cl_2	***cis*-PN**·$CHCl_3$	**PP**·CH_2Cl_2
Formula	$C_{61}H_{48.5}BClN_{4.5}PRu$	$C_{39}H_{32}Cl_2F_{12}N_5P_3Ru$	$C_{39}H_{31}Cl_3F_{12}N_5P_3Ru$	$C_{48}H_{40}Cl_2F_{12}N_4P_4Ru$
Formula weight	1022.84	1063.58	1139.07	1196.69
T, ºC	−150	−150	−150	−150
Crystal color, habit	deep purple, needle	red, needle	orange, needle	yellow, platelet
Crystal system	triclinic	monoclinic	triclinic	orthorhombic
Crystal size, mm^3	0.40 × 0.10 × 0.05	0.30 × 0.10 × 0.03	0.45 × 0.18 × 0.11	0.30 × 0.15 × 0.05
Space group	$P\bar{1}$	$P2_1/c$	$P\bar{1}$	*Pbca*
a, Å	8.9568(17)	8.9011(15)	8.641(3)	13.2623(11)
b, Å	18.690(3)	12.595(2)	13.060(4)	22.7489(19)
c, Å	31.427(4)	38.632(7)	20.571(6)	32.187(3)
α, º	69.100(5)	90	92.619(2)	90
β, º	80.584(8)	90.336(3)	98.711(5)	90
γ, º	86.525(8)	90	102.589(6)	90
V, Å^3	4848.6(14)	4330.9(12)	2232.1(12)	9710.9(15)
Z	4	4	2	8
D calc, g cm^{-3}	1.401	1.631	1.634	1.637
μ, mm^{-1}	0.458	0.684	0.725	0.652
F (000)	2108	2128	1096	4816
$R_1{}^a$	0.0608	0.0620	0.0320	0.0554
w$R_2{}^b$	0.1721	0.1643	0.0980	0.1491
Goodness-of-fit S	1.059	1.139	1.078	1.086

Complex	***trans*-PN^{DMF}**·CH_2Cl_2	***trans*-PN^{H2O}**·$2Me_2CO$	**trpyMeCN2Cl**·CH_3CN
Formula	$C_{40}H_{36}Cl_2F_{12}N_5OP_3Ru$	$C_{42}H_{41}F_{12}N_4O_3P_3Ru$	$C_{21}H_{20}ClF_6N_6PRu$
Formula weight	1095.62	1071.77	637.92
T, ºC	−150	−150	−150
Crystal color, habit	red, needle	red, needle	violet, block
Crystal system	monoclinic	triclinic	monoclinic
Crystal size, mm^3	0.55 × 0.12 × 0.05	0.65 × 0.23 × 0.14	0.36 × 0.24 × 0.08
Space group	$P2_1/c$	$P\bar{1}$	$P2_1/c$
a, Å	8.8914(11)	8.963(2)	14.882(2)
b, Å	12.7270(16)	12.895(4)	11.7261(16)
c, Å	38.449(5)	19.927(6)	15.094(2)
α, º	90	102.043(4)	90
β, º	91.640(3)	90.214(4)	108.890(3)
γ, º	90	90.759(4)	90
V, Å^3	4349.1(9)	2252.2(11)	2492.2(6)
Z	4	2	4
D calc, g cm^{-3}	1.673	1.580	1.700
μ, mm^{-1}	0.686	0.548	0.868
F (000)	2200	1084	1272
$R_1{}^a$	0.0451	0.0435	0.0308
w$R_2{}^b$	0.1137	0.1251	0.0747
Goodness-of-fit S	1.047	1.075	1.065

[a] $R_1 = -\Sigma||Fo|-|Fc|| / \Sigma|Fo|$. [b] $wR_2 = [\Sigma(w(Fo^2-Fc^2)^2) / \Sigma w(Fo^2)^2]^{1/2}$

Table 3. Selected bond distances (Å) and angles (°) for ***cis*-Cl'**, ***trans*-PN**, ***cis*-PN**, **PP**, ***trans*-PN^{DMF}**, ***trans*-PN^{H2O}**, and **trpyMeCN2Cl**.

***cis*-Cl'**·0.5MeCN				***trans*-PN**·CH_2Cl_2		***cis*-PN**·$CHCl_3$	
Ru1–Cl1	2.4049(11)	Ru2–Cl2	2.4102(12)	Ru1–N1	2.081(5)	Ru1–N1	2.105(2)
Ru1–N1	2.097(4)	Ru2–N5	2.093(4)	Ru1–N2	1.967(5)	Ru1–N2	2.033(2)
Ru1–N2	2.018(3)	Ru2–N6	2.011(4)	Ru1–N3	2.077(5)	Ru1–N3	2.103(2)
Ru1–N3	2.094(4)	Ru2–N7	2.091(4)	Ru1–N4	2.119(5)	Ru1–N4	2.076(2)
Ru1–N4	2.060(4)	Ru2–N8	2.064(3)	Ru1–N5	2.127(5)	Ru1–N5	2.041(2)
Ru1–P1	2.2767(12)	Ru2–P2	2.2875(12)	Ru1–P1	2.2646(15)	Ru1–P1	2.2973(10)
N1–Ru1–N2	78.38(14)	N5–Ru2–N6	78.28(15)	N1–Ru1–N2	79.3(2)	N1–Ru1–N2	77.86(9)
N2–Ru1–N3	78.11(13)	N6–Ru2–N7	78.09(15)	N2–Ru1–N3	79.7(2)	N2–Ru1–N3	78.00(9)
N4–Ru1–P1	83.50(10)	N8–Ru2–P2	83.54(11)	N4–Ru1–P1	83.00(13)	N4–Ru1–P1	83.24(7)

PP·CH_2Cl_2		***trans*-PN^{DMF}**·CH_2Cl_2		***trans*-PN^{H2O}**·$2Me_2CO$		**trpyMeCN2Cl**·MeCN	
Ru1–N1	2.117(3)	Ru1–N1	2.075(3)	Ru–N1	2.070(3)	Ru1–Cl1	2.4111(6)
Ru1–N2	2.024(3)	Ru1–N2	1.959(3)	Ru–N2	1.963(3)	Ru1–N1	2.0628(17)
Ru1–N3	2.103(3)	Ru1–N3	2.080(3)	Ru–N3	2.082(3)	Ru1–N2	1.9527(17)
Ru1–N4	2.110(3)	Ru1–N4	2.107(3)	Ru–N4	2.108(3)	Ru1–N3	2.0716(17)
Ru1–P1	2.2860(9)	Ru1–O1	2.160(10)	Ru1–O1	2.187(2)	Ru1–N4	2.0583(18)
Ru1–P2	2.3077(9)	Ru1–P1	2.2418(11)	Ru1–P1	2.2348(10)	Ru1–N5	2.0095(19)
N1–Ru1–N2	77.56(11)	N1–Ru1–N2	79.67(14)	N1–Ru1–N2	79.91(11)	N1–Ru1–N2	80.18(7)
N2–Ru1–N3	78.48(11)	N2–Ru1–N3	79.79(14)	N2–Ru1–N3	79.47(11)	N2–Ru1–N3	79.97(7)
P1–Ru1–P2	83.85(3)	N4–Ru1–P1	83.23(10)	N4–Ru1–P1	83.42(8)	N4–Ru1–N5	87.73(7)

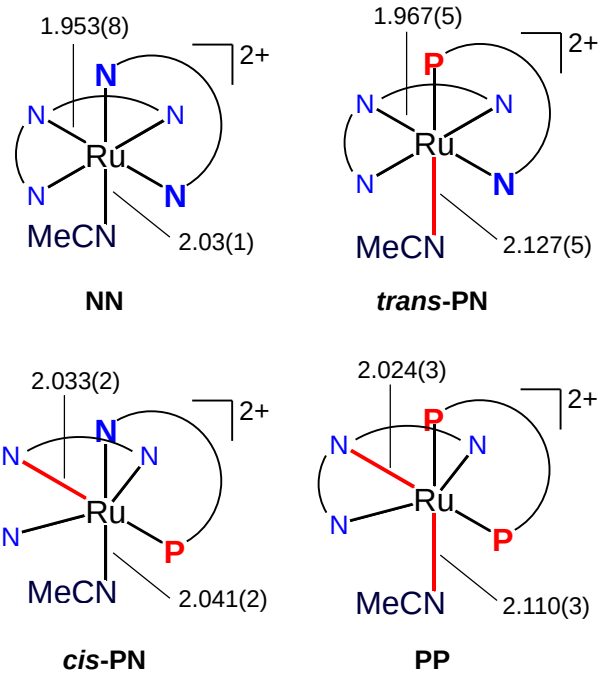

Figure 3. Comparison of bond distances (Å) around ruthenium centers of **NN**, ***trans*-PN**, ***cis*-PN**, and **PP**.

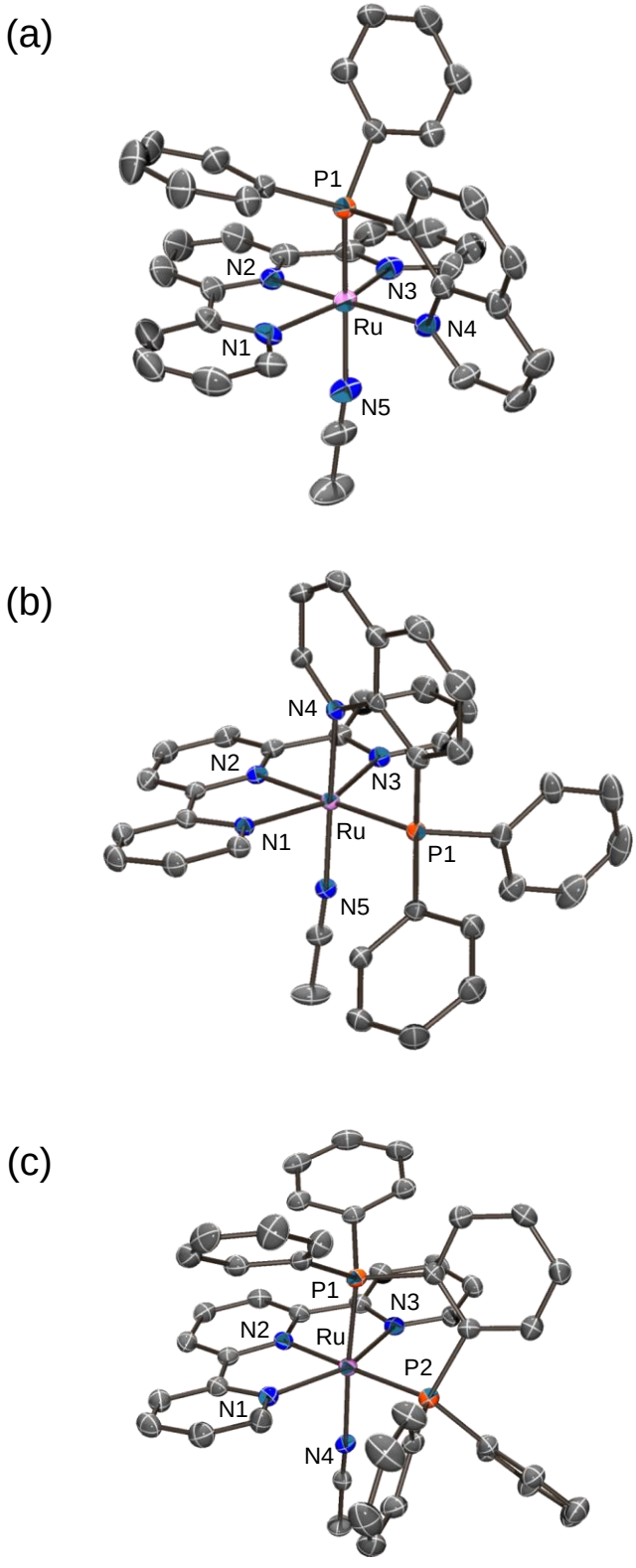

Figure 4. ORTEP drawings (50% probability level) of cataionic complexes in (a) ***trans*-PN**, (b) ***cis*-PN**, and (c) **PP**. Hydrogen atoms are omitted for clarity.

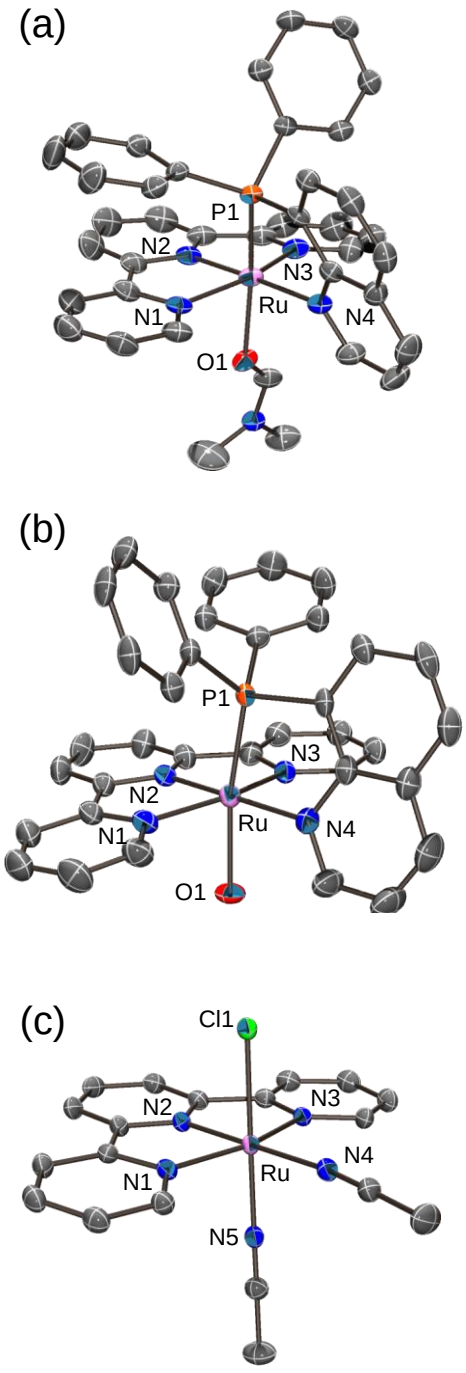

Figure 5. ORTEP drawings (50% probability level) of cataionic complexes in (a) ***trans*-PN^{DMF}**, (b) ***trans*-PN^{H2O}**, and (c) **trpyMeCN2Cl**. Hydrogen atoms are omitted for clarity.

UV-Vis Absorption Spectra.

Figure 6 shows the UV-Vis absorption spectra of a series of [Ru(trpy)(BL)(MeCN)]$(PF_6)_2$ (**NN**, ***trans*-PN**, ***cis*-PN**, and **PP**), where BL is a bidentate ligand such as bpy, Pqn, or dppbz. Spectral data for these four complexes and related compounds[29] are listed in Table 4. All of the complexes display intense absorption bands in the UV region, assigned to ligand-based π–π* transitions. Additionally, a moderately intense band in the visible region for each complex is assigned to the metal-to-ligand charge transfer (MLCT) transition from the dπ orbitals of ruthenium to the π* orbitals of trpy and BL. The absorption maxima (λ_{max}) of the MLCT transition of ***trans*-PN**, ***cis*-PN**, and **PP** were blue-shifted compared with that of **NN**. The degree of the blue shifts ($\Delta\lambda_{complex}$(MLCT) = $\lambda_{max,\mathbf{NN}}$(MLCT) − $\lambda_{max,complex}$(MLCT)) were 18 nm for ***trans*-PN**, 41 nm for ***cis*-PN**, and 66 nm for **PP**. The similar blue shift of MLCT band was also observed in a series of $[Ru(bpy)_2(BL)]^{2+}$ (Table 4),[29] which attributes to the stabilization of the dπ orbitals of the ruthenium center upon introduction of the phosphine donors. Note that the MLCT transition energy of ***cis*-PN** experienced a larger shift than that of ***trans*-PN** despite the isomeric relationship between ***trans*-PN** and ***cis*-PN**, suggesting that the position of phosphorus atom affects the electronic structure of the complexes (For detailed explanation of phosphorus atom affects, please see Phosphine as σ-donor and π-acceptor section in the Discussion part). The molar absorption coefficient of **PP** was nearly one-half that of **NN**, ***trans*-PN**, and ***cis*-PN**.

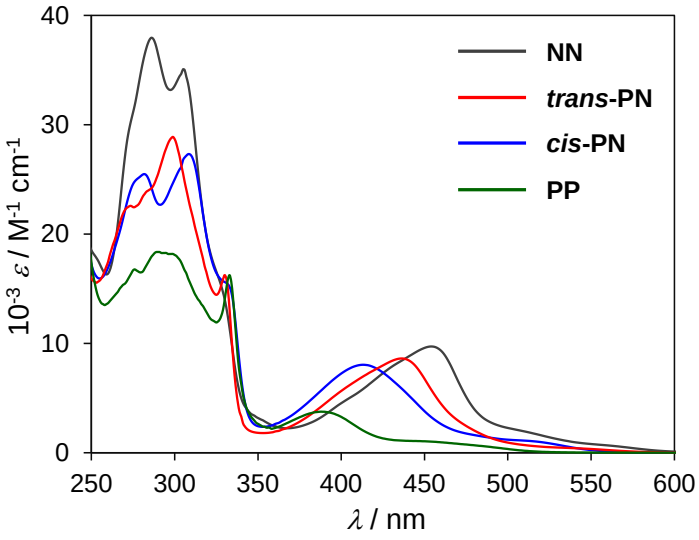

Figure 6. UV-Vis absorption spectra of **NN**, ***trans*-PN**, ***cis*-PN**, and **PP** in acetonitrile at room temperature.

Table 4. UV-Vis absorption data (λ_{max}/nm (10^{-3} ε/M^{-1} cm^{-1})) and redox potentials ($E_{1/2}$/V vs Fc/Fc^{+}) for **NN**, ***trans*-PN**, ***cis*-PN**, **PP**, and related compounds in acetonitrile at room temperature.

	λ_{max}		reduction			oxidation	
complex	MLCT	π–π* transition	$E_{1/2}(1)$	$E_{1/2}(2)$	$E_{1/2}(3)$	$E_{1/2}(Ru^{II/III})$	reference
NN	454 (7.65)	325 (16.6), 305 (27.2), 286 (37.9), 273 (29.8)	–1.65	–1.95		+0.92	23
***trans*-PN**	435 (7.72)	330 (16.2), 299 (28.9), 279 (24.0)[a], 274 (22.6)	–1.70[b]	–1.77[b]	–2.13	+0.97	this work
***cis*-PN**	412 (7.52)	334 (14.6), 310 (26.1), 282 (24.7), 275 (24.7)	[c]	[c]	[c]	+1.05	this work
PP	388 (3.97)	333 (16.2), 301 (18.0)[a], 290 (18.4), 276 (16.8)	–1.50[b]	–1.46[b]	–2.49	+1.27	this work
$[Ru(bpy)_3](PF_6)_2$	452 (13.2), 410 (7.48)[a]	287 (77.2)	–1.86	–2.02		+0.75	29
$[Ru(bpy)_2(Pqn)](PF_6)_2$	418 (10.0)	285 (47.0)	–1.80	–2.03		+0.91	29
$[Ru(bpy)_2(dppbz)](PF_6)_2$	377 (8.09)	319 (15.6)[a], 278 (34.9)	–1.82	–2.07		+1.18	29
$[Ru(trpy)_2](PF_6)_2$	475 (14.7)	308 (63.4), 270 (38.8)	–1.66	–1.90		+0.89	31

[a]Absorption shoulder. [b]Simulated values. See also Table 5. These two redox couples of **PP** at −1.50 and −1.46 V were observed as a single wave with $E_{1/2}$ of −1.47 V. [c]***cis*-PN** underwent a isomerization to ***trans*-PN** upon reduction.

Electrochemistry.

The cyclic voltammograms (CVs) of **NN**, ***trans*-PN**, ***cis*-PN**, and **PP** are shown in Figure 7. Electrochemical data of these complexes and related compounds are listed in Table 4. The CVs were measured in 0.1 M tetraethylammonium perchlorate (TEAP) / acetonitrile, respectively. All complexes displayed one reversible oxidation wave, which is assigned to a Ru(III)/Ru(II) redox couple. The half wave potentials ($E_{1/2}$) of **NN**, ***trans*-PN**, ***cis*-PN**, and **PP** were 0.92, 0.97, 1.05, and 1.27 V vs ferrocene/ferrocenium (Fc/Fc^+), respectively. The positive shift on introduction of the phosphine donors is due to the stabilizationof the dπ orbitals of the ruthenium center (For details, see Phosphine as σ-donor and π-acceptor section in the Discussion part). This tendency was also observed in the series of $[Ru(bpy)_2(BL)]^{2+}$ (Table 4).[29] Note that the oxidation potential of ***cis*-PN** was more positive than that of ***trans*-PN**.

CVs in the negative potential region are shown in Figure 7b. Each complex exhibited distinct electrochemical behavior unlike those in the positive potential region. The effect of light shielding on CVs is negligible (Figure 8). The CV of ***trans*-PN** showed two redox waves at $E_{1/2}$ = −1.73 and −2.13 V. The results of square wave voltammetry (SWV, Figure 9), the CV simulation (Figure 10) of the wave at $E_{1/2}$ = −1.73 V, and controlled potential electrolysis (CPE, Figure 11) indicates that two one-electron processes with similar redox potential ($E^{\circ'}_1$(***trans*-PN**) = −1.70 V and $E^{\circ'}_2$(***trans*-PN**) = −1.77 V, Table 5) exists in this region. The first reduction potentials ($E_{1/2}$(1)) of **NN** (−1.65 V) and ***trans*-PN** (−1.70 V) are assigned to reduction of the trpy ligand.[32]

The CV of ***cis*-PN** at a scan rate of 100 mV/s showed an irreversible reduction peak at E_{pc} = −1.56 V, followed by two reversible redox waves at $E_{1/2}$ = −1.73 and −2.13 V. The two reversible redox waves of ***cis*-PN** are very similar to those of ***trans*-PN** (Figure 12a), which implies that irreversible and rapid isomerization of ***cis*-PN** to ***trans*-PN** occurred on the electrode surface along with reduction of ***cis*-PN** (For detailed mechanism of electrochemically induced isomerization behavior of the complex, see Mechanism of Isomerization and Electrochemical Behavior section).

To further investigate the *cis-trans* transformation, potentials were swept in a positive or negative direction from the open circuit potential (−0.19 V) at a scan rate of 1.0 V/s in a ***cis*-PN** solution (Figure 12b). The positive-direction sweeping showed an oxidation wave at $E_{1/2}$ = 1.05 V, which is assigned to a Ru(II)/Ru(III) redox couple of ***cis*-PN**. In contrast, the negative-direction sweeping showed the $E_{1/2}$ value matched to that of ***trans*-PN** ($E_{1/2}$ = 0.97 V). Figure 13 shows CVs of ***cis*-PN** at a scan rate of 1.0 V/s, for which the negative edges of potential sweeping were changed between −1.5 V

and −2.0 V at an interval of 0.1 V. Results clearly indicate that ***cis*-PN** is converted to ***trans*-PN** upon the electrochemical reduction reaction, and that the *cis-trans* conversion occurs after the first irreversible reduction around −1.6 V. The first irreversible reduction peak of ***cis*-PN** (−1.6 V) is probably due to electron insertion into the π* orbital of trpy ligand. The electrochemical behavior of ***cis*-PN** and ***trans*-PN** is summarized in Scheme 4.

For **PP**, the first reduction wave was observed at $E_{1/2}$ = −1.47 V with a peak potential separation ΔE_p of 41 mV (where $\Delta E_p = E_{pa} - E_{pc}$). The $E_{1/2}$ value was relatively positive compared to those of the analogs **NN** (−1.65 V), ***trans*-PN** (−1.73 V), and $[Ru(bpy)_2(dppbz)](PF_6)_2$ (−1.82 V).[29] The number of electrons transferred in the first reduction wave of **PP** was determined to be 2.13 by CPE (Figure 11). The results of CV simulation gave two redox potentials of $E^{\circ\prime}_1$(**PP**) = −1.50 V and $E^{\circ\prime}_2$(**PP**) = −1.46 V vs Fc/Fc^+, indicating the potential inversion of two redox processes (Figure 10 and Table 5). These results indicate that the first reduction step of **PP** is a two-electron transfer process with potential inversion. Subsequent reduction was observed in much lower negative potential region (−2.49 V).

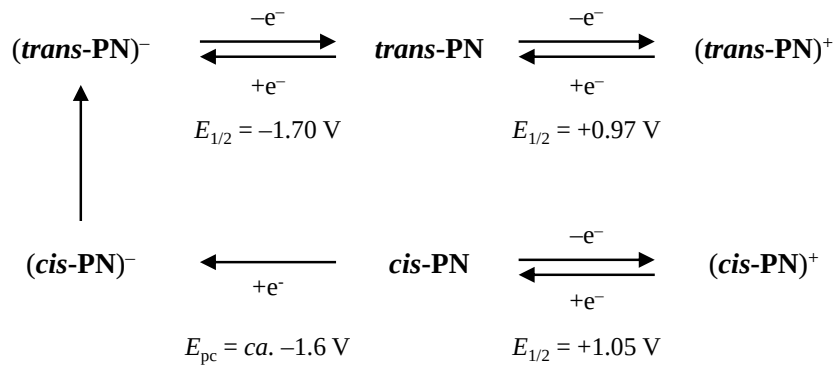

Scheme 4. Electrochemical behavior of ***trans*-PN** and ***cis*-PN**.

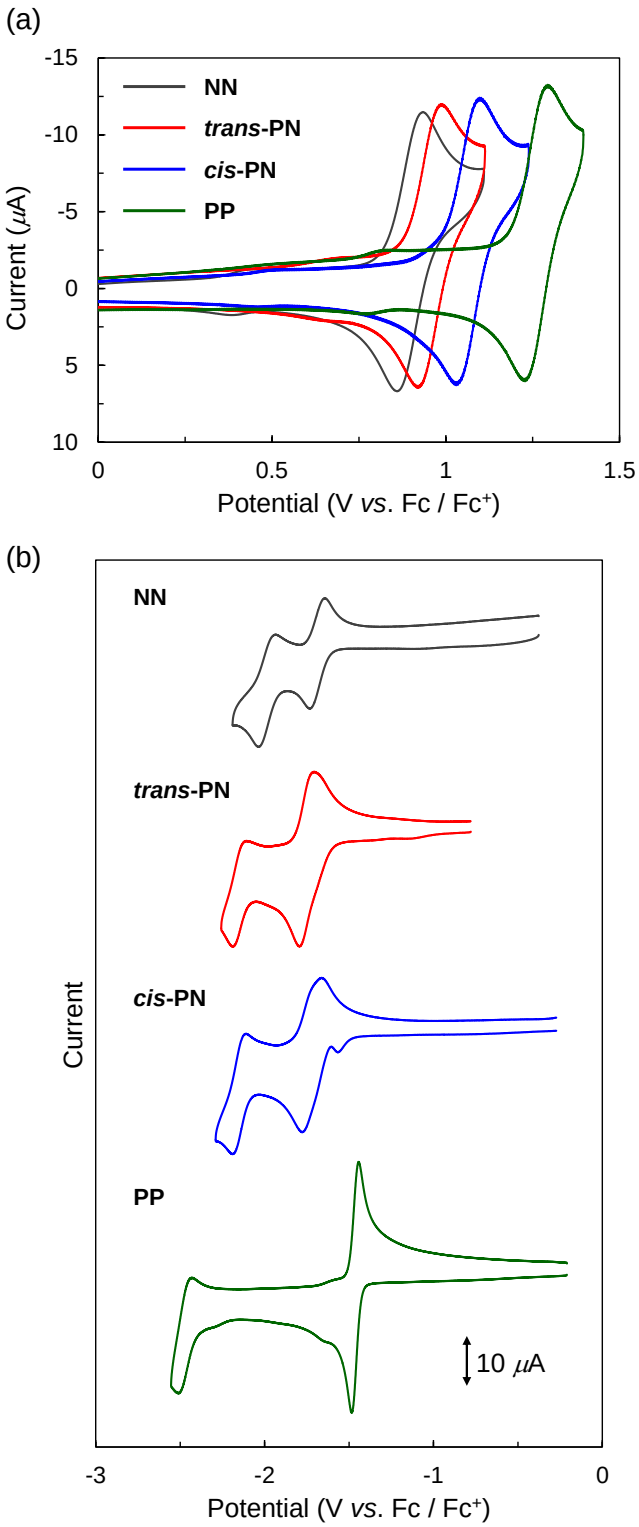

Figure 7. Cyclic voltammograms of **NN**, ***trans*-PN**, ***cis*-PN**, and **PP** (0.5 mM) in 0.1 M TEAP/acetonitrile under an Ar atmosphere scanned in the (a) positive and (b) negative region (WE: GC, CE: Pt wire, RE: Ag/Ag^{+}; Scan rate: 100 mV/s).

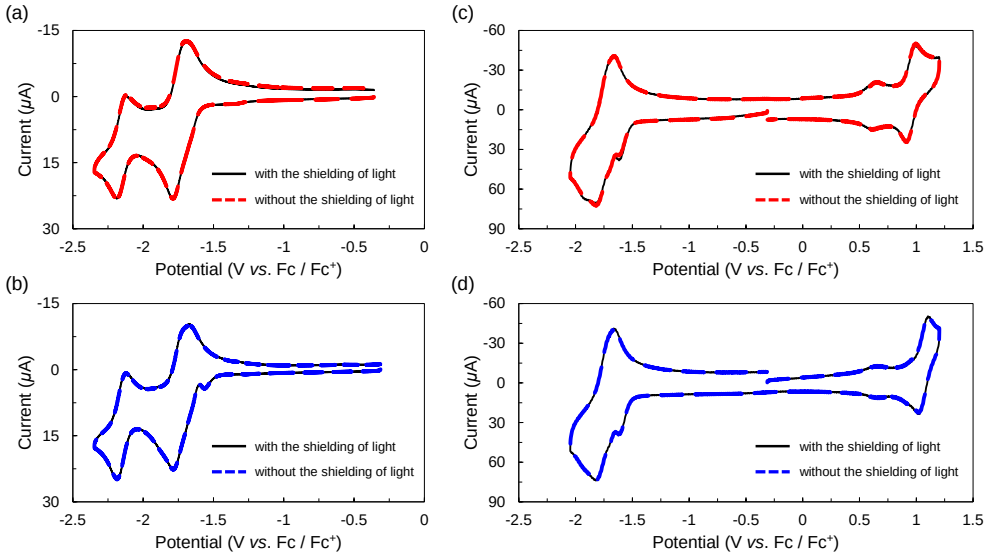

Figure 8. Comparison of CVs between with (solid lines) and without (dashed lines) the shielding of light. CVs of 0.5 mM (a) ***trans*-PN** and (b) ***cis*-PN** in 0.1 M TEAP/acetonitrile solution scanned in positive at a scan rate of 0.10 V/s. CVs of 0.5 mM ***cis*-PN** in 0.1 M TEAP/acetonitrile solution scanned from (c) positive and (d) negative region at a scan rate of 1.0 V/s. The results show that the effect of the shielding of light is negligible in these experimental conditions.

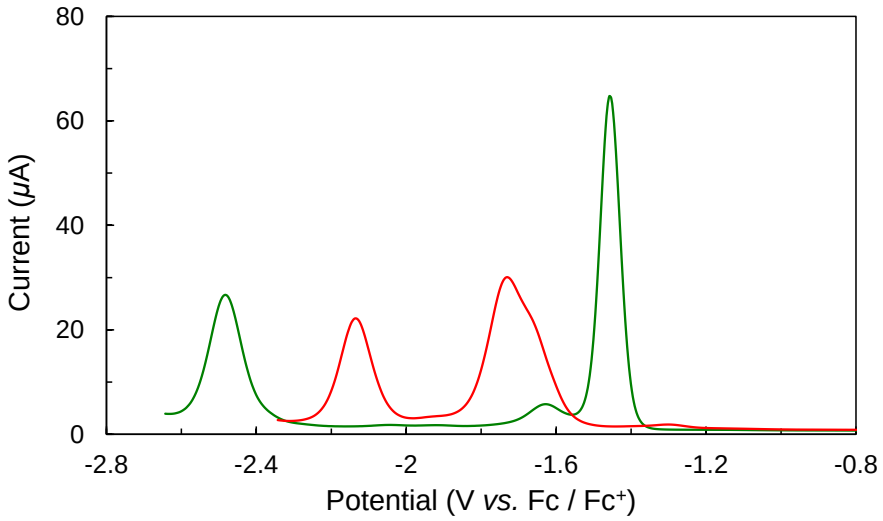

Figure 9. Square Wave Voltammograms (SWV) of ***trans*-PN** (red-line) and **PP** (green-line) in acetonitrile ([complex] = 0.6 mM; 0.1 M TEAP). SWVs were recorded on a BAS ALS Model 650DKMP electrochemical analyzer. (WE: GC, CE: Pt wire, RE: Ag/Ag^{+}; amplitude: 25 mV, frequency 10 Hz, step 5 mV).

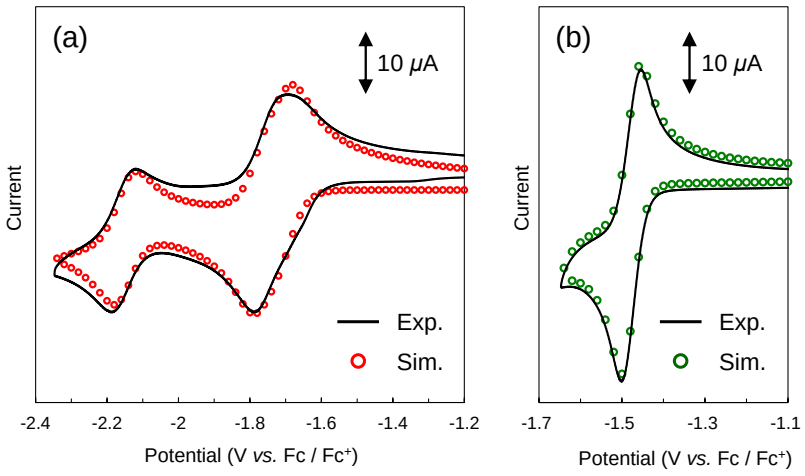

Figure 10. Simulated voltammograms of (a) ***trans*-PN** and (b) **PP** in acetonitrile (dotted lines, [complex] = 0.6 mM; 0.1 M TEAP) under an Ar atmosphere scanned at room temperature and their cyclic voltammograms (solid lines, WE: GC, CE: Pt wire, RE: Ag/Ag^{+};). Elchsoft DigiElch 7.FD software was used for simulation of cyclic voltammograms to obtain redox potentials of ***trans*-PN** and **PP**.

Table 5. Simulation parameters for the cyclic voltammograms. Elchsoft DigiElch 7.0. software was used for simulation.

	***trans* -PN**	**PP**
Sweep rate [v] (V)	0.10	0.10
Resistance [R] (Ω)	2.0×10^{2}	2.0×10^{2}
Capacitance [CdI] (F)	1.0×10^{-6}	1.0×10^{-6}
Temperature [T] (K)	293.2	293.2
Surface area [A] (cm^{2})	7.069×10^{-2}	7.069×10^{-2}
Diffusion constant [D] ($cm^{2}\cdot s^{-1}$)	1.0×10^{-5}	1.0×10^{-5}
Concentration [c] ($mol\cdot dm^{-3}$)	6.2×10^{-4}	6.3×10^{-4}
$E°'_1$ (V)	–1.70	–1.50
k_{s1} ($cm\cdot s^{-1}$)	1.0×10^{4}	1.0×10^{4}
α_1	0.50	0.50
$E°'_2$ (V)	–1.77	–1.46
k_{s2} ($cm\cdot s^{-1}$)	1.0×10^{4}	1.0×10^{4}
α_2	0.50	0.50
$E°'_3$ (V)	–2.15	–
k_{s3} ($cm\cdot s^{-1}$)	1.0×10^{4}	–
α_3	0.50	–
$\Delta E°'$ (V)	+0.07	–0.04

[a] $E°'_1$, $E°'_2$, and $E°'_3$ are referred to Fc/Fc^{+}. [b] $\Delta E°' = (E°'_2 - E°'_1)$.

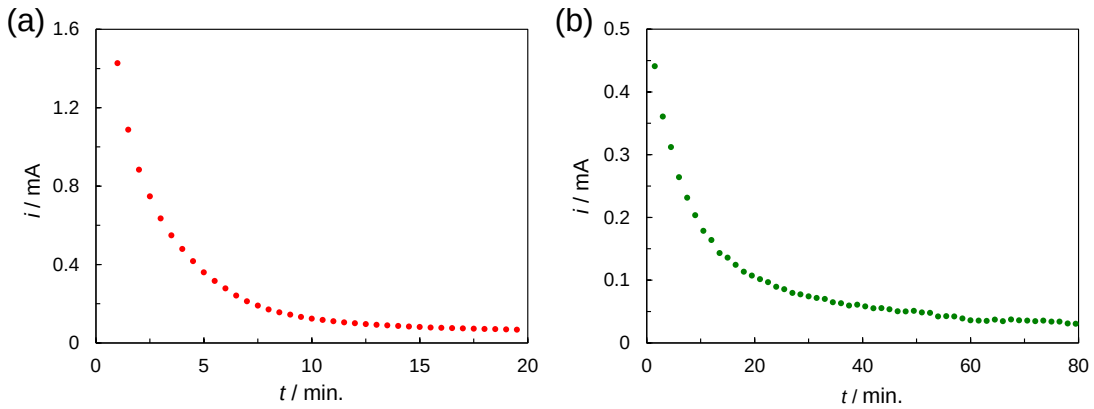

Figure 11. Controlled potential electrolysis (CPE) data (*i*-*t* plot) of (a) ***trans*-PN** and (b) **PP**. The potentials were kept at –1.84 V (*vs.* Fc/Fc^+) for ***trans*-PN** and –1.72 V for **PP**. Coulometry was carried out in a two compartment cell separated by an anion-exchange membrane. The working electrode was a 1.0 cm × 3.5 cm piece of glassy carbon. Typically, the electrode was partially immersed (surface area immersed area was 1.0 × 1.5 cm^2) in the solution. 4.0 mL (***trans*-PN**) or 6.0 mL (**PP**) of the electrolyte solution in acetonitrile solvent ([complex] = 0.5 mM; 0.1 M TEAP) degassed with vacuum/Ar cycles was electrolyzed with stirring. The counter and reference electrodes were platinum-wire and Ag/Ag^+, respectively.

The number of electrons transferred during the reduction was determined by using Eq. 1 shown below.

$$Q(\infty) = nFVC(0) \quad \text{(Eq. 1)}$$

$Q(\infty)$: total electric charge, n: the number of electrons transferred in the reduction, F: faraday constant, V: volume of solution for electrolysis, $C(0)$: initial concentration.

The estimated number of electrons is as follows.

$$n(\textbf{\textit{trans}-PN}) = 2.09,\ n(\textbf{PP}) = 2.13$$

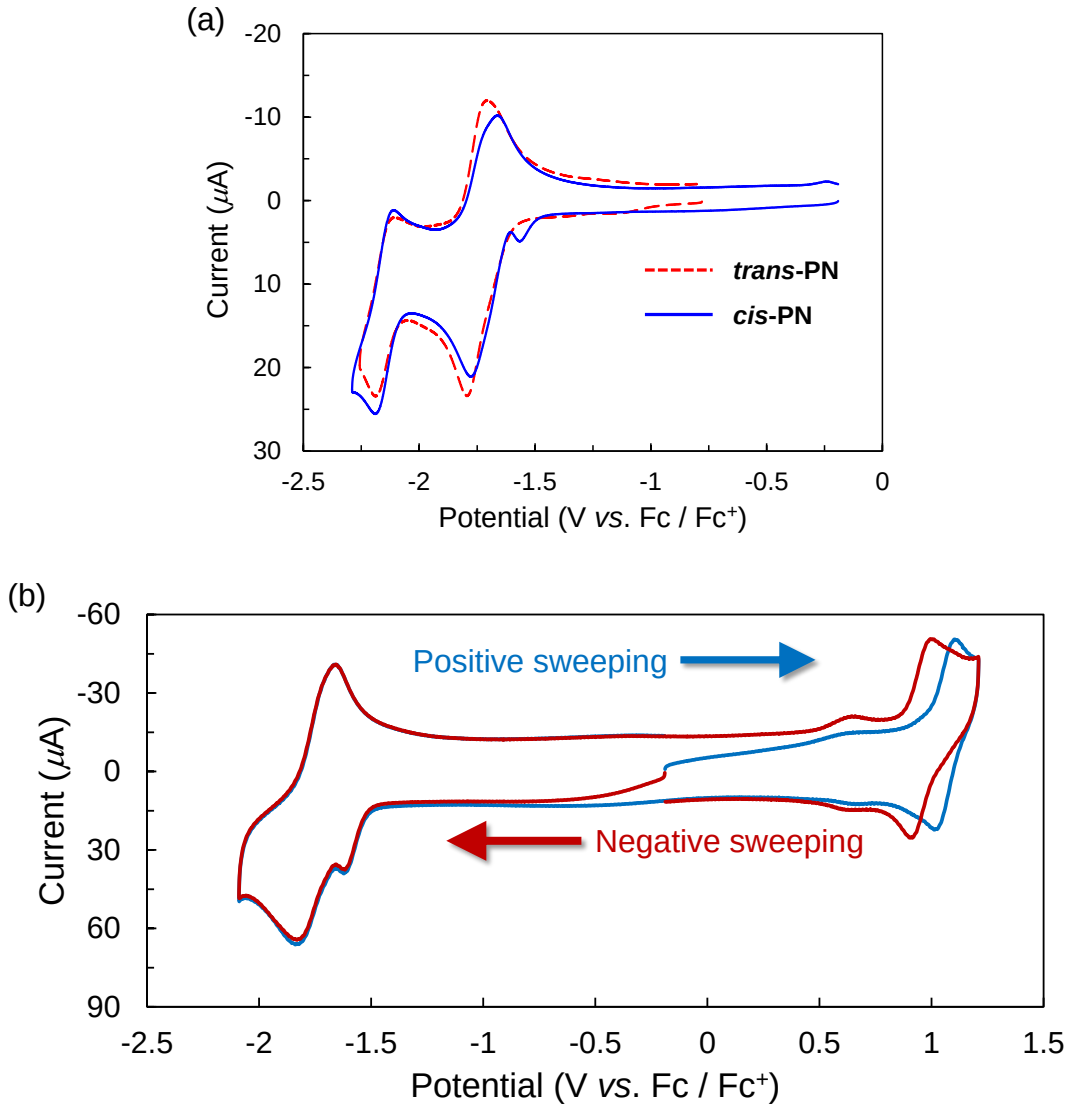

Figure 12. (a) Cyclic voltammograms of ***trans*-PN** and ***cis*-PN** (0.5 mM) in 0.1 M TEAP/acetonitrile solution scanned in positive at a scan rate of 0.10 V/s. (b) Cyclic voltammograms of ***cis*-PN** (0.5 mM) in 0.1 M TEAP/acetonitrile solution scanned in positive and negative at a scan rate of 1.0 V/s.

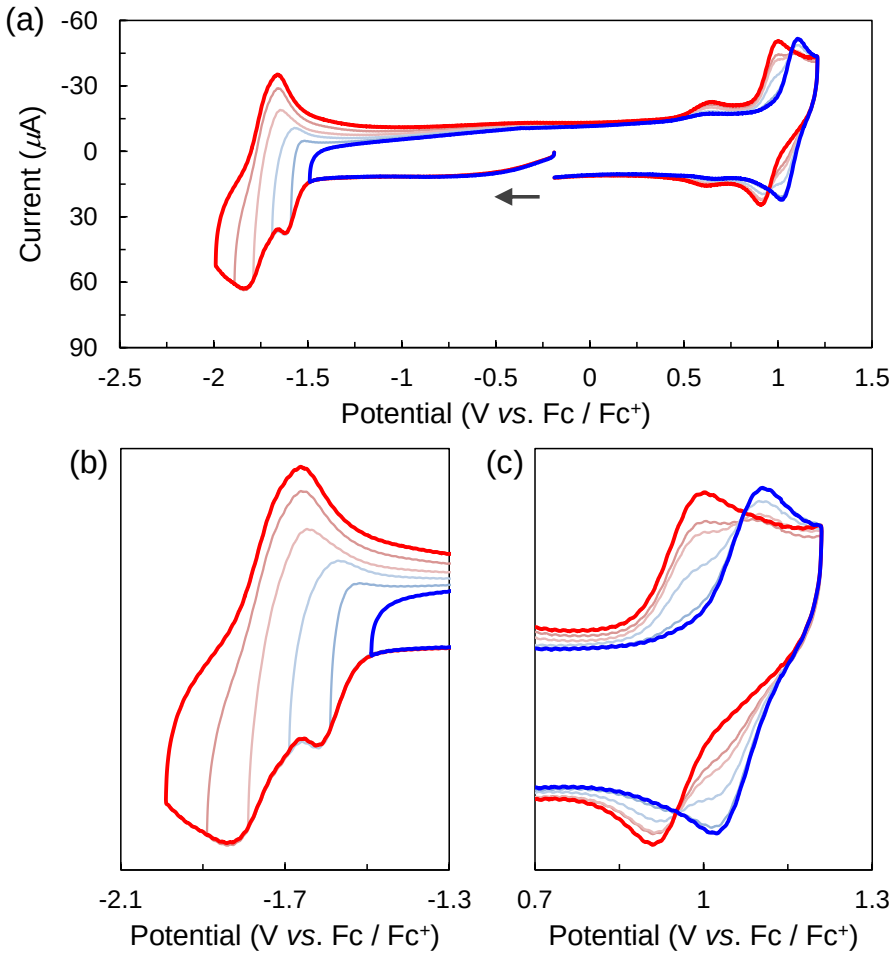

Figure 13. Cyclic voltammograms of ***cis*-PN** (0.5 mM) in 0.1 M TEAP/acetonitrile under an Ar atmosphere (WE: GC, CE: Pt wire, RE: Ag/Ag^+; Scan rate: 1.0 V/s). Negative edges of potential sweeping were switched between −1.5 V (blue) and −2.0 V (red) at an interval of 0.1 V. Potential sweeps were started from the open circuit potential (−0.19 V). (a) Full scale view. (b) Magnified view in the range of −2.1 V to −1.3 V. (c) Magnified view in the range of 0.7 V to 1.3 V.

DFT Calculations.

To discuss the electronic structures of ***trans*-PN**, ***cis*-PN**, and **PP**, density functional theory (DFT) calculations were conducted using the Gaussian 09 programs with the B3LYP functional and LanL2DZ basis set. All calculations were performed with the polarizable continuum model (PCM)[37] to account for solvent effects in acetonitrile. All optimized structures were shown in Figure 14.

The highest occupied molecular orbitals (HOMOs, HOMO to HOMO−2) and the lowest unoccupied molecular orbitals (LUMOs, LUMO to LUMO+2) are illustrated in Figure 15. The HOMOs of ***trans*-PN** and ***cis*-PN** contain dπ (d_{xy}, d_{yz}, and d_{zx}) characteristics of ruthenium with distribution to the π* orbitals of trpy, Pqn, and acetonitrile ligands and σ* orbitals of P−C bonds in the phosphine donors. The LUMOs are dominated mainly by π* orbitals of trpy or Pqn. The frontier orbitals of **PP** are similar to those of ***trans*-PN** and ***cis*-PN**, except that the π* orbitals of dppbz are not involved in orbitals from HOMO−2 to LUMO+2. The HOMO energy levels of ***trans*-PN**, ***cis*-PN**, and **PP** were −6.24, −6.30, and −6.53 eV (Figure 16), respectively, indicating a tendency similar to that observed in the oxidation potentials in cyclic voltammograms (0.97, 1.05, and 1.27 V vs Fc/Fc^+, see Table 4), as discussed above.

Electronic transitions for the complexes were investigated using the time-dependent density functional theory (TD-DFT) method.[38] Calculated excitation wavelengths and oscillator strengths for selected transitions are listed in Table 6, and absorption spectra based on these calculated transitions with Gaussian functions are depicted in Figure 17. The profiles of convoluted absorption spectra are similar to those observed experimentally. For ***trans*-PN** and ***cis*-PN**, transitions in the visible light region arise mainly from the MLCT transition from the dπ orbitals of ruthenium (HOMOs) to the π* orbitals of trpy (LUMO and LUMO+1) and Pqn (LUMO+2). For **PP**, the transitions arise mainly from dπ orbitals of ruthenium (HOMOs) to π* orbitals of trpy (LUMO and LUMO+1), which do not involve the π* orbitals of dppbz. Intensity of the simulated absorption of **PP** was nearly 50% of those of ***trans*-PN** and ***cis*-PN**, which is consistent with the experimental results (Figure 6).

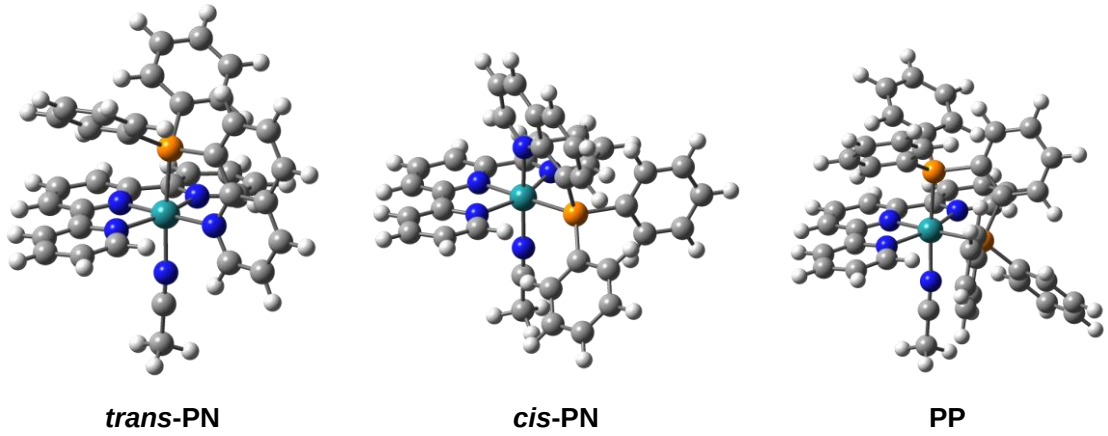

Figure 14. Optimized structures of cationic moieties of ***trans*-PN**, ***cis*-PN**, and **PP**.

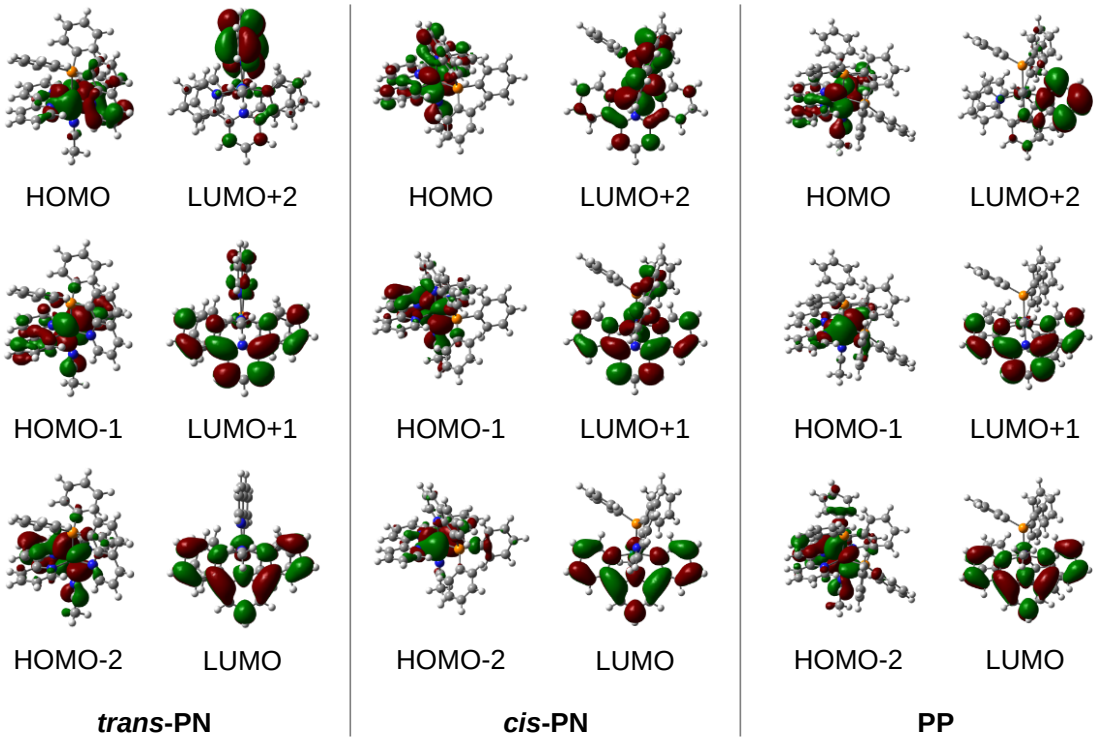

Figure 15. Isodensity surface plots of selected frontier molecular orbitals of ***trans*-PN**, ***cis*-PN**, and **PP** based on the optimized ground-state geometry.

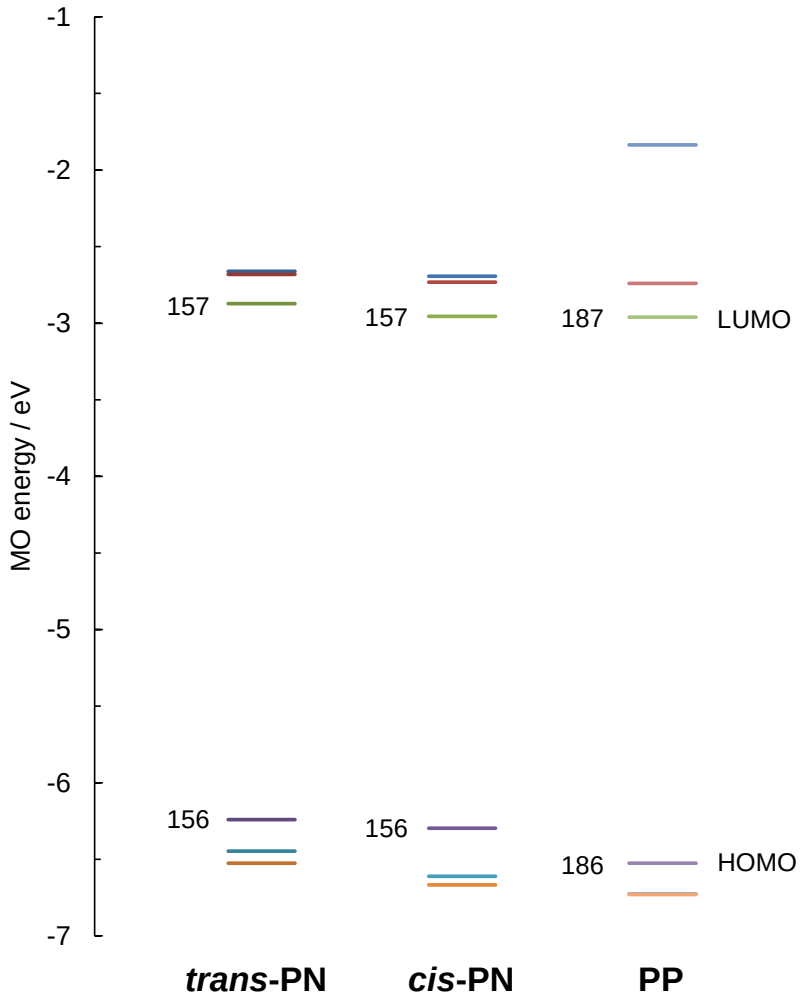

Figure 16. Diagram of DFT-derived molecular orbital energies of ***trans*-PN**, ***cis*-PN**, and **PP**.

Complex	λ / nm	f	Transition			|CI coef| (> 0.25)
***trans*-PN**	432.70	0.0622	HOMO–2	→	LUMO	0.56714
			HOMO–1	→	LUMO+1	0.26813
			HOMO	→	LUMO+2	0.30506
	422.02	0.0839	HOMO–1	→	LUMO+1	0.29811
			HOMO	→	LUMO+2	0.57823
	404.69	0.0293	HOMO–2	→	LUMO+1	0.67754
***cis*-PN**	422.24	0.0916	HOMO	→	LUMO+2	0.67258
	405.84	0.0628	HOMO–1	→	LUMO	0.43370
			HOMO	→	LUMO+1	0.43810
	401.78	0.0262	HOMO–1	→	LUMO+1	0.67054
PP	398.01	0.0355	HOMO–2	→	LUMO	0.35846
			HOMO–1	→	LUMO+1	0.42195
			HOMO	→	LUMO+1	0.41949
	385.95	0.0262	HOMO–2	→	LUMO+1	0.57866
			HOMO–1	→	LUMO+1	0.32709
	382.86	0.0477	HOMO–2	→	LUMO+1	0.38021
			HOMO–1	→	LUMO+1	0.44940
			HOMO	→	LUMO+1	0.28421

Table 6. Calculated TD-DFT excitation energies of ***trans*-PN**, ***cis*-PN**, and **PP** in acetonitrile media. *f* denotes the oscillator strength calculated for each transition.

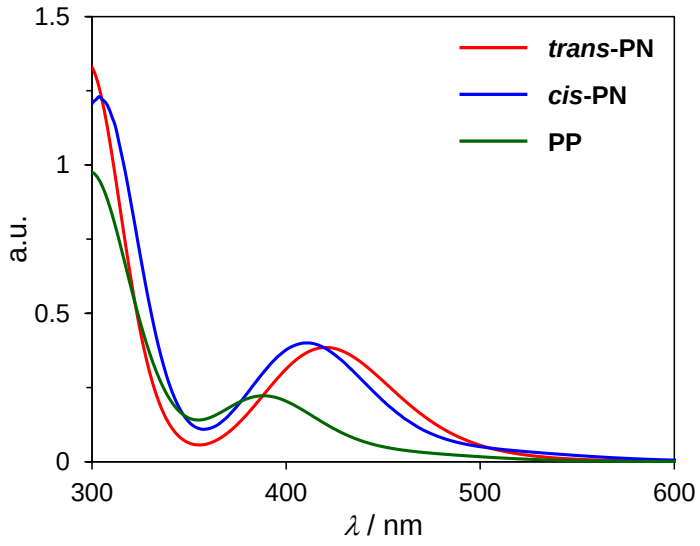

Figure 17. Simulated absorption spectra of ***trans*-PN**, ***cis*-PN**, and **PP** in acetonitrile based on TD-DFT calculations.

Solvent-induced Isomerization.

Isomerization of ***cis*-PN** to ***trans*-PN** does not occur in acetonitrile, even upon heating to temperatures near the boiling point (75 °C) for 24 hours (Figure 18). In contrast, the isomerization proceeded upon moderate heating in *N*,*N*-dimethylformamide (DMF).

The time course of spectral changes of ***cis*-PN** in DMF heated at 110 °C are shown in Figure 21. Note that the dissociation of the acetonitrile ligand was not observed for ***cis*-PN** in DMF (Figures 18 and 19) at room temperature and the spectrum at 0 min was consistent with that of ***cis*-PN** at room temperature. The anchored isosbestic points at λ = 314 and 432 nm indicate that only two species were involved without the formation of side products or intermediates. Based on comparisons with the absorption spectrum of ***trans*-PN** in DMF (Figure 19), the product of this isomerization reaction was identified as the DMF-coordinated *trans*-isomer, *trans(P,DMF)*-[Ru(trpy)(Pqn)(DMF)]$(PF_6)_2$ (***trans*-PN^{DMF}**, λ_{max} for MLCT transition = 462 nm). Therefore the spectral change observed at 110 °C is attributed to the transformation from ***cis*-PN** to ***trans*-PN^{DMF}**.

Reaction kinetics of the transformation was investigated using UV-Vis spectroscopy in DMF at 70, 80, 90, 100, and 110 °C. The spectral changes were analyzed using the singular value decomposition (SVD) method. The SVD-based spectral analysis in SPECFIT[39] confirms that the isomerization is first-order at 70-110 °C with rate constants of k = 2.10(11)×10^{-5}, 7.5(4)×10^{-5}, 2.36(15)×10^{-4}, 6.05(14)×10^{-4}, and 1.52(5)×10^{-3} s^{-1}, respectively. The thermodynamic parameters for the conversion of ***cis*-PN** to ***trans*-PN^{DMF}** were calculated using the Eyring equation.[40] The Eyring plot shown in Figure 22 affords an entropy of activation ($\Delta S^{\ddagger}$) of 111(8) J·mol^{-1}·K^{-1} and an enthalpy of activation ($\Delta H^{\ddagger}$) of 120(3) kJ·mol^{-1}. The large positive value of $\Delta S^{\ddagger}$ indicates a dissociative mechanism of this transformation.[40] The $\Delta H^{\ddagger}$ value (120(3) kJ·mol^{-1}) appears to correspond to the dissociative energy of the Ru−N(MeCN) bond.[41] Therefore, the dissociation of an acetonitrile ligand is the isomerization rate-determining step, followed by the coordination of a DMF molecule to give ***trans*-PN^{DMF}**. The half-life for the transformation from ***cis*-PN** to ***trans*-PN^{DMF}** in DMF is estimated to be longer than a year at room temperature ($\tau \approx$ 400 days at 20 °C), consistent with the fact that the acetonitrile ligand of ***cis*-PN** barely dissociates in DMF at room temperature.

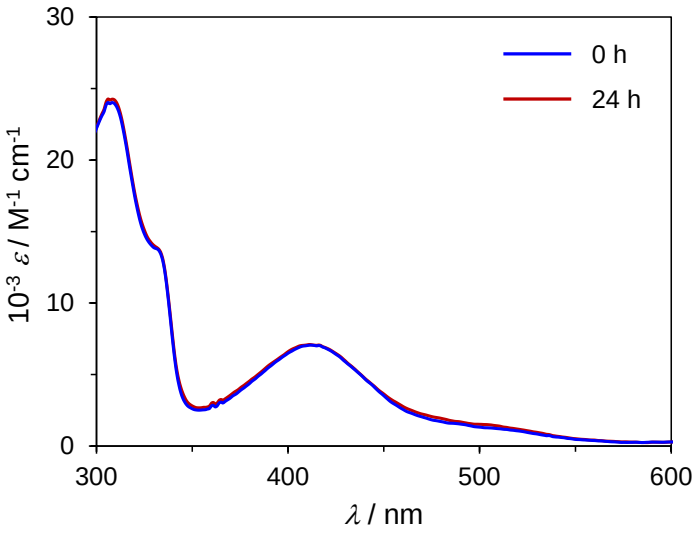

Figure 18. UV-vis absorption spectra of ***cis*-PN** in acetonitrile before and after heating at 75 °C for 24 hours.

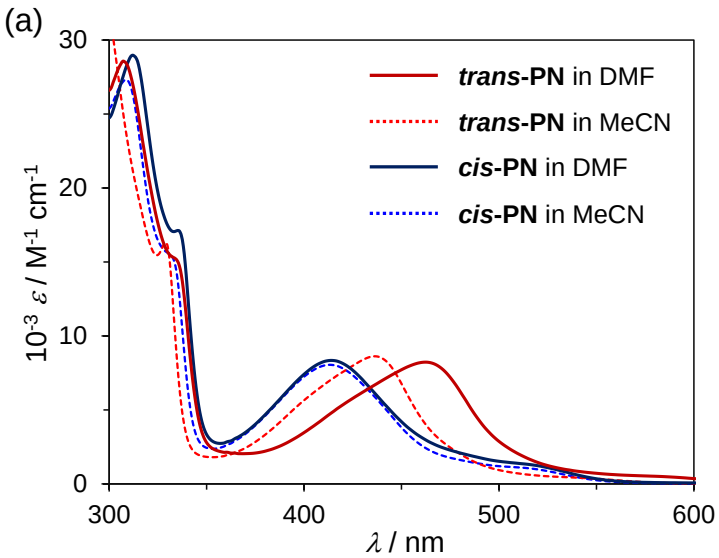

Figure 19. UV-vis absorption spectra of ***trans*-PN** and ***cis*-PN** in acetonitrile and DMF at room temperature. The UV-vis spectra indicate that the acetonitrile ligand of ***trans*-PN** can easily undergo a ligand substitution, whereas that of ***cis*-PN** is barely substituted.

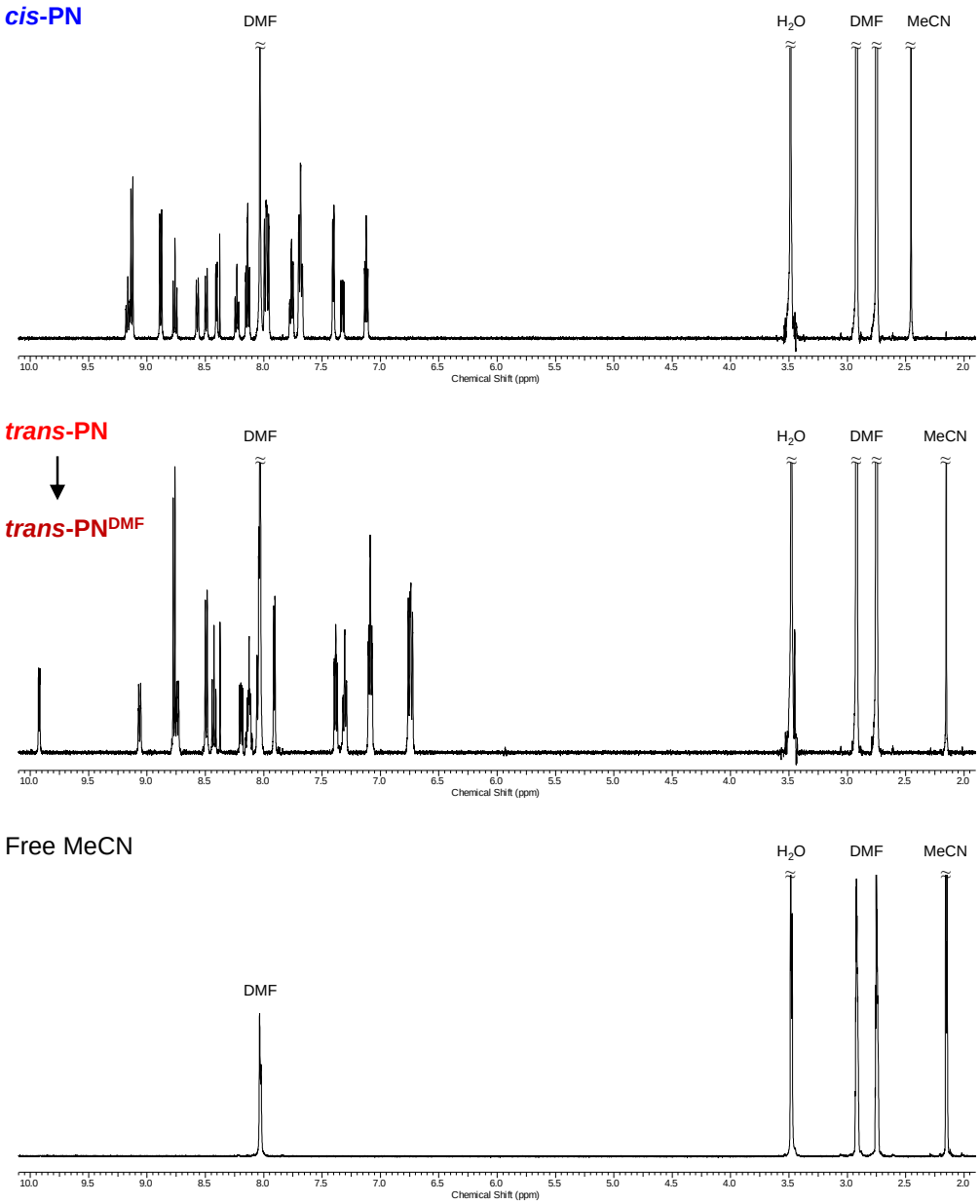

Figure 20. ^{1}H NMR spectra of ***cis*-PN**, ***trans*-PN**, and free acetonitrile in DMF-d_7 at room temperature. According to ^{1}H NMR spectrum of ***trans*-PN** in DMF-d_7, the signal of acetonitrile ligand is consistent with that of free acetonitrile molecule at δ 2.15 (s), whereas that of ***cis*-PN** appeared at δ 2.46 (s). The results indicate that the acetonitrile ligand of ***trans*-PN** could easily undergo a ligand substitution to form *trans(P,DMF)*-[Ru(trpy)(Pqn)(DMF)]$(PF_6)_2$ (***trans*-PN^{DMF}**).

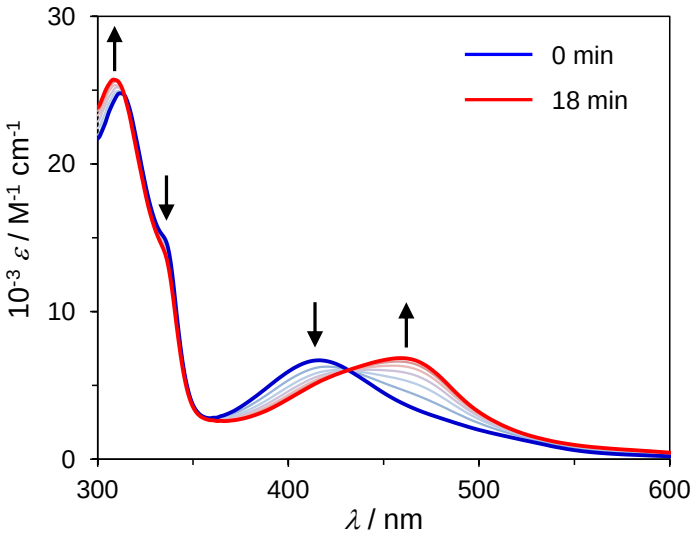

Figure 21. Time course of spectral changes of ***cis*-PN** in DMF at 110°C. Spectra were recorded at 3-min intervals.

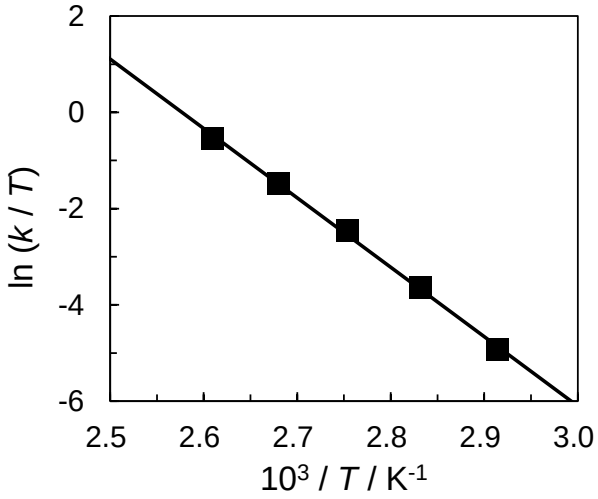

Figure 22. Eyring plot for the transformation of ***cis*-PN** to ***trans*-PN**$^{\mathbf{DMF}}$.

Photo-induced Isomerization.

Photo responses of obtained complexes were investigated by irradiating visible light to an acetonitrile solution of complexes. In this experimental condition, ***cis*-Cl** and ***trans*-PN** did not show photo response (Figure 23). In contrast, irradiation of visible light to an acetonitrile solution of ***cis*-PN** resulted in the isomerization to ***trans*-PN**, which was monitored by UV-Vis spectroscopy as shown in Figure 24. The existence of isosbestic points at λ = 307, 325, 332, 419, and 488 nm indicates that the isomerization proceeds without side products or stable intermediates. The kinetic profile of the photoisomerization process was first order with respect to the concentration of the complex. The rate constant was determined using the SVD method to be k = 4.2(6)×10^{-4} s^{-1} at room temperature. Along with the dissociative mechanism of solvent-induced isomerization in DMF, the photochemical isomerization is probably related to ligand dissociation from the triplet metal-centered (^{3}MC) state, which has anti-bonding nature between a metal ion and an acetonitrile ligand and is thermally accessible from the ^{3}MLCT photoexcited state.[10d]

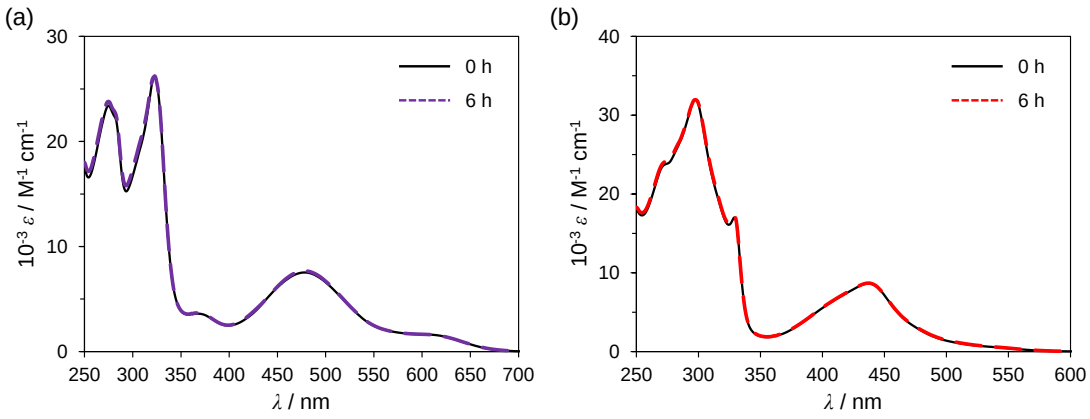

Figure 23. UV-vis absorption spectra of (a) ***cis*-Cl** and (b) ***trans*-PN** in acetonitrile before and after photo-irradiation (λ > 370 nm) for 6 hours. The complexes did not show photo response.

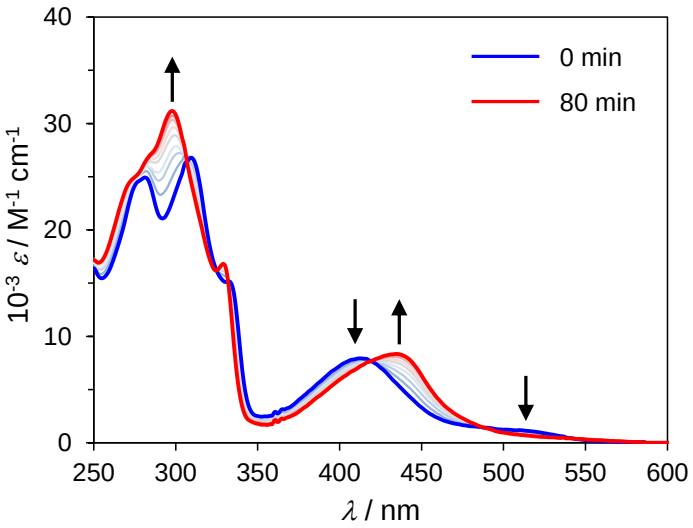

Figure 24. The time course of spectral changes of ***cis*-PN** under photo-irradiation (λ > 370 nm) in acetonitrile at room temperature. Spectra were recorded at 10-min intervals.

Water Oxidation.

As mentioned earlier, three $[Ru(N{-}N{-}N)(N{-}N)(L)]^{n+}$-type ruthenium polypyridine complexes can serve as catalysts for some chemical conversions.[7-14] Because the reduction or photo-irradiation can lead to the *cis-trans* isomerization (see the section of electrochemistry), in the present study, water oxidation catalyses of ***trans*-PN** and ***cis*-PN**, together with **PP**, were investigated in order to examine difference in reactivities between the geometrical isomers. The reaction was initiated by adding a solution of a catalyst in acetonitrile (0.1 mL) to a solution of $Ce(NH_4)_2(NO_3)_6$ (0.40 mmol) in water (1.9 mL) at 20 °C under Ar atmosphere, where acetonitrile was used to improve the solubility of the PF_6^- salt of the catalyst. The oxygen evolved was monitored using an oxygen probe (YSI 5331/5300) and the results are shown in Figure 25. The turnover numbers (TON) of ***trans*-PN**, ***cis*-PN** and **PP** after one hour were determined to be 24.8, 6.7, and 0.4, respectively. The order of the catalytic activities is ***trans*-PN** > ***cis*-PN** > **PP**, although their activities are less than that of **NN**.[9] This order of catalytic activities match to the order of oxidation potentials of ruthenium center shown in Table 4.

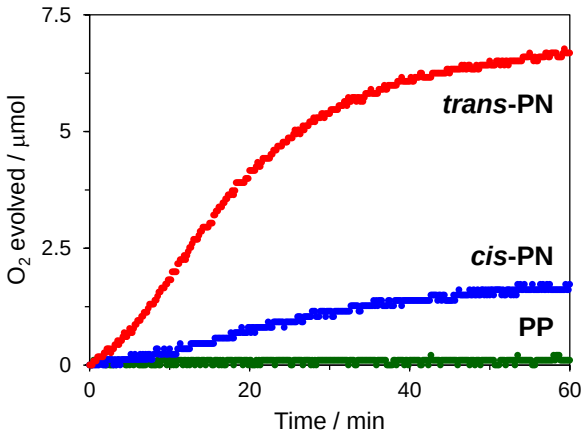

Figure 25. Oxygen evolution from a 19:1 water/acetonitrile mixture (2 mL) containing $Ce(NH_4)_2(NO_3)_6$ (200 mM) in the presence of either ***trans*-PN**, ***cis*-PN,** or **PP** (0.125 mM) as a catalyst.

Discussion

Phosphine as σ-donor and π-acceptor.

The differences in the redox potentials and UV-vis absorption spectra between ***trans*-PN**, ***cis*-PN**, **PP** and **NN** can be reasonably interpreted by considering the properties of phosphine group.

The σ-donor character of phosphine group significantly elongates the bond length between the ruthenium center and the ligand located at the *trans* position of the phosphine group, called the *trans* influence. The red lines in Figure 3 correspond to the elongated bonds. The σ-donation also affects kinetics of ligand substitution reactions. ***Trans*-Cl**, the geometrical isomer of ***cis*-Cl**, was not isolated because the chloride ligand at the *trans* position of the phosphino group in ***trans*-Cl** easily dissociates to afford *trans(P,L)*-$[Ru(trpy)(Pqn)(L)]^{2+}$ due to the *trans* labilizing effect.[28] A chloro ligand of $[Ru(trpy)(dppbz)Cl]^{+}$ was more labile than that of ***cis*-Cl**, allowing the transformation of $[Ru(trpy)(dppbz)Cl]^{+}$ to **PP** in acetonitrile without addition of silver ion (Ag^{+}). The *trans* labilizing effect also explains the difference in ligand substitution rates of ***cis*-PN** and ***trans*-PN**; ***trans*-PN** immediately converted to ***trans*-PN^{DMF}** in DMF at room temperature, whereas the structure of ***cis*-PN** was preserved under the same conditions (Figures 19 and 20).

In contrast, the π-acceptor character of phosphines stabilizes the energy levels of the dπ orbitals of the ruthenium center. As the number of phosphine donors increases, the dπ orbitals are more stabilized. Indeed, the oxidation potential of Ru(II)/Ru(III) for **PP** is higher than those of ***trans*-PN** and ***cis*-PN**, while that of **NN** is the lowest (Figure 7a). The blue shifts observed in the UV-Vis absorption spectra upon introduction of phosphine moieties (Figure 6) also can be explained by stabilization of the dπ orbitals of the ruthenium center. These observations are supported by DFT and TD-DFT calculations (Figures 16 and 17), and are consistent with the results reported for a series of $[Ru(bpy)_2(BL)](PF_6)_2$ (see Table 4).[29]

The difference in the stabilization of the dπ orbitals between ***trans*-PN** and ***cis*-PN** can be explained by considering interactions with the π* orbitals of trpy, Pqn, and acetonitrile ligands, as well as σ* orbitals of the P−C bonds of Pqn. The σ* orbitals of the P−C bonds can interact with two of the three dπ orbitals (d_{yz} and d_{zx} orbitals, with the Ru−P bond along the z-axis). For both ***trans*-PN** and ***cis*-PN**, the two dπ orbitals stabilized by π-back bonding of the phosphine compose HOMO−2 and HOMO−1 (Scheme 5a and Figure 15). As a result, the remaining dπ orbital without contribution from the π-back bonding of phosphine forms the HOMO. The HOMO of ***trans*-PN** lies

in-plane with the trpy ligand, and can interact only with the π* orbitals of the quinoline moiety of Pqn. In contrast, that of ***cis*-PN** lies perpendicular to the trpy ligand and quinolone moiety of Pqn, and thus is stabilized by the π* orbitals of trpy, Pqn, and acetonitrile ligands (Scheme 5b and Figure 15). Therefore, the HOMO of ***cis*-PN** was stabilized to a greater extent than that of ***trans*-PN**, resulting in a positive shift of the Ru(II)/Ru(III) potential and the blue shift of the MLCT band (Figures 6 and 7a).

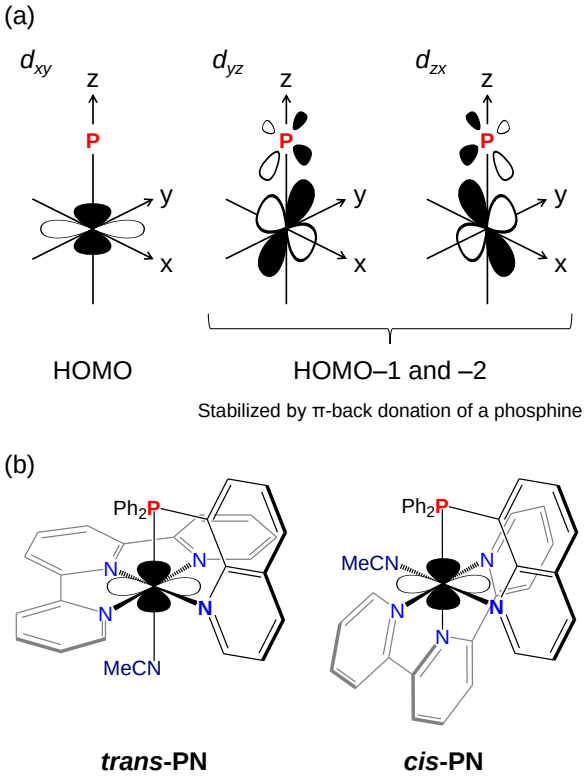

Scheme 5. (a) Two of the three dπ orbitals stabilized by π-back donation of a phosphine. (b) HOMOs of ***trans*-PN** and ***cis*-PN**. The HOMO of ***trans*-PN** lies in-plane with the trpy ligand, and can interact only with π* orbitals of the quinoline moiety of Pqn. The HOMO of ***cis*-PN** lies perpendicularly to the trpy ligand and the quinolone moiety of Pqn, and thus is stabilized by the π* orbitals of trpy, Pqn, and MeCN.

Mechanism of Isomerization and Electrochemical Behavior.

Although the results of X-ray crystallography, UV-Vis absorption spectroscopy, and CVs in the positive potential region can be understood based on σ-donation and π-back donation of phosphine donors, the CVs of phosphine containing complexes in the negative potential region exhibited distinct behavior with each other. Reduction of ***cis*-PN** led to *cis-trans* isomerization (Figure 13), and that of **PP** went through a two-electron transfer (Figure 7). The mechanism of these various electrochemical behaviors is discussed in the combination with *cis-trans* transformation behavior of ***cis*-PN** by heating or photoirradiation.

The *cis-trans* transformation proceeded upon moderate heating in DMF (Figure 21) and *via* visible-light irradiation (Figure 24). The positive values of $\Delta S^{\ddagger}$ and $\Delta H^{\ddagger}$ for solvent-induced isomerization in DMF indicate that the isomerization proceeds *via* a short-lived intermediate, $[Ru(trpy)(Pqn)]^{2+}$, after dissociation of the acetonitrile ligand (Scheme 6, top). Photochemical isomerization also can be explained by ligand-dissociation from the ^{3}MC excited state to produce the short-lived five-coordinated species (Scheme 6, middle).[10d]

The concept of the five-coordinated species also can be used to explain the two-electron transfer process of **PP** (Figure 7) and the reduction-induced *cis-trans* isomerization of ***cis*-PN** (Figure 13). The two-electron process of **PP** implies that the reduction potential for **PP** lies at more negative potential than that for the one-electron-reduced species of **PP**. Similar electrochemical behavior was reported for a ruthenium-arene complex, $[Ru(\eta^6\text{-}C_6Me_6)(bpy)(MeCN)]^{2+}$, for which the acetonitrile ligand was lost upon electrochemical reduction of $[Ru(\eta^6\text{-}C_6Me_6)(bpy)(MeCN)]^{2+}$. The $[Ru(\eta^6\text{-}C_6Me_6)(bpy)]^0$ was assumed to be the dominant form of the doubly reduced species.[13] Based on comparisons with the ruthenium-arene complex, the two-electron reduction of **PP** may involve the five-coordinated doubly-reduced species $[Ru(trpy)(dppbz)]^0$.

To discuss the electrochemical behaviors of ***cis*-PN** and **PP** in conjunction with five-coordinated species, bond dissociation free energies (BDFEs) upon liberation of the acetonitrile ligand were estimated. Table 7 shows BDFEs for the one-electron reduced species of ***trans*-PN**, ***cis*-PN**, and **PP** (***trans*-PN**$^-$, ***cis*-PN**$^-$, and **PP**$^-$), determined by DFT calculation. The negative BDFEs suggest that dissociation of the acetonitrile ligand is favored in the equilibrium. Therefore, ligand dissociations are favored for ***cis*-PN**$^-$ and **PP**$^-$ (reactions 2 and 3, respectively, in Table 7), while dissociation is not favored for ***trans*-PN**$^-$ (reaction 1). In particular, the large negative $\Delta G°$ value for **PP**$^-$ implies that the equilibrium is largely shifted toward formation of the five-coordinated

species, $[Ru(trpy)(dppbz)]^+$ (reaction 3). The reduction potential for $[Ru(trpy)(dppbz)]^+/[Ru(trpy)(dppbz)]^0$ may be more positive than that for $[Ru(trpy)(dppbz)(MeCN)]^{2+}/[Ru(trpy)(dppbz)(MeCN)]^+$, leading to the two-electron process.[13,42] The generation of $[Ru(trpy)(dppbz)]^0$ upon reduction is also supported by the BDFE (reaction 4). For ***cis*-PN**, one-electron reduction may lead to ligand dissociation to give the five-coordinated species $[Ru(trpy)(Pqn)]^+$ ($\Delta G° < 0$, for reaction 2), followed by rapid coordination of an acetonitrile molecule to the five-coordinated species to afford ***trans*-PN**$^-$ ($\Delta G° > 0$, for reaction 1). Thus the equilibrium of ***cis*-PN**$^-$, ***trans*-PN**$^-$, and $[Ru(trpy)(Pqn)]^+$ seems to be shifted toward ***trans*-PN**$^-$ to some extent, although the $|\Delta G°|$ values are too small to explain the fact that only ***trans*-PN** was formed by the re-oxidation of the equilibrium mixture (Figure 13). A reasonable explanation of the irreversible *cis-trans* conversion is given by considering the first reduction potentials of ***cis*-PN** ($E_{pc} \approx -1.6$ V) and ***trans*-PN** ($E^{\circ\prime}_1 = -1.70$ V). In the potential region between these two potentials ($E \approx -1.6 \sim -1.7$ V), ***cis*-PN** is reduced to ***cis*-PN**$^-$ and the generated ***cis*-PN**$^-$ reaches equilibrium with ***trans*-PN**$^-$ and $[Ru(trpy)(Pqn)]^+$. Then, ***trans*-PN**$^-$ in the equilibrium mixture can be oxidized to ***trans*-PN** in the same potential region (Scheme 7). Therefore, the potential sweeping over $E \approx -1.6 \sim -1.7$ V results in the irreversible conversion from ***cis*-PN** to ***trans*-PN** *via* the five-coordinated species (Scheme 6, bottom).

Table 7. Bond dissociation free energies (BDFEs) for the one-electron reduced species of ***trans*-PN**, ***cis*-PN**, and **PP** (***trans*-PN**$^-$, ***cis*-PN**$^-$, and **PP**$^-$, respectively), and two-electron reduced species of **PP** (**PP**$^{2-}$) estimated by DFT calculations (see also Table 8).

reaction	$\Delta G°$ (kJ / mol)
One-Electron Reduction	
trans(P,MeCN) -$[Ru(trpy)(Pqn)(MeCN)]^+$ → $[Ru(trpy)(Pqn)]^+$ + MeCN (1)	2.5
cis(P,MeCN) -$[Ru(trpy)(Pqn)(MeCN)]^+$ → $[Ru(trpy)(Pqn)]^+$ + MeCN (2)	–1.4
$[Ru(trpy)(dppbz)(MeCN)]^+$ → $[Ru(trpy)(dppbz)]^+$ + MeCN (3)	–45.3
Two-Electron Reduction	
$[Ru(trpy)(dppbz)(MeCN)]^0$ → $[Ru(trpy)(dppbz)]^0$ + MeCN (4)	–19.3

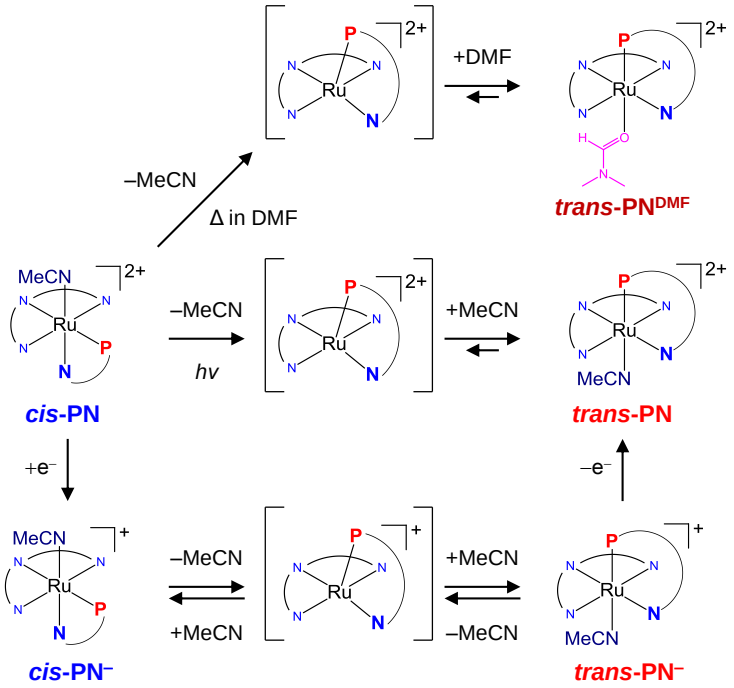

Scheme 6. Three paths for isomerization from ***cis*-PN** to ***trans*-PN**. (Top) Solvent-induced isomerization. (Middle) Photo-induced isomerization. (Bottom) Reduction-induced isomerization. All isomerization reactions from *cis* to *trans* proceed though the short-lived intermediates.

at *ca.* –1.6 V

(a) ***cis*-PN** + e⁻ ⟶ (***cis*-PN**)⁻

(b) (***cis*-PN**)⁻ ⟶ (***trans*-PN**)⁻

(c) (***trans*-PN**)⁻ + ***cis*-PN** ⟶ ***trans*-PN** + (***cis*-PN**)⁻

(d) (***trans*-PN**)⁻ ⟶ ***trans*-PN** + e⁻

at –1.70 V

(e) ***trans*-PN** + e⁻ ⟶ (***trans*-PN**)⁻

Scheme 7. Reduction induced isomerization behavior of ***cis*-PN**. Initially, ***cis*-PN** was reduced to **(*cis*-PN)**$^-$ around –1.6 V by the electrode (a), and **(*cis*-PN)**$^-$ undergoes isomerization reaction to **(*trans*-PN)**$^-$ (b). Electron transfer from **(*trans*-PN)**$^-$ to ***cis*-PN** (c) or electron transfer to the electrode (d) affords ***trans*-PN**. Further potential sweep initiates the reduction of ***trans*-PN** at –1.70 V (e).

Table 8. Sums of electronic and thermal free energies for cationic moieties of ***trans*-PN**, ***cis*-PN**, and **PP**, and the corresponding one-electron reduced species, two-electron reduced species, and possible intermediates in acetonitrile media (in Hartree). Details of DFT calculations are described in Experimental Section in the main text.

Species	Sum of Free Energy
Neutral species	
trans(P,MeCN)-[Ru(trpy)(Pqn)(MeCN)]$^{2+}$ (***trans*-PN**)	–1839.313460
cis(P,MeCN)-[Ru(trpy)(Pqn)(MeCN)]$^{2+}$ (***cis*-PN**)	–1839.308112
[Ru(trpy)(dppbz)(MeCN)]$^{2+}$ (**PP**)	–2138.635483
One electron reduced species	
trans(P,MeCN)-[Ru(trpy)(Pqn)(MeCN)]$^{+}$ (***trans*-PN**$^{-}$)	–1839.433623
cis(P,MeCN)-[Ru(trpy)(Pqn)(MeCN)]$^{+}$ (***cis*-PN**$^{-}$)	–1839.432149
[Ru(trpy)(dppbz)(MeCN)]$^{+}$ (**PP**$^{-}$)	–2138.741912
Two electron reduced species	
trans(P,MeCN)-[Ru(trpy)(Pqn)(MeCN)]^{0} (***trans*-PN**$^{2-}$)	–1839.537686
[Ru(trpy)(dppbz)(MeCN)]^{0} (**PP**$^{2-}$)	–2138.852228
5-coordinated species	
[Ru(trpy)(Pqn)]$^{2+}$	–1706.582449
[Ru(trpy)(Pqn)]$^{+}$	–1706.717557
[Ru(trpy)(Pqn)]^{0}	–1706.822581
[Ru(trpy)(dppbz)]$^{2+}$	–2005.901237
[Ru(trpy)(dppbz)]$^{+}$	–2006.044054
[Ru(trpy)(dppbz)]^{0}	–2006.144458
5-coordinated species + acetonitrile	
[Ru(trpy)(Pqn)]$^{2+}$ + MeCN	–1839.297569
[Ru(trpy)(Pqn)]$^{+}$ + MeCN	–1839.432677
[Ru(trpy)(Pqn)]^{0} + MeCN	–1839.537701
[Ru(trpy)(dppbz)]$^{2+}$ + MeCN	–2138.616357
[Ru(trpy)(dppbz)]$^{+}$ + MeCN	–2138.759174
[Ru(trpy)(dppbz)]^{0} + MeCN	–2138.859578
MeCN	–132.715120

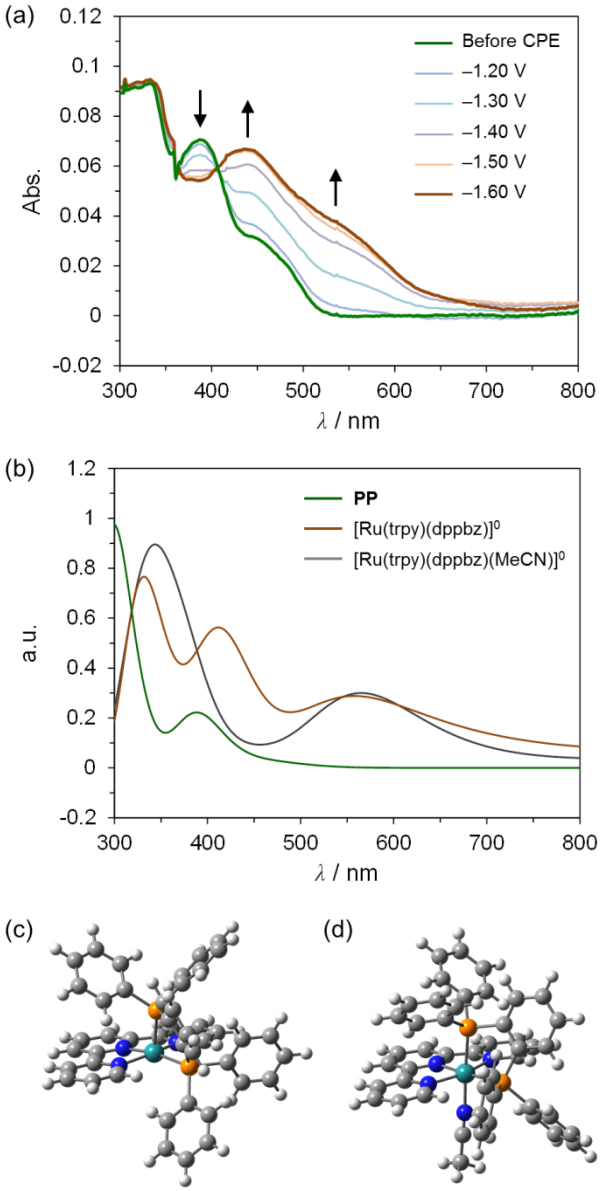

Figure 26. (a): UV-vis spectra under controlled potential electrolysis (CPE) in acetonitrile solvent ([complex] = 2.0 mM; 0.1 M TEAP) for 2 min using BAS Spectroelectrochemical Cell. The electrolytic potentials were switched between –1.20 V and –1.60 V at an interval of 0.10 V (WE: GC, CE: Pt wire, RE: Ag/Ag^{+}). The isosbestic point at λ = 407 nm indicates that only two species were involved without the formation of side products or intermediates. (b): Simulated absorption spectra of **PP** and two possible two-electron reduced species. Optimized structures of (c) $[Ru(trpy)(dppbz)]^{0}$ and (d) $[Ru(trpy)(dppbz)(MeCN)]^{0}$.

Conclusion

This study describes the effects of the substitution of phosphines for pyridine in a series of ruthenium(II) polypyridine complexes with a monodentate labile ligand. The structures and electronic properties of ruthenium(II) complexes were expected to be systematically controlled by the number and position of the phosphines. Indeed, the σ-donating and π-accepting character of the phosphines clearly influenced the dσ and dπ orbitals of a metal center, respectively, which was supported by crystallographic, spectroscopic, and electrochemical analyses. Furthermore, electrochemical behaviors of these complexes in their reduction reactions were totally different among them. The mechanisms explaining these results were elucidated by considering five-coordinated species formed *via* liberation of the monodentate labile ligand. These results are significant because they show a clear relation between the redox properties of the metal complexes and the liberation of a labile ligand, and therefore provide important information for the development of new catalysts for electrochemical and photochemical reactions.

Experimental Section

General Methods.

The ^{1}H and $^{31}P\{^{1}H\}$ NMR spectra were recorded at room temperature on a JEOL JNM-LA500 spectrometer using tetramethylsilane as an internal reference for ^{1}H NMR spectra and phosphoric acid as an external reference for $^{31}P\{^{1}H\}$ NMR spectra. UV-Vis absorption spectra were obtained on a Shimadzu UV-2450SIM spectrophotometer at room temperature. Elemental analyses were conducted on a J-Science Lab Micro Corder JM10 elemental analyzer. ESI-TOF mass spectra were recorded on a JEOL JMS-T100LC mass spectrometer. All of the ESI-TOF mass spectrometric measurements were obtained in the positive ion mode at a cone voltage of 20 V. Typically, each sample solution was introduced into the spectrometer at a flow rate of 10 mL min^{-1} using a syringe pump. Cyclic voltammograms were measured at room temperature on a BAS ALS Model 650DKMP electrochemical analyzer in acetonitrile ([complex] = 0.5 mM; 0.1 M tetraethylammonium perchlorate (TEAP)). A glassy carbon disk, platinum wire, and Ag/Ag^{+} electrode (Ag/0.01 M $AgNO_3$) were used as the working, auxiliary, and reference electrodes, respectively. The redox potentials of samples were calibrated against the redox signal for the ferrocene/ferrocenium (Fc/Fc^{+}) couple. The photoisomerization was performed using a 150 W xenon lamp (CX-04E, Eagle Engineering) as a probe with a cut filter (λ > 370 nm). Global kinetic analysis was conducted using the singular value decomposition (SVD) method in SPECFIT, [36] in the range of 300-600 nm. The amount of O_2 evolved was monitored using a YSI model 5300A oxygen meter at room temperature under Ar atmosphere.[9a]

Materials.

Pqn [8-(diphenylphosphanyl)quinoline],[43] $[RuCl_3(trpy)]\cdot H_2O$ (trpy = 2,2':6',2"-terpyridine)[27] and $[Ru(trpy)(bpy)(MeCN)](PF_6)_2$ (**NN**)[25] were prepared by methods reported previously. Dppbz [1,2-bis(diphenylphosphanyl)benzene] and $NaPF_6$ were purchased from Wako Pure Chemical Industries, Ltd. The $AgPF_6$ was purchased from Sigma-Aldrich Co. All solvents and reagents were of the highest quality available and were used as received.

Synthesis of *cis(P,Cl)*-[Ru(trpy)(Pqn)Cl]PF_6 (*cis*-Cl).

A mixture of $[RuCl_3(trpy)]\cdot H_2O$ (94.0 mg, 0.205 mmol), Pqn (64.6 mg, 0.206 mmol), and ascorbic acid (68.7 mg, 0.390 mmol) in ethanol (100 cm^3) was refluxed for 4 h and then cooled to room temperature. The solution was filtered and the purple filtrate

concentrated to ca. 5 cm^3 under reduced pressure. A saturated $NaPF_6$/water solution was added to the solution under refrigeration and resulted in a purple precipitate. The crude product was further purified by gel permeation chromatography (Sephadex LH-20) using acetonitrile−methanol (1:1) mixture as the eluent. The product was recrystallized from dichloromethane and a small amount of acetonitrile/diethyl ether to yield deep purple crystals of ***cis*-Cl** (0.089 mmol, 43%). ESI-TOF MS (positive ion, acetonitrile): *m/z* 683 ($[Ru(trpy)(Pqn)Cl]^+$). ^1H NMR (CD_3CN): δ 6.70 (t, 2H, J = 6.5 Hz), 6.95 (t, 1H, J = 8.5 Hz), 7.38 (d, 2H, J = 6.0 Hz), 7.50 (t, 4H, J = 7.0 Hz), 7.57 (t, 2H, J = 7.5 Hz), 7.75 (t, 2H, J = 7.5 Hz), 8.08 (m, 7H), 8.20 (d, 1H, J = 9.0 Hz), 8.30 (t, 1H, J = 7.5 Hz), 8.35 (d, 2H, J = 8.0 Hz), 8.56 (d, 2H, J = 8.5 Hz), 9.01 (t, 1H, J = 7.5 Hz). $^{31}P\{^1H\}$ NMR (CD_3CN): δ 51.16 (s). Anal. Found: C, 50.52; H, 3.44; N, 6.54%. Calcd for $C_{36.5}H_{28}F_6Cl_2N_4P_2Ru$ (***cis*-Cl**·$0.5CH_2Cl_2$): C, 50.36; H, 3.24; N, 6.44%.

Synthesis of *cis(P,Cl)*-[Ru(trpy)(Pqn)Cl]BPh_4 (*cis*-Cl').

This complex was prepared by counter ion exchange of ***cis*-Cl** (16.9 mg, 0.0194 mmol) with excess $NaBPh_4$. The product was recrystallized from dichloromethane and a small amount of acetonitrile / diethyl ether to afford purple crystals of ***cis*-Cl'** (0.0124 mmol, 64%). Anal. Found: C, 71.72; H, 4.74; N, 5.59%. Calcd for $C_{60}H_{47}BClN_4PRu$ (***cis*-Cl'**): C, 71.90; H, 4.73; N, 5.59%.

Synthesis of *trans(P,MeCN)*-[Ru(trpy)(Pqn)(MeCN)]$(PF_6)_2$ (*trans*-PN).

A mixture of ***cis*-Cl** (108 mg, 0.124 mmol) and $AgPF_6$ (34.8 mg, 0.138 mmol) in 2-butanone (10 cm^3)/water (5 cm^3) was heated at 100 ºC for 1 day. The resulting red solution was evaporated to dryness under reduced pressure. The residue was extracted with a small amount of acetonitrile and the precipitate of AgCl was removed by filtration. The product was recrystallized from dichloromethane and a few drops of acetonitrile/diethyl ether to afford orange crystals of ***trans*-PN** (0.102 mmol, 82%). ESI-TOF MS (positive ion, acetonitrile): *m/z* 324 ($[Ru(trpy)(Pqn)]^{2+}$), 345 ($[Ru(trpy)(Pqn)(MeCN)]^{2+}$). ^1H NMR (CD_3CN): δ 6.59 (t, 4H, J = 8.5 Hz), 6.99 (t, 4H, J = 7.5 Hz), 7.15 (d, 2H, J = 6.5 Hz), 7.24 (t, 2H, J = 7.5 Hz), 7.57 (t, 2H, J = 6.0 Hz), 7.84 (t, 2H, J = 8.5 Hz), 7.96 (m, 3H), 8.07 (d, 2H, J = 9.0 Hz), 8.22 (t, 1H, J = 7.5 Hz), 8.32 (d, 2H, J = 8.0 Hz), 8.52 (d, 1H, J = 7.5 Hz), 8.83 (d, 1H, J = 8.0 Hz), 9.85 (d, 1H, J = 7.5 Hz). $^{31}P\{^1H\}$ NMR (CD_3CN): δ 58.80 (s). Anal. Found: C, 44.12; H, 3.24; N, 6.59%. Calcd for $C_{39}H_{32}F_{12}Cl_2N_5P_3Ru$ (***trans*-PN**·CH_2Cl_2): C, 44.04; H, 3.03; N, 6.58%.

Synthesis of *cis(P,MeCN)*-[Ru(trpy)(Pqn)(MeCN)](PF$_6$)$_2$ (*cis*-PN).

A mixture of ***cis*-Cl** (85.1 mg, 0.103 mmol) and $AgPF_6$ (28.0 mg, 0.111 mmol) in acetonitrile (15 cm^3) was heated at 70 ºC for 2 days and then cooled to room temperature. The resulting orange solution was evaporated to dryness under reduced pressure. The residue was extracted with a small amount of acetonitrile and the precipitate of AgCl was removed by filtration. The product was recrystallized from chloroform and a few drops of acetonitrile / diethyl ether to afford orange crystals of ***cis*-PN** (0.096 mmol, 93%). ESI-TOF MS (positive ion, acetonitrile): *m/z* 324 ([Ru(trpy)(Pqn)]$^{2+}$), 345 ([Ru(trpy)(Pqn)(MeCN)]$^{2+}$). ^{1}H NMR (CD_3CN): δ 6.83 (t, 2H, *J* = 6.5 Hz), 7.10 (d, 1H, *J* = 8.0 Hz), 7.26 (d, 2H, *J* = 6.5 Hz), 7.57 (t, 4H, *J* = 7.0 Hz), 7.67 (t, 2H, *J* = 7.5 Hz), 7.77 (d, 2H, *J* = 8.0 Hz), 7.79 (d, 2H, *J* = 8.0 Hz), 7.89 (t, 2H, *J* = 8.0 Hz), 7.97 (d, 1H, *J* = 5.5 Hz), 8.04 (t, 1H, *J* = 7.5 Hz), 8.24 (d, 1H, *J* = 8.0 Hz), 8.28 (d, 1H, *J* = 8.0 Hz), 8.41 (d, 2H, *J* =8.0 Hz), 8.50 (t, 1H, *J* =8.0 Hz), 8.65 (d, 2H, *J* = 8.0 Hz), 8.89 (t, 1H, *J* = 8.0 Hz). ^{31}P{^{1}H} NMR (CD_3CN): δ 55.96 (s). Anal. Found: C, 44.38; H, 3.13; N, 6.73%. Calcd for $C_{38.5}H_{31}Cl_{1.5}N_5P_3Ru$ (***cis*-PN**·0.5$CHCl_3$): C, 44.53; H, 2.96; N, 6.74%.

Synthesis of [Ru(trpy)(dppbz)(MeCN)](PF$_6$)$_2$ (PP).

A mixture of [$RuCl_3$(trpy)]·H_2O (62.0 mg, 0.135 mmol), dppbz (63.1 mg, 0.141 mmol), and ascorbic acid (52.3 mg, 0.297 mmol) in ethanol (50 cm^3) was refluxed for 4 h and then cooled to room temperature. The solution was filtered and the purple filtrate concentrated to ca. 5 cm^3 under reduced pressure. A saturated $NaPF_6$/water solution was added to the solution under refrigeration, which resulted in a purple precipitate. Purification of the crude product by gel permeation chromatography (Sephadex LH-20) using acetonitrile−methanol (1:1) mixture as the eluent produced an orange band followed by a purple band of *cis(MeCN,MeCN)*-[Ru(trpy)($MeCN)_2$Cl]PF_6 (**trpyMeCN2Cl**) [see the synthesis of **trpyMeCN2Cl** in Supporting Information]. The orange solution was evaporated and a saturated $NaPF_6$/acetonitrile solution (30 cm^3) was added to the residue. The mixture was refluxed for 3 h, cooled to room temperature, and then evaporated to dryness under reduced pressure. The residue was extracted with dichloromethane and salts were removed by filtration. After evaporation of the solvent, the dried solid was dissolved in a minimum amount of dichloromethane and then loaded onto a silica gel column. The column was eluted with dichloromethane−acetonitrile (9 : 1) to give an orange band followed by a yellow band. The **PP** was obtained from the yellow band after evaporation and recrystallization from dichloromethane−acetonitrile mixture (1 : 1) / diethyl ether as yellow crystals (0.034 mmol, 25%). ESI-TOF MS

(positive ion, acetonitrile): *m/z* 391 ($[Ru(trpy)(dppbz)]^{2+}$), 411 ($[Ru(trpy)(dppbz)(MeCN)]^{2+}$). ^{1}H NMR ($CD_3CN$): 6.56 (t, 4H, *J* = 8.0 Hz), 6.76 (t, 2H, *J* = 5.5 Hz), 6.83 (d, 2H, *J* = 6.0 Hz), 6.91 (t, 4H, *J* = 8.0 Hz), 7.20 (t, 2H, *J* = 7.5 Hz), 7.51 (t, 4H, *J* = 8.0 Hz), 7.63 (m, 6H), 7.70 (t, 1H, *J* = 8.0 Hz), 7.82 (m, 3H), 7.99 (t, 1H, *J* = 7.5 Hz), 8.09 (d, 2H, *J* = 8.5 Hz), 8.37 (m, 3H), 8.53 (t, 1H, *J* = Hz). $^{31}P\{^1H\}$ NMR (CD_3CN): δ 68.57 (d, $^2J_{P\text{-}P}$ = 20.2 Hz), 69.77 (d, $^2J_{P\text{-}P}$ = 20.2 Hz). Anal. Found: C, 48.32; H, 3.52; N, 4.81%. Calcd for $C_{48}H_{40}F_{12}Cl_2N_4P_4Ru$ (**PP**·CH_2Cl_2): C, 48.17; H, 3.37; N, 4.68%.

Synthesis of *trans(P,DMF)*-[Ru(trpy)(Pqn)(DMF)](PF$_6$)$_2$ (*trans*-PN^{DMF}).

It is prepared by ligand exchange from ***trans*-PN** (0.0186 mmol) in *N*,*N*-dimethylformamide (DMF) solution. The product was recrystallized from dichloromethane and a few drops of DMF/diethyl ether affording red crystals of ***trans*-PN^{DMF}** (0.0130 mmol, 70%). ESI-TOF MS (positive ion, DMF): *m/z* 361 ($[Ru(trpy)(Pqn)(DMF)]^{2+}$), 693 ($[Ru(trpy)(Pqn)(HCOO)]^{+}$). ^{1}H NMR (DMF-$d_7$): δ 2.15 (s, 3H), 6.74 (t, 4H, *J* = 8.5 Hz), 7.09 (t, 4H, *J* = 8.0 Hz), 7.31 (t, 2H, *J* = 7.0 Hz), 7.38 (t, 2H, *J* = 6.5 Hz), 7.91 (d, 2H, *J* = 5.5 Hz), 8.04 (m, 2H), 8.12 (m, 2H), 8.19 (d, 1H, *J* = 8.5 Hz), 8.42 (t, 1H, *J* = 8.0 Hz), 8.49 (d, 2H, *J* = 8.0 Hz), 8.74 (m, 1H), 8.77 (d, 2H, *J* = 8.0 Hz), 9.06 (d, 1H, *J* = 8.5 Hz), 9.92 (d, 1H, *J* = 5.0 Hz). $^{31}P\{^1H\}$ NMR (DMF-d_7): δ 65.62 (s). Anal. Found: C, 44.97; H, 3.39; N, 6.68%. Calcd for $C_{39.5}H_{35}ClF_{12}N_5OP_3Ru$ (***trans*-PN^{DMF}**·0.5CH_2Cl_2): C, 45.05; H, 3.35; N, 6.65%.

Synthesis of *trans(P,H$_2$O)*-[Ru(trpy)(Pqn)(H$_2$O)](PF$_6$)$_2$ (*trans*-PN^{H2O}).

This complex was prepared from ***cis*-Cl** (0.0491 mmol) by a method similar to that for complex ***trans*-PN**. The extraction solvent was acetone instead of acetonitrile. Single crystals of ***trans*-PN^{H2O}** suitable for X-ray crystallography were grown by the slow evaporation of acetone in an acetone–water mixed solution (0.0272 mmol, 55%). ESI-TOF MS (positive ion, methanol): *m/z* 333 ($[Ru(trpy)(Pqn)(H_2O)]^{2+}$). ^{1}H NMR (acetone-$d_6$): δ 6.58 (d, 1H, *J* = 8.5 Hz), 6.80 (t, 4H, *J* = 8.5 Hz), 7.08 (t, 4H, *J* = 8.5 Hz), 7.28 (t, 2H, *J* = 7.5 Hz), 7.34 (t, 2H, *J* = 7.5 Hz), 7.90 (d, 1H, *J* = 8.0 Hz), 8.01 (t, 2H, *J* = 7.5 Hz), 8.15 (m, 3H), 8.40 (t, 3H, *J* = 8.5 Hz), 8.66 (d, 2H, *J* = 8.5 Hz), 8.69 (d, 1H, *J* = 8.0 Hz), 9.01 (d, 1H, *J* = 8.0 Hz), 10.07 (d, 1H, *J* = 7.5 Hz). $^{31}P\{^1H\}$ NMR (acetone-d_6): δ 67.02 (s). Anal. Found: C, 44.26; H, 3.06; N, 5.86%. Calcd for $C_{36}H_{31}F_{12}N_4O_2P_3Ru$ (***trans*-PN^{H2O}**·H_2O): C, 44.41; H, 3.21; N, 5.75%.

Synthesis of *cis(MeCN,MeCN)*-[Ru(trpy)(MeCN)$_2$Cl]PF$_6$ (trpyMeCN2Cl).

It was obtained from the purple band on the Sephadex LH-20 in synthesis of complex **PP**. Single crystals suitable for X-ray crystallography was grown by the slow diffusion of diethyl ether into dichloromethane−acetonitrile mixture of **trpyMeCN2Cl**. (0.046 mmol, 34%) ESI-TOF MS (positive ion, acetonitrile): *m/z* 452 ($[Ru(trpy)(MeCN)Cl]^+$). Anal. Found: C, 37.53; H, 3.15; N, 11.93%. Calcd for $C_{21}H_{20.25}F_6Cl_2N_{5.75}PRu$ (**trpyMeCN2Cl**·$0.5CH_2Cl_2$·$0.75CH_3CN$): C, 37.64; H, 3.05; N, 12.02%.

Crystallography.

Diffraction data at 123 K were obtained using a Rigaku AFC8 diffractometer with a Rigaku Saturn CCD system. Graphite-monochromated Mo-Kα radiation (0.71075 Å) was used. Cell parameters were retrieved using Crystal Clear-SM 1.4.0 software and refined using Crystal Clear-SM 1.4.0 on all observed reflections. Data reduction and empirical absorption correction using equivalent reflections and Lorentzian polarization were performed with the Crystal Clear-SM 1.4.0 software. The structure was solved by the direct method using *SIR-92*[44]and refined on F^2 with the full-matrix least squares technique using *SHELXL-97*.[45] All non-hydrogen atoms were refined anisotropically. Molecular graphics were generated using *ORTEP-3* for *Windows*[46] and *POV-RAY*.[47] For ***cis*-PN**, the diffused electron densities resulting from residual solvent molecules were removed from the data set using the SQUEEZE routine of PLATON and refined further using the data generated.

Crystallographic data have been deposited with Cambridge Crystallographic Data Center: Deposition numbers CCDC 971295, 971296, 971297, 971298, 971299, 971300, and 971301 for ***cis*-Cl'**, ***trans*-PN**, ***cis*-PN**, **PP**, ***trans*-PN^{DMF}**, ***trans*-PN^{H2O}**, and **trpyMeCN2Cl**, respectively. Copies of the data can be obtained free of charge *via* www.ccdc.cam.ac.uk/data_request/cif.

DFT calculations.

Calculations were performed using the DFT method implemented in the Gaussian 09 package of programs.[33] The structures were fully optimized using the B3LYP method, which uses hybrid Becke's three-parameter exchange functional[34] with the correlation energy functional of Lee, Yang, and Parr.[35] All calculations were performed using the standard double-ζ type LanL2DZ basis set[36] implemented in Gaussian 09, without adding any extra polarization or diffuse function. The LanL2DZ basis set also uses relativistic effective core potentials (RECP) for the Ru atom to account for the scalar relativistic effects of the inner 28 core electrons ($[Ar]3d^{10}$) for Ru. All calculations were performed using the polarizable continuum model (PCM)[37] to compute the structures in

acetonitrile. All stationary points were characterized by their harmonic vibrational frequencies as minima. The free energies at 298 K and 1 atm were obtained through thermochemical analysis of the frequency calculation, using the thermal correction to Gibbs free energy as reported by Gaussian 09. The excited states were calculated using the TD-DFT[38] method within the Tamm-Dancoff approximation as implemented in Gaussian 09. These calculations employ the hybrid B3LYP functional along with the basis sets described above. At least 100 excited states were computed in each calculation. To obtain the simulated spectrum of each species, transition energies and oscillator strengths have been interpolated by a Gaussian convolution with a common σ value of 0.2 eV.

References

1 (a) Kalyanasundaram, K. *Coord. Chem. Rev.* **1982**, *46*, 159−244. (b) Juris, A.; Balzani, V. Barigelletti, F.; Campagna, S.; Belser, P.; von Zelewsky, A. *Coord. Chem. Rev.* **1988**, *84*, 85−277.

2 (a) Sutin, N. *Journal of Photochemistry*, **1979**, *10*, 19−40. (b) Dodsworth, E. S.; Lever, A. B. P.; *Chem. Phys. Lett.* **1986**, *124*, 152−158. (c) Lever, A. B. P. *Inorg. Chem.* **1990**, *29*, 1271−1285. (d) Thompson, D. W.; Wishart, J. F.; Brunschwig, B. S.; Sutin, N. *J. Phys. Chem. A*, **2001**, *105*, 8117−8122.

3 (a) Clark, C. D.; Hoffman, M. Z. *Coord. Chem. Rev.* **1997**, *159*, 359−373. (b) De Cola, L.; Belser, P. *Coord. Chem. Rev.* **1998**, *177*, 301−346. (c) Ward, M. D.; Barigelletti, F. *Coord. Chem. Rev.* **2001**, *216−217*, 127−154.

4 (a) Beer, P. D. *Acc. Chem. Res.* **1998**, *31*, 71−80. (b) Wu, A.; Yoo, D.; Lee, J.-K.; Rubner, M. F. *J. Am. Chem. Soc.* **1999**, *121*, 4883−4891. (c) Gao, F. G.; Bard, A. J. *J. Am. Chem. Soc.* **2000**, *122*, 7426−7427. (d) Demas, J. N.; DeGraff, B. A. *Coord. Chem. Rev.* **2001**, *211*, 317−351. (d) Polo, A. S.; Itokazu, M. K.; Iha, N. Y. M. *Coord. Chem. Rev.* **2004**, *248*, 1343−1361.

5 (a) Wilson, G. J.; Launikonis, A.; Sasse, W. H. F.; Mau, A. W.-H. *J. Phys. Chem. A* **1997**, *101*, 4860−4866. (b) Simon, J. A.; Curry, S. L.; Schmehl, R. H.; Schatz, T. R.; Piotrowiak, P.; Jin, X.; Thummel, R. P. *J. Am. Chem. Soc.* **1997**, *119*, 11012−11022. (c) Guerzo, A. D.; Leroy, S.; Fages, F.; Schmehl, R. H. *Inorg. Chem.* **2002**, *41*, 359−366. (d) Tyson, D. S.; Luman, C. R.; Zhou, X.; Castellano, F. N. *Inorg. Chem.* **2001**, *40*, 4063−4071.

6 (a) Barton, J. K. *Science* **1986**, *233*, 727−734. (b) Turro, C.; Bossmann, S. H.; Jenkins, Y.; Barton, J. K.; Turro, N. J. *J. Am. Chem. Soc.* **1995**, *117*, 9026−9032. (c) Gray, H. B.; Winkler, J. R. *Ann. Rev. Biochem.* **1996**, *65*, 537−561. (d) Guerzo, A. D.; Mesmaeker, A. K.-D. *Inorg. Chem.* **2002**, *41*, 938−945.

7 (a) Meyer, T. J.; Huynh, M. H. V. *Inorg. Chem.* **2003**, *42*, 8140−8160. (b) Masllorens, E.; Rodriguez, M.; Romero, I.; Roglans, A.; Parella, T.; Benet-Buchholz, J.; Poyatos, M.; Llobet, A. *J. Am. Chem. Soc.* **2006**, *128*, 5306−5307.

8 (a) Concepcion, J. J.; Jurss, J. W.; Templeton, J. L.; Meyer, T. J. *J. Am. Chem. oc.* **2008**, *130*, 16462−16463. (b) Tseng, H.-W.; Zong, R.; Muckerman, J. T.; Thummel, R. P. *Inorg. Chem.* **2008**, *47*, 11763−11773. (c) Romain, S.; Vigara, L.; Llobet, A. *Acc. Chem. Res.* **2009**, *42*, 1944−1953. (d) Concepcion, J. J.; Jurss, J. W.; Brennaman, M. K.; Hoertz, P. G.; Patrocinio, A. O. T.; Murakami Iha, N. Y.;

Templeton, J. L.; Meyer, T. J. *Acc. Chem. Res.* **2009**, *42*, 1954−1965. (e) Duan, L.; Tong, L.; Xu, Y.; Sun, L. *Energy Environ. Sci.* **2011**, *4*, 3296−3313. (f) Wasylenko, D. J.; Palmer, R. D.; Berlinguette, C. P. *Chem. Commun.* **2013**, *49*, 218−227.

9 (a) Masaoka, S.; Sakai, K. *Chem. Lett.* **2009**, *38*, 182−183. (b) Yoshida, M.; Masaoka, S.; Sakai, K. *Chem. Lett.*, **2009**, *38*, 702−703. (c) Yoshida, M.; Masaoka, S.; Abe, J.; Sakai, K. *Chem. Asian J.* **2010**, *5*, 2369−2378. (d) Kiyota, J.; Yokoyama, J.; Yoshida, M.; Masaoka, S.; Sakai, K. *Chem. Lett.*, **2010**, *39*, 1146−1148. (e) Kimoto, A.; Yamauchi, K.; Yoshida, M.; Masaoka, S.; Sakai, K. *Chem. Commun.*, **2012**, *48*, 239−241. (f) Okamura, M.; Yoshida, M.; Kuga, R.; Sakai, K.; Kondo, M.; Masaoka, S. *Dalton Trans.*, **2012**, *41*, 13081−13089.

10 (a) Yamazaki, H.; Hakamata, T.; Komi, M.; Yagi, M. *J. Am. Chem. Soc.* **2011**, *133*, 8846−8849. (b) Boyer, J. L.; Polyansky, D. E.; Szalda, D. J.; Zong, R.; Thummel, R. P.; Fujita, E. *Angew. Chem. Int. Ed.* **2011**, *50*, 12600−12604. (c) Padhi, S. K.; Fukuda, R.; Ehara, M.; Tanaka, K. *Inorg. Chem.* **2012**, *51*, 5386−5392. (d) Hirahara, M.; M. Ertem, Z.; Komi, M.; Yamazaki, H.; Cramer, C. J.; Yagi, M. *Inorg. Chem.* **2013**, *52*, 6354−6364.

11 (a) Nagao, H.; Mizukawa, T.; Tanaka, K. *Chem. Lett.* **1993**, *22*, 955−958. (b) Nakajima, H.; Kushi, Y.; Nagao, H.; Tanaka, K. *Organometallics*, **1995**, *14*, 5093−5098. (c) Tanaka, K.; Ooyama, D. *Coord. Chem. Rev.* **2002**, *226*, 211−218. (d) Savéant, J.-M. *Chem. Rev.* **2008**, *108*, 2348−2378.

12 Chen, Z.; Chen, C.; Weinberg, D. R.; Kang, P.; Concepcion, J. J.; Harrison, D. P.; Brookhart, M. S.; Meyer, T. J. *Chem. Commun.* **2011**, *47*, 12607−12609.

13 Matsubara, Y.; Fujita, E.; Doherty, M. D.; Muckerman, J. T.; Creutz, C. *J. Am. Chem. Soc.* **2012**, *134*, 15743−15757.

14 (a) Kobayashi, A.; Takatori, R.; Kikuchi, I.; Konno, H.; Sakamoto, K.; Ishitani, O. *Organometallics* **2001**, *20*, 3361−3363. (b) Kobayashi, A.; Konno, H.; Sakamoto, K.; Sekine, A.; Ohashi, Y.; Iida, M.; Ishitani, O. *Chem. Eur. J.* **2005**, *11*, 4219−4226. (c) Kimura, M.; Tanaka, K. *Angew. Chem. Int. Ed.* **2008**, *47*, 9768−9771. (d) Matsubara, Y.; Kosaka, T.; Koga, K.; Nagasawa, A.; Kobayashi, A.; Konno, H.; Creutz, C.; Sakamoto, K.; Ishitani, O. *Organometallics*, **1995**, *14*, 5093−5098.

15 Kinoshita, T.; Dy, J. T.; Uchida, S.; Kubo, T.; Segawa, H. *Nat. Photonics* **2013**, *7*, 535−539.

16 (a) Noyori, R.; Ohkuma, T. *Angew. Chem. Int. Ed.* **2001**, *40*, 40−73. (b) Noyori, R. *Angew. Chem. Int. Ed.* **2002**, *41*, 2008−2022.

17 (a) Schwab, P.; France, M. B.; Ziller, J. W.; Grubbs, R. H. *Angew. Chem. Int. Ed.* **1995**, *34*, 2039−2041. (b) Vougioukalakis, G. C.; Grubbs, R. H. *Chem. Rev.* **2010**, *110*, 1746−1787. (c) Samec, J. S. M.; Keitz, B. K.; Grubbs, R. H. *J. Organomet. Chem.* **2010**, *695*, 1831−1837.

18 (a) Clavier, H.; Nolan, S. P. *Chem. Eur. J.* **2007**, *13*, 8029−8036. (b) Nolan, S. P.; Clavier, H. *Chem. Soc. Rev.* **2010**, *39*, 3305−3316.

19 (a) Dutta, D. K.; Deb, B. *Coord. Chem. Rev.* **2011**, *255*, 1686−1712. (b) Yi, C. S. *J. Organomet. Chem.* **2011**, *696*, 76−80. (c) Mellone, I.; Peruzzini, M.; Rosi, L.; Mellmann, D.; Junge, H.; Beller, M.; Gonsalvi, L. *Dalton Trans.* **2013**, *42*, 2495−2501.

20 (a) Leising, R. A.; Grzybowski, J. J.; Takeuchi, K. J. *Inorg. Chem.* **1988**, *27*, 1020−1025. (b) Coe, B. J.; Thompson, D. W.; Culbertson, C. T.; Schoonover, J. R.; Meyer, T. J. *Inorg. Chem.* **1995**, *34*, 3385−3395. (c) Szczepura, L. F.; Kubow, S. A.; Leising, R. A.; Perez, W. J.; Huynh, M. H. V.; Lake, C. H.; Churchill, D. G.; Churchill, M. R.; Takeuchi, K. J. *J. Chem. Soc., Dalton Trans.: Inorg. Chem.* **1996**, *7*, 1463−1470. (d) Lim, J. W.; Yeo, H. J.; Jeong, J. H. *Acta Cryst.* **1997**, *C53*, 1405−1407. (e) Perez, W. J.; Lake, C. H.; See, R. F.; Toomey, L. M.; Churchill, M. R.; Takeuchi, K. J.; Radano, C. P.; Boyko, W. J.; Bessel, C. A. *J. Chem. Soc., Dalton Trans.* **1999**, 2281−2292. (f) Billings, S. B.; Mock, M. T.; Wiacek, K.; Turner, M. B.; Kassel, W. S.; Takeuchi, K. J.; Rheingold, A. L.; Boyko, W. J.; Bessel, C. A. *Inorg, Chim. Acta* **2003**, *355*, 103−115. (g) Spivak, G. J.; Beach, N. J. *Inorg. Chim. Acta.* **2003**, *343*, 244−252. (h) Sharma, S.; Singh, S. K.; Chandra, M.; Pandey, D. S. *J. Inorg. Biochem.* **2005**, *99*, 458−466. (i) Mishra, D.; Naskar, S.; Chattopadhyay, S. K.; Maji, M.; Sengupta, P.; Dinda, R.; Ghosh, S.; Mak, T. C. W. *Transit. Met. Chem.* **2005**, *30*, 352−356. (j) Mishra, D.; Barbieri, A.; Sabatini, C.; Drew, M. G. B.; Figgie, H. M.; Sheldrick, W. S.; Chattopadhyay, S. K. *Inorg. Chim. Acta.* **2007**, *360*, 2231−2244. (k) Ye, W.; Zhao, M.; Du, W.; Jiang, Q.; Wu, K.; Wu, P.; Yu, Z. *Chem. Eur. J.* **2011**, *17*, 4737−4741. (l) Małecki, J. G.; Maroń, A. *Polyhedron* **2012**, *44*, 221−227. (m) Tseng, K.-N. T.; Kampf, J. W.; Szymczak, N. K. *Organometallics* **2013**, *32*, 2046−2049. (n) Moore, C. M.; Szymczak, N. K. *Chem. Commun.* **2013**, *49*, 400−402.

21 (a) Sullivan, B. P.; Salmon, D. J.; Meyer, T. J. *Inorg. Chem.* **1978**, *17*, 3334−3341. (b) Sullivan, B. P.; Conrad, D.; Meyer, T. J. *Inorg. Chem.* **1985**, *24*, 3640−3645. (c) Otruba, J. P.; Neyhart, G. A.; Dressick, W. J.; Marshall, J. L.; Sullivan, B. P.; Watkins, P. A.; Meyer, T. J. *J. Photochem.* **1986**, *35*, 133−153. (d) Leising, R. A.; Takeuchi, K. J. *Inorg. Chem.* **1987**, *26*, 4391−4393. (e) Leising, R. A.; Ohman, J.

S.; Takeuchi, K. J. *Inorg. Chem.* **1988**, *27*, 3804−3809. (f) Bessel, C. A.; Margarucci, J. A.; Acquaye, J. H.; Rubmo, R. S.; Crandall, J.; Jircitano, A. J.; Takeuchi, K. J. *Inorg. Chem.* **1993**, *32*, 5779−5784. (g) Churchill, M. R.; Krajkowski, L. M.; Huynh, M. H. V.; Takeuchi, K. J. *J. Chem. Crystallogr.* **1997**, *27*, 589−597. (h) Salierno, M.; Marceca, E.; Peterka, D. S.; Yuste, R.; Etchenique, R. *J. Inorg. Biochem.* **2010**, *104*, 418−422. (i) Litke, S. V.; Ershov, A. Y.; Meyer, T. J. *J. Phys. Chem. A* **2011**, *115*, 14235−14242. (j) Miguel, V. S.; Álvarez, M.; Filevich, O.; Etchenique, R.; Campo, A. del *Langmuir* **2012**, *28*, 1217−1221. (k) Araya, R.; Andino-Pavlovsky, V.; Yuste, R.; Etchenique, R. *ACS Chem. Neurosci.* **2013**, *4*, 1163−1167. (l) Ogweno, A. O.; Ojwach, S. O.; Akerman, M. P. *Dalton Trans.* **2014**, *43*, 1228−1237. (m) Huang, J.; Chen, J.; Gao, H.; Chen, L. *Inorg. Chem.* **2014**, *53*, 9570−9580.

22 (a) Nikol'skii, A. B.; Egorova, M. B.; Repinskaya, T. S.; Gindin, V. A.; Popov, A. M. *Zhurnal Obshchei Khimii* **1986**, *56*, 2415−2416. (b) Sussuchi, E. M.; De Lima, A. A.; De Giovani, W. F. *Polyhedron* **2006**, *25*, 1457−1463. (c) Sinha, P.; Raghuvanshi, D. S.; Singh, K. N.; Mishra, L. *Polyhedron* **2012**, *31*, 227−234.

23 (a) Hecker, C. R.; Fanwick, P. E.; McMillin, D. R. *Inorg. Chem.* **1991**, *30*, 659−666. (b) Tsai, C.-N.; Allard, M. M.; Lord, R. L.; Luo, D.-W.; Chen, Y.-J.; Schlegel, H. B.; Endicott, J. F. *Inorg. Chem.* **2011**, *50*, 11965−11977.

24 Rasmussen, S. C.; Ronco, S. E.; Mlsna, D. A.; Billadeau, M. A.; Pennington, W. T.; Kolis, J. W.; Petersen, J. D. *Inorg. Chem.* **1995**, *34*, 821−829.

25 Takeuchi, K. J.; Thompson, M. S.; Pipes, D. W.; Meyer, T. J. *Inorg. Chem.* **1984**, *23*, 1845−1851.

26 Wehman, P.; van Donge, H. M. A.; Hagos, A.; Kamer, P. C. J.; van Leeuwen, P. W. N. M. *J. Organomet. Chem.* **1997**, *535*, 183−193.

27 Sullivan, B. P.; Calver, J. M.; Meyer, T. J. *Inorg. Chem.* **1980**, *19*, 1404−1407.

28 (a) Simándi, L. I.; Neméth, S. *Inorg. Chim. Acta* **1998**, *270*, 326−329. (b) Coe, B. J.; Glenwright, S. J. *Coord. Chem. Rev.* **2000**, *203*, 5−80. (c) Smithback, J. L.; Helms, J. B.; Schutte, E.; Woessner, S. M.; Sullivan, B. P. *Inorg. Chem.* **2006**, *45*, 2163−2174.

29 (a) Suzuki, T.; Kuchiyama, T.; Kishi, S.; Kaizaki, S.; Kato, M. *Bull. Chem. Soc. Jpn.* **2002**, *75*, 2433−2439. (b) Suzuki, T.; Kuchiyama, T.; Kishi, S.; Kaizaki, S.; Takagi, H. D.; Kato, M. *Inorg. Chem.* **2003**, *42*, 785−795.

30 (a) Suen, H.-F.; Wilson, S. W.; Pomerantz, M.; Walsh, J. L. *Inorg. Chem.* **1989**, *28*, 786−791. (b) Fanni, S.; Weldon, F. M.; Hammarstrom, L.; Mukhtar, E.; Browne, W. R.; Keyes, T. E.; Vos, J. G. *Eur. J. Inorg. Chem.* **2001**, *2*, 529−534.

31 Taketoshi, A.; Koizumi, T.; Kanbara, T. *Tetrahedron Lett.* **2010**, *51*, 6457−6459.
32 Wadman, S. H.; Lutz, M.; Tooke, D. M.; Spek, A. L.; Hartl, F.; Havenith, R. W. A.; van Klink, G. P. M.; van Koten, G. *Inorg. Chem.* **2009**, *48*, 1887−1900.
33 Frisch, M. J.; Trucks, G. W.; Schlegel, H. B.; Scuseria, G. E.; Robb, M. A.; Cheeseman, J. R.; Scalmani, G.; Barone, V.; Mennucci, B.; Petersson, G. A.; Nakatsuji, H.; Caricato, M.; Li, X.; Hratchian, H. P.; Izmaylov, A. F.; Bloino, J.; Zheng, G.; Sonnenberg, J. L.; Hada, M.; Ehara, M.; Toyota, K.; Fukuda, R.; Hasegawa, J.; Ishida, M.; Nakajima, T.; Honda, Y.; Kitao, O.; Nakai, H.; Vreven, T.; Montgomery Jr., J. A.; Peralta, J. E.; Ogliaro, F.; Bearpark, M.; Heyd, J. J.; Brothers, E.; Kudin, K. N.; Staroverov, V. N.; Keith, T.; Kobayashi, R.; Normand, J.; Raghavachari, K.; Rendell, A.; Burant, J. C.; Iyengar, S. S.; Tomasi, J.; Cossi, M.; Rega, N.; Millam, J. M.; Klene, M.; Knox, J. E.; Cross, J. B.; Bakken, V.; Adamo, C.; Jaramillo, J.; Gomperts, R.; Stratmann, R. E.; Yazyev, O.; Austin, A. J.; Cammi, R.; Pomelli, C.; Ochterski, J. W.; Martin, R. L.; Morokuma, K.; Zakrzewski, V. G.; Voth, G. A.; Salvador, P.; Dannenberg, J. J.; Dapprich, S.; Daniels, A. D.; Farkas, O.; Foresman, J. B.; Ortiz, J. V.; Cioslowski, J.; Fox, D. J. *Gaussian 09 (Revision C.01)*, Gaussian, Inc. Wallingford CT, **2010**.
34 Becke, A. D. *J. Chem. Phys.* **1993**, *98*, 5648−5652.
35 Lee, C.; Yang, W.; Parr, R. G. *Phys. Rev. B* **1988**, *37*, 785−789.
36 (a) Dunning Jr., T. H.; Hay, P. J. in *Modern Theoretical Chemistry*, ed. Schaefer III, H. F.; Plenum, New York, **1976**. (b) Hay, P. J.; Wadt, W. R. *J. Chem. Phys*. **1985**, *82*, 270−283. (c) Hay, P. J.; Wadt, W. R. *J. Chem. Phys*. **1985**, *82*, 299−310.
37 Cossi, M.; Scalmani, G.; Rega, N.; Barone, V. *J. Chem. Phys.* **2002**, *117*, 43−54.
38 (a) Casida, M. E.; Jamorski, C.; Casida, K. C.; Salahub, D. R. *J. Chem. Phys.* **1998**, *108*, 4439−4449. (b) Stratmann, R. E.; Scuseria, G. E.; Frisch, M. J. *J. Chem. Phys.* **1998**, *109*, 8218−8224. (c) Bauernschmitt, R.; Ahlrichs, R. *Chem. Phys. Lett.* **1996**, *256*, 454−464.
39 SPECFIT. Spectrum Research Associate: Chapel Hill, NC.
40 (a) Casado, A. L.; Espinet, P. *Organometallics* **1998**, *17*, 954−959. (b) Casado, A. L.; Casares, J. A.; Espinet, P. *Inorg. Chem.* **1998**, *37*, 4154−4156. (c) Robertus, J.; Reker, S. F.; Pijper, T. C.; Deuzeman, A.; Browne, W. R.; Feringa, B. L. *Phys. Chem. Chem. Phys.* **2012**, *14*, 4374−4382. (d) Glöckner, A.; Banneberg, T.; Ibrom, K.; Daniliuc, C. G.; Freytag, M.; Jones, P. G.; Walter, M. D.; Tamm, M. *Organometallics* **2012**, *31*, 4480−4494. (e) Howarth, A. J.; Davies, D. L.; Lelj, F.; Wolf, M. O.; Patrick, B. O. *Dalton Trans.* **2012**, *41*, 10150−10152.
41 Helm, L.; Merbach, A. E. *Chem. Rev.* **2005**, *105*, 1923−1959.

42 Kaim, W.; Reinhardt, R.; Sieger, M. *Inorg. Chem.* **1994**, *33*, 4453−4459.
43 Feltham, R. D.; Metzger, H. G. *J. Organomet. Chem.* **1971**, *33*, 347−345.
44 Altomare, A.; Cascarano, G.; Giacovazzo, C.; Guagliardi, A. J. *J. Appl. Cryst.* **1993**, *26*, 343−350.
45 Sheldrick, G. M. *Acta Crystallogr. Sect. A* **2008**, *64*, 112−122.
46 Farrugia, L. J. *J. Appl. Crystallogr.* **1997**, *30*, 565.
47 Fenn, T. D.; Ringe, D.; Petsko, G. A. *J. Appl. Crystallogr.* **2003**, *36*, 944−947.

Chapter 2

Synthesis and Properties of Phosphine-Substituted Ruthenium(II) Polypyridine Complexes with Nitrogen Oxide

To be submitted to Dalton Transactions.

Introduction

Ruthenium(II) polypyridine complexes are an intriguing class of materials not only for the fundamental understanding of coordination chemistry including electrochemistry, photochemistry, and photophysics,[1] but also for the potential applications to energy conversion,[2] luminescent sensors,[3] electroluminescence displays,[4] and biotechnology.[5] Of particular interest are ruthenium(II) complexes composed of tridentate and bidentate polypyridine ligands and a monodentate labile ligand, $[Ru(TL)(BL)(L)]^{n+}$ (TL = tridentate polypyridine ligand, BL = bidentate polypyridine ligand, and L = monodentate labile ligand) due to their catalytic activity for various reactions such as oxidation,[6-9] reduction,[10-12] and photo-induced reactions.[13]

Phosphine containing ruthenium(II) complexes are also attractive targets for potential applications to energy conversion system[14] and catalysis.[15-17] In these examples, electronic structures of the ruthenium centre are finely tuned thanks to the σ-donating and π-accepting abilities of phosphine ligands. Thus, the substitution of coordinating N atom to P atom in ruthenium(II) polypyridine complexes should be one of the key strategies to develop the metal complexes with novel properties and reactivity.

In our previous report,[18] we have succeeded for the first time in the syntheses and structural determination of a series of phosphine containing ruthenium(II) polypyridine complexes with $[Ru(TL)(BL)(L)]^{n+}$-type structure. 8-(Diphenylphosphanyl)quinoline (Pqn) and 1,2-bis(diphenylphosphanyl)benzene (dppbz) were selected as phosphine containing ligand and acetonitrile (MeCN) was used as a labile ligand (Scheme 1), and the effects of the number and position of phosphine donors on the structures and electronic properties were investigated. Furthermore, unique isomerization behaviours of complexes were observed and the coordinating P atom revealed to play crucial role on these isomerization reactions. These results encouraged us to investigate the effect of

P atom on the physical properties of Ru-based metal complexes in more detail.

Here we show the syntheses, structural characterization, and electrochemical and spectroscopic properties of a series of ruthenium(II) polypyridine complexes containing Pqn or dppbz with nitric oxides. Three novel nitrite complexes, *trans(P,NO_2)*-, and *cis(P,NO_2)*-[Ru(trpy)(Pqn)(NO_2)]PF_6 (***trans*-NO_2** and ***cis*-NO_2**, trpy = 2,2':6',2"-terpyridine), and **[**Ru(trpy)(dppbz)(NO_2)]PF_6 (**PP-NO_2**), were successfully synthesized and their electronic structure were analysed by single crystal X-ray structural determination, UV-vis absorption spectra and electrochemical measurements. Furthermore, one nitrosyl complex, *cis(P,NO)*-[Ru(trpy)(Pqn)(NO)]$(PF_6)_3$ (***cis*-NO**), was synthesised from ***cis*-NO_2** and its properties were examined. We also investigated the reactivity of labile sites for nitrite and nitrosyl complexes in comparison with corresponding acetonitrile complexes and found that their stability are determined not only by the number and position of phosphine donor but also by the properties of labile ligands.

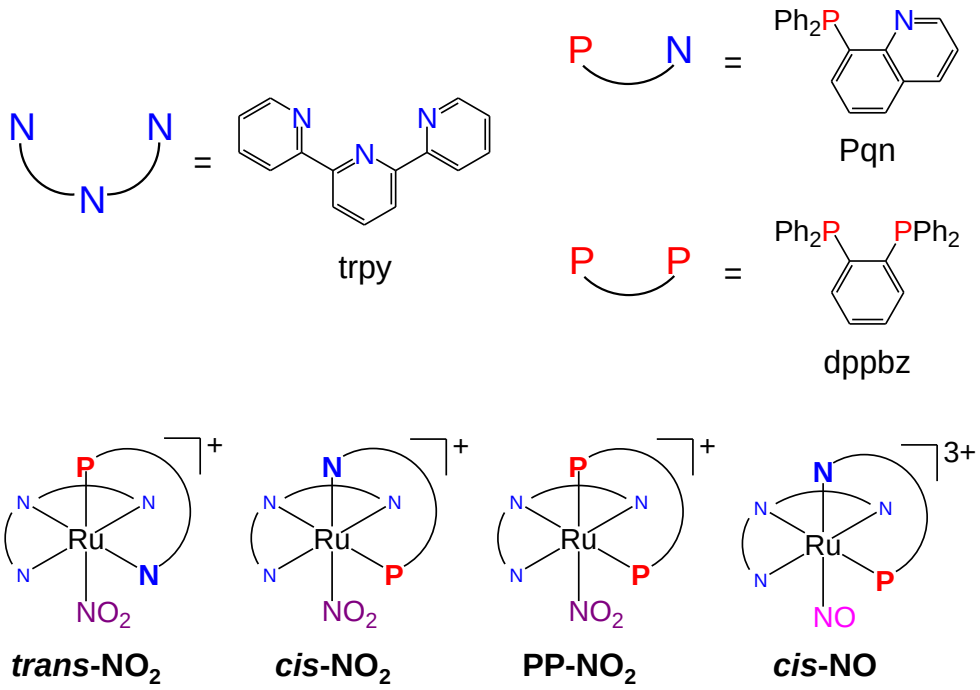

Scheme 1. Structures of a tridentate ligand (trpy), bidentate ligands (Pqn and dppbz), and metal complexes (***trans*-NO_2**, ***cis*-NO_2**, **PP-NO_2**, and ***cis*-NO**) used in this study.

Results and Discussion

Synthesis and Characterization

Synthetic procedures to obtain ***trans*-NO_2**, ***cis*-NO_2**, and **PP-NO_2** are shown in Scheme 2. ***trans*-MeCN**, ***cis*-MeCN**, and **PP-MeCN** were synthesized following the method we previously reported.[18] Reaction of obtained acetonitrile complexes with excess amount of $NaNO_2$ in 1:1 mixture of ethanol:water at 100°C gave the corresponding nitro complexes[19] (***trans*-NO_2**, ***cis*-NO_2**, and **PP-NO_2**) and the desired products were characterized by the ^{1}H NMR and $^{31}P\{^1H\}$ NMR spectroscopy and elemental analysis. The $^{31}P\{^1H\}$ NMR spectra of ***trans*-NO_2** and ***cis*-NO_2** in CD_3CN gave a singlet at δ 53.10 and 54.06, showing upfield shifts ($\Delta\delta$ = 5.70 and 1.90) compared to the signals in the spectra of corresponding acetonitrile complex, ***trans*-MeCN** and ***cis*-MeCN** (δ 58.80 and 55.96), respectively. The $^{31}P\{^1H\}$ NMR spectrum of **PP-NO_2** in CD_3CN afforded two doublets at δ 62.65 and 68.59 with coupling constants of 14.2 Hz, showing upfield shifts ($\Delta\delta$ = 5.85 and 1.18) compared to the signals in the spectrum of **PP-MeCN** (68.57 and 69.77, $^2J_{P-P}$ = 20.2 Hz).

The syntheses of ruthenium nitrosyl complexes were performed by adding excess amount of HPF_6 to the acetone solution of nitrito complex at 0°C. Although the preparation of ***trans*-NO** and **PP-NO** from trans-NO_2 and **PP-NO_2** were not successful due to the instability of nitrosyl complex or reaction intermediate under acidic condition (For detail, see Figure 1), ***cis*-NO** was isolated in moderate yield (85%) and was characterized by ^{1}H NMR and $^{31}P\{^1H\}$ NMR spectroscopy and elemental analysis. The $^{31}P\{^1H\}$ NMR spectra of ***cis*-NO** in acetone-d_6 gave a singlet at δ 54.23. ***cis*-NO** immediately converted to a solvent-coordinated complex in highly coordinative solvent such as acetonitrile, but was stable in less-coordinative solvent such as acetone and γ-butyrolactone.

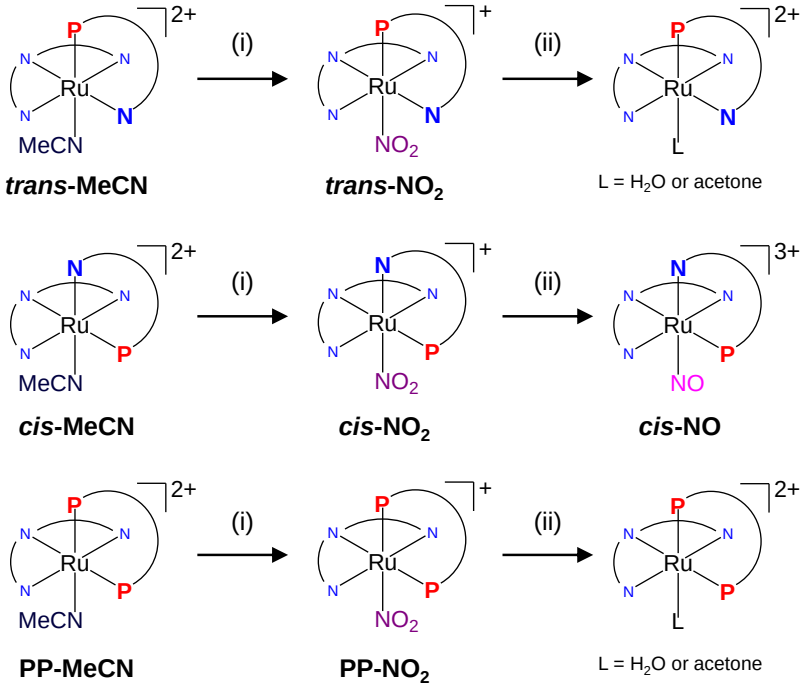

Scheme 2. Syntheses of ***trans*-NO_2**, ***cis*-NO_2**, **PP-NO_2**, and ***cis*-NO**. (i) $NaNO_2$ in 1:1 mixture of ethanol:water at 100ºC. (ii) HPF_6 in acetone at 0ºC.

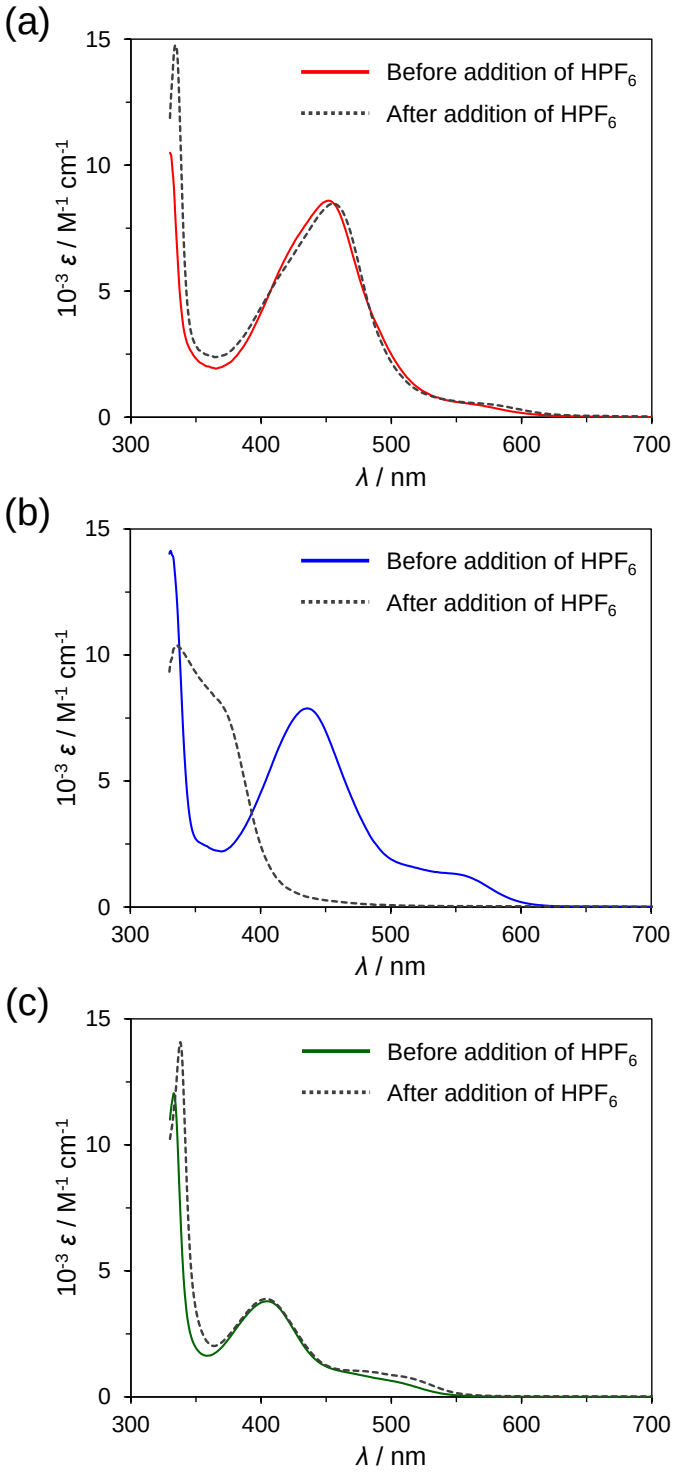

Figure 1. UV-vis absorption spectra of (a) ***trans*-NO_2**, (b) ***cis*-NO_2**, and (c) **PP-NO_2** in acetone at 0 °C before and after addition of a few drops of HPF_6. Only ***cis*-NO_2** showed large blue shift (100 nm) to 336 nm, suggesting the formation of a corresponding nitrolsyl complex.

Crystal Structures

Single crystals of ***trans*-NO_2** and **PP-NO_2** suitable for structural determination was obtained by recrystallization from diethyl ether/methanol/acetonitrile. Single crystals of *cis*-nitrite complex were obtained as the BPh_4^- salt, *cis(P,NO_2)*-[Ru(trpy)(Pqn)(NO_2)]BPh_4 (***cis*-NO_2'**), prepared by adding excess amount of $NaBPh_4$ instead of NH_4PF_6 after the reaction. The molecular structures of ***trans*-NO_2**, ***cis*-NO_2'** and **PP-NO_2** determined by single-crystal X-ray crystallography and the summary of crystallographic data are shown in Figure 2 and Table 1-2, respectively. The asymmetric unit of the monoclinic $P2_1/n$ crystal of ***trans*-NO_2** contained one cationic ruthenium complex, one PF_6 anion, and one acetonitrile molecule. The ***cis*-NO_2'** crystallizes with two crystallographically independent ruthenium complexes, two BPh_4 anions, and one acetonitrile molecule as the crystal solvent in the asymmetric unit of the triclinic $P\bar{1}$ space group. The asymmetric unit of the monoclinic $P2_1/c$ crystal of **PP-NO_2** contained one cationic ruthenium complex, one PF_6 anion, and two methanol molecules. For all complexes, the ratio of ruthenium to counter anion indicates that the oxidation states of ruthenium centre are two. The coordination geometry at each Ru atom is that of a distorted octahedron composed of a meridionally coordinated terpyridine ligand, a bidentate ligand, and a nitrite ligand.

Bond distances between the ruthenium atom and nitrogen atom of the nitrite ligand of ***trans*-NO_2** and **PP-NO_2** were 2.141(3) (Ru1–N5) and 2.124(2) Å (Ru1–N4), respectively (Figure 3), and are longer than that found in [Ru(trpy)(bpm)(NO_2)]PF_6 (2.034(5) Å, bpm = 2,2'-bipyrimidine).[20] In contrast, the Ru–N(NO_2) distances of ***cis*-NO_2'** (2.0362(18) and 2.0290(18) Å for Ru1–N5 and Ru2–N10, respectively, Figure 3) were similar to that of [Ru(trpy)(bpm)(NO_2)]PF_6 (2.034(5) Å).[20] These results indicate the stronger *trans* influence of the phosphorous atom of Pqn or dppbz compared to that of the nitrogen atom of bpm or bpy. This tendency was also observed in ***trans*-MeCN**, ***cis*-MeCN**, and **PP-MeCN** in our previous study.[18]

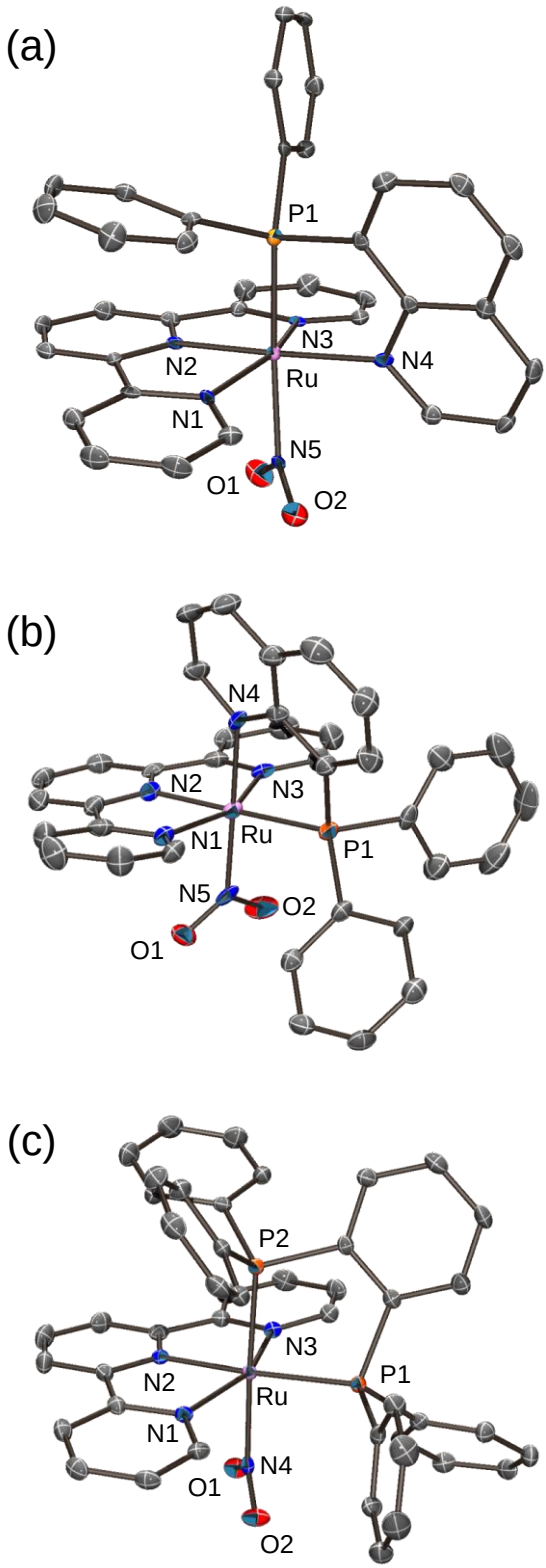

Figure 2. ORTEP drawings (50% probability level) of cataionic complexes in (a) ***trans*-NO_2**, (b) ***cis*-NO_2'**, and (c) **PP-NO_2**. Hydrogen atoms are omitted for clarity.

Table 1. Crystallographic data for ***trans*-NO_2**, ***cis*-NO_2'**, **PP-NO_2**.

Complex	***trans*-NO_2**·CH_3CN	***cis*-NO_2'**·0.5CH_3CN	**PP-NO_2**·2CH_3OH
Formula	$C_{38}H_{30}F_6N_6O_2P_2Ru$	$C_{61}H_{48.5}BN_{5.5}O_2PRu$	$C_{47}H_{43}F_6N_4O_4P_3Ru$
Formula weight	879.69	1033.40	1035.83
T, ºC	−170	−170	−170
Crystal color, habit	red, needle	orange-red, platelet	orange, block
Crystal system	monoclinic	triclinic	monoclinic
Crystal size, mm^3	0.30 × 0.05 × 0.05	0.15 × 0.15 × 0.10	0.15 × 0.10 × 0.05
Space group	$P\,2_1/n$	$P\,\bar{1}$	$P\,2_1/c$
a, Å	12.1909(17)	10.2764(2)	17.1049(6)
b, Å	11.9003(17)	21.2343(4)	13.0763(6)
c, Å	25.260(4)	24.3802(4)	20.1547(8)
α, º	90	77.0060(10)	90
β, º	99.579(3)	78.9530(10)	106.853(3)
γ, º	90	74.9360(10)	90
V, $Å^3$	3613.5(9)	4955.30(16)	4314.4(3)
Z	4	4	4
D calc, g cm^{-3}	1.617	1.385	1.595
μ, mm^{-1}	0.599	0.400	0.552
F (000)	1776	2132	2112
R_1 [a]	0.0596	0.0337	0.0397
wR_2 [b]	0.1678	0.1071	0.0941
Goodness-of-fit S	1.032	1.178	1.004

[a] $R_1 = -\Sigma||Fo|-|Fc|| / \Sigma|Fo|$. [b] $wR_2 = [\Sigma(w(Fo^2-Fc^2)^2) / \Sigma w(Fo^2)^2]^{1/2}$

Table 2 Selected bond distances (Å) and angles (°) for ***trans*-NO_2**, ***cis*-NO_2'**, and **PP-NO_2**.

***trans*-NO_2**·CH_3CN		***cis*-NO_2'**·0.5CH_3CN				**PP-NO_2**·2CH_3OH	
Ru1–N1	2.085(4)	Ru1–N1	2.1066(18)	Ru2–N6	2.1353(19)	Ru1–N1	2.125(2)
Ru1–N2	1.971(4)	Ru1–N2	2.0153(18)	Ru2–N7	2.0248(19)	Ru1–N2	2.020(2)
Ru1–N3	2.081(4)	Ru1–N3	2.1066(18)	Ru2–N8	2.1012(19)	Ru1–N3	2.095(2)
Ru1–N4	2.143(4)	Ru1–N4	2.1080(18)	Ru2–N9	2.1241(18)	Ru1–N4	2.124(2)
Ru1–N5	2.146(4)	Ru1–N5	2.0362(18)	Ru2–N10	2.0290(18)	Ru1–P1	2.2958(7)
Ru1–P1	2.2952(13)	Ru1–P1	2.2981(6)	Ru2–P2	2.3005(6)	Ru1–P2	2.3270(7)
N5–O1	1.199(6)	N5–O1	1.251(3)	N10–O3	1.253(3)	N4–O1	1.252(3)
N5–O2	1.246(6)	N5–O2	1.251(3)	N10–O4	1.253(3)	N4–O2	1.229(3)
N1–Ru1–N2	79.00(17)	N1–Ru1–N2	78.31(7)	N6–Ru2–N7	77.74(8)	N1–Ru1–N2	77.59(9)
N2–Ru1–N3	79.43(17)	N2–Ru1–N3	78.35(8)	N7–Ru2–N8	78.25(7)	N2–Ru1–N3	78.46(9)
N4–Ru1–P1	82.00(12)	N4–Ru1–P1	82.65(5)	N9–Ru2–P2	82.51(5)	P1–Ru1–P2	84.10(3)
O1–N5–O2	122.4(5)	O1–N5–O2	117.75(19)	O3–N10–O4	118.00(18)	O1–N4–O2	118.5(2)

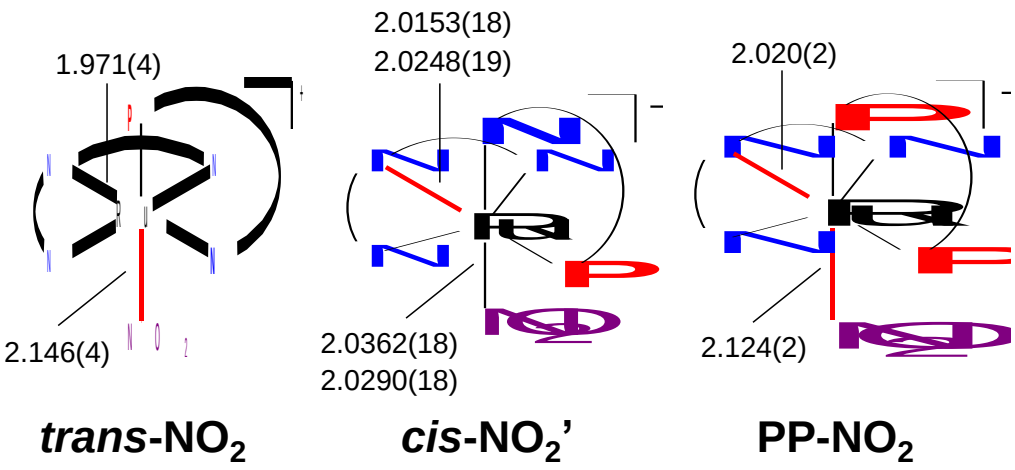

Figure 3. Comparison of bond distances (Å) around ruthenium centers of ***trans*-NO_2**, ***cis*-NO_2'**, and **PP-NO_2**.

UV-Vis Absorption Spectra.

Figure 4 shows the UV-Vis absorption spectra of a series of nitrite complexes (***trans*-NO_2**, ***cis*-NO_2**, and **PP-NO_2**) in acetonitrile solution. Spectral data for these three complexes and related compounds are listed in Table 3. All complexes display intense absorption bands in the UV region, assigned to ligand-based π–π* transitions. Additionally, a moderately intense band was observed in the visible region for each complex. TD-DFT calculations performed using the B3LYP/LandL2DZ basis sets indicate that the band can be assigned to the metal-to-ligand charge transfer (MLCT) transition from the dπ orbitals of ruthenium to the π* orbitals of trpy, and Pqn or dppbz (For detail, see Table 5 and Figures 6-9). The molar absorption coefficient of **PP-NO_2** was nearly half those of ***trans*-NO_2** and ***cis*-NO_2**.The absorption maxima (λ_{max}) of the MLCT transition of ***trans*-NO_2**, ***cis*-NO_2**, and **PP-NO_2** are 443, 431, and 402 nm, respectively and was blue-shifted compared with that of $[Ru(trpy)(bpm)(NO_2)]PF_6$,[20] suggesting the stabilization of the dπ orbitals of the ruthenium centre upon the introduction of the phosphine donors. Note that the MLCT transition energy of ***cis*-NO_2** was larger than that of ***trans*-PN** despite their isomeric relationship, which indicate that the position of phosphorus atom affects the electronic structure of the complexes. The similar the tendency of blue shift was also observed in a series of acetonitrile complexes, ***trans*-MeCN**, ***cis*-MeCN**, and **PP-MeCN**.[18]

UV-vis absorption spectra of *cis*-isomers with different labile ligands, *cis(P,L)*-$[Ru(trpy)(Pqn)(L)]^{n+}$ (L = Cl^-, NO_2^-, MeCN and NO^+), in ethylene glycol are shown in Figure 5. All complexes exhibit ligand-based π–π* transitions in the UV region and MLCT transition in the visible region. MLCT transition of ***cis*-NO** was observed at λ_{max} = 383 nm and is comparable to the related compounds[19-21] as shown in Table 4. The energy of lowest energy transitions of *cis*-isomers are in the order of L = Cl^- (468 nm) < NO_2^- (423 nm) < MeCN (413 nm) < NO^+ (383 nm), reflecting the coordinating ability of labile ligand, L. This result suggests that the donation of electron from L destabilizes the ruthenium based filled MOs, and the strength of ligand field has changed. These observations in absorption spectra indicate that the electronic structure of complex can be controlled not only by the number and the position of P atoms but also by the donating ability of labile ligands.

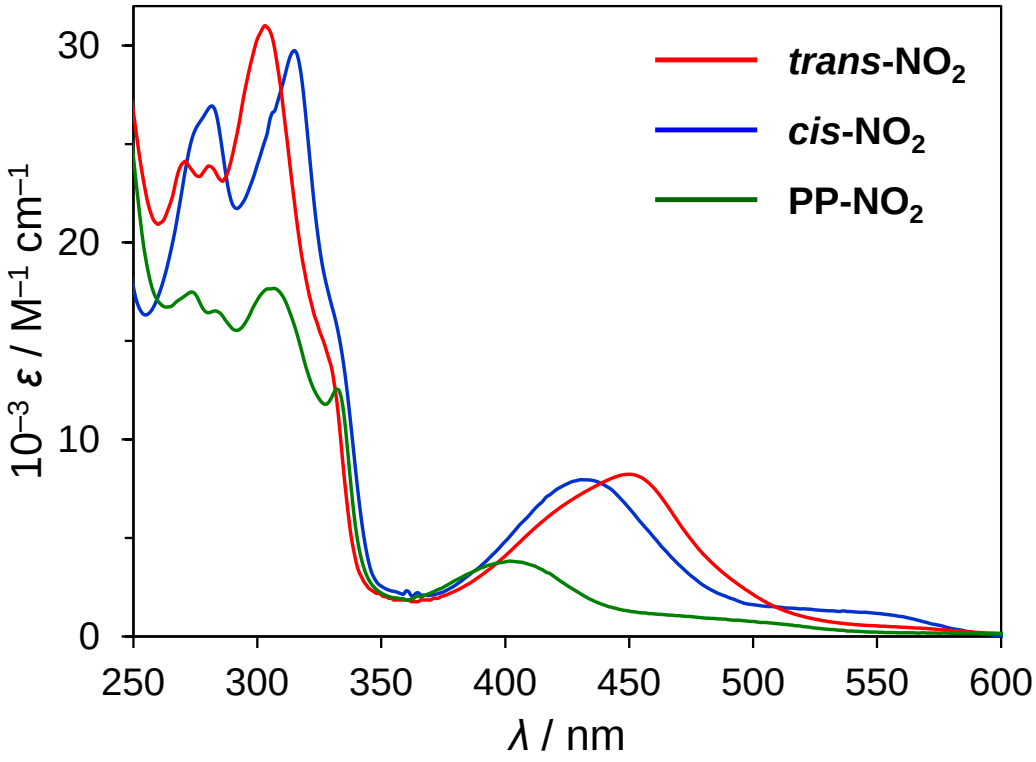

Figure 4. UV-Vis absorption spectra of **NN**, ***trans*-PN**, ***cis*-PN**, and **PP** in acetonitrile at room temperature.

Table 3. UV-Vis absorption data (λ_{max}/nm (10^{-3} ε/M^{-1} cm^{-1})) in acetonitrile and infrared data (ν/cm^{-1}) for ***trans*-NO_2**, ***cis*-NO_2**, **PP-NO_2**, and [Ru(trpy)(bpm)(NO_2)]PF_6 at room temperature.

		IR[c]	
complex	λ_{max}	$\nu_{as}(NO_2)$	$\nu_{s}(NO_2)$
***trans*-NO_2**	443 (8.02), 327[b], 303 (31.0), 281 (23.9), 271 (24.1)	1349	1304
***cis*-NO_2**	431 (7.95), 331[b], 315 (29.7), 282 (26.9), 276[b]	1339	1286
PP-NO_2	402 (3.82), 332 (12.6), 307 (17.7), 283 (16.5), 273 (17.5)	1354	1311
[Ru(trpy)(bpm)(NO_2)]PF_6[a]	470 (6.50), 362 (6.10), 330[b], 308 (25.6), 264 (23.3)	1342	1286

[a] Reference 20. [b] Absorption shoulder. [c] Infrared data for $NaNO_2$: 1335 ($\nu_{as}(NO_2)$) and 1250 ($\nu_{s}(NO_2)$) cm^{-1}. Reference 28.

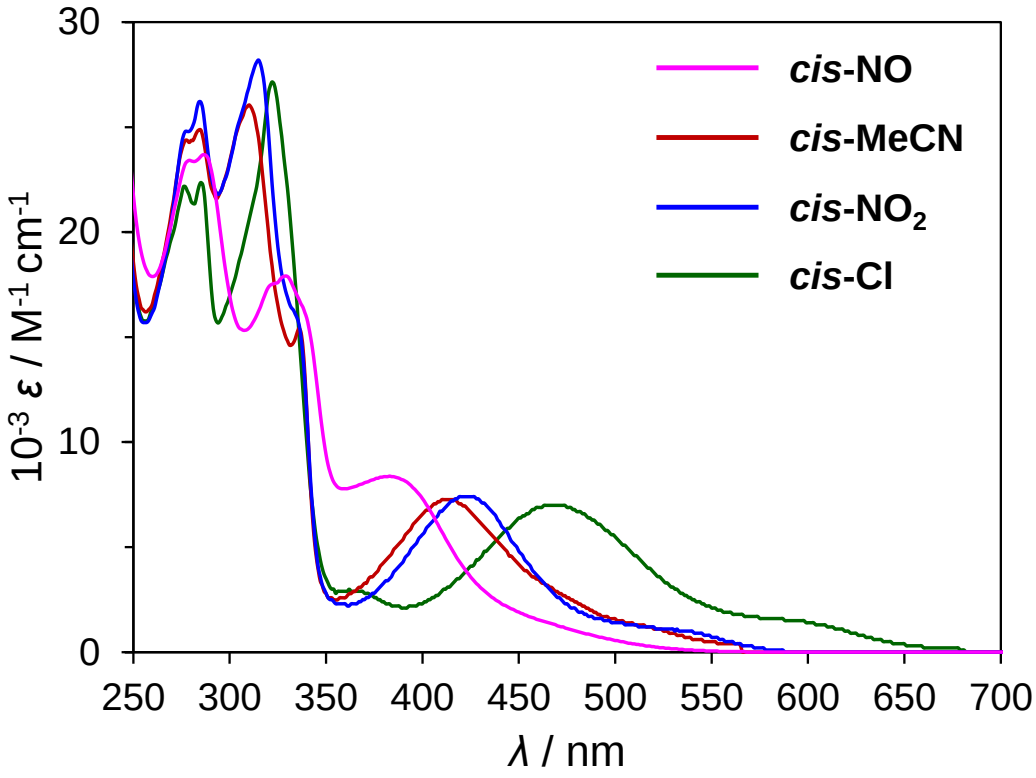

Figure 5. UV-Vis absorption spectra of *cis(P,X)*-[Ru(trpy)(Pqn)(L)]^{n} (L = Cl^{-}, NO_2, MeCN, NO^{+}) in ethylene glycol at room temperature.

Table 4. UV-Vis absorption data (λ_{max}/nm (10^{-3} ε/M^{-1} cm^{-1})) in acetonitrile and infrared data (ν/cm^{-1}) for ***cis*-NO** and related compounds at room temperature.

complex	λ_{max}	ν_{N-O}
***cis*-NO**[a]	383 (8.38), 329 (17.9), 323[e], 287 (23.7), 279[e]	1929
[Ru(trpy)(bpy)(NO)]$(PF_6)_3$[b]	336[e], 305, 292(10.00)	1952
[Ru(trpy)(bpm)(NO)]$(PF_6)_3$[c]	362 (5.12), 331[e], 312[e], 291 (8.93), 265 (10.8)	1957
trans(P,P)-[Ru(trpy)$(PPh_3)_2$(NO)]$(ClO_4)_3$[d]	393[e], 330 (32)	1900

[a] UV-Vis data in ethylene glycol. [b] Reference 21. [c] Reference 20. [d] Reference 19. [e] Absorption shoulder.

DFT Calculations.

To discuss the electronic structures of ***trans*-NO_2**, ***cis*-NO_2**, and **PP-NO_2**, density functional theory (DFT) calculations were conducted using the Gaussian 09 programs[21] with the B3LYP[22,23] functional and LanL2DZ basis set.[24] All calculations were performed with the polarizable continuum model (PCM)[25] to account for solvent effects in acetonitrile. All optimized structures were shown in Figure 6.

The highest occupied molecular orbitals (HOMOs, HOMO to HOMO−2) and the lowest unoccupied molecular orbitals (LUMOs, LUMO to LUMO+2) are illustrated in Figure 7. The HOMOs of ***trans*-NO_2** and ***cis*-NO_2** contain dπ (d_{xy}, d_{yz}, and d_{zx}) characteristics of ruthenium with distribution to the π* orbitals of trpy, Pqn, and acetonitrile ligands and σ* orbitals of P−C bonds in the phosphine donors. The LUMOs are dominated mainly by π* orbitals of trpy or Pqn. The frontier orbitals of **PP-NO_2** are similar to those of ***trans*-NO_2** and ***cis*-NO_2**, except that the π* orbitals of dppbz are not involved in orbitals from HOMO−2 to LUMO+2. The HOMO energy levels of ***trans*-NO_2**, ***cis*-NO_2**, and **PP-NO_2** were −6.04, −6.06, and −6.31 eV (Figure 8), respectively, indicating a tendency similar to that observed in the oxidation potentials (E_{pc}) in cyclic voltammograms (0.79, 0.82, and 0.95 V vs Fc/Fc^+), as discussed later.

Electronic transitions for the complexes were investigated using the time-dependent density functional theory (TD-DFT) method.[26] Calculated excitation wavelengths and oscillator strengths for selected transitions are listed in Table 5, and absorption spectra based on these calculated transitions with Gaussian functions are depicted in Figure 9. The profiles of convoluted absorption spectra are similar to those observed experimentally. For ***trans*-NO_2** and ***cis*-NO_2**, transitions in the visible light region arise mainly from the MLCT transition from the dπ orbitals of ruthenium (HOMOs) to the π* orbitals of trpy (LUMO and LUMO+1) and Pqn (LUMO+2). For **PP-NO_2**, the transitions arise mainly from dπ orbitals of ruthenium (HOMOs) to π* orbitals of trpy (LUMO and LUMO+1), which do not involve the π* orbitals of dppbz. Intensity of the simulated absorption of **PP-NO_2** was nearly 50% of those of ***trans*-NO_2** and ***cis*-NO_2**, which is consistent with the experimental results (Figure 4).

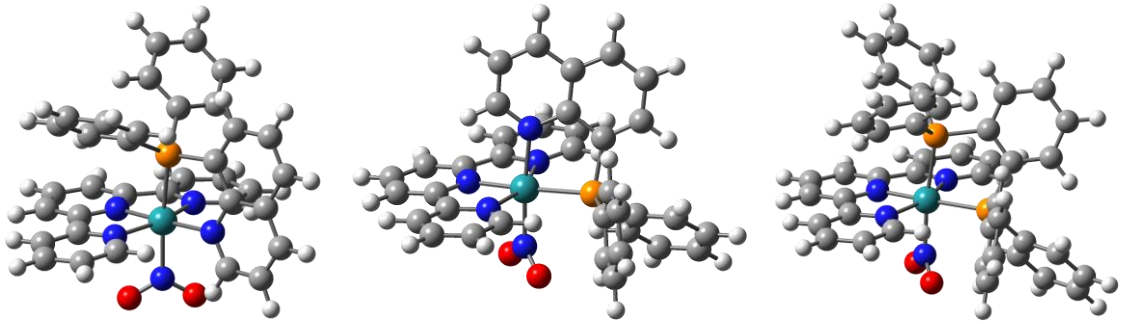

Figure 6. Optimized structures of cationic moieties of ***trans*-NO$_2$**, ***cis*-NO$_2$**, and **PP-NO$_2$**.

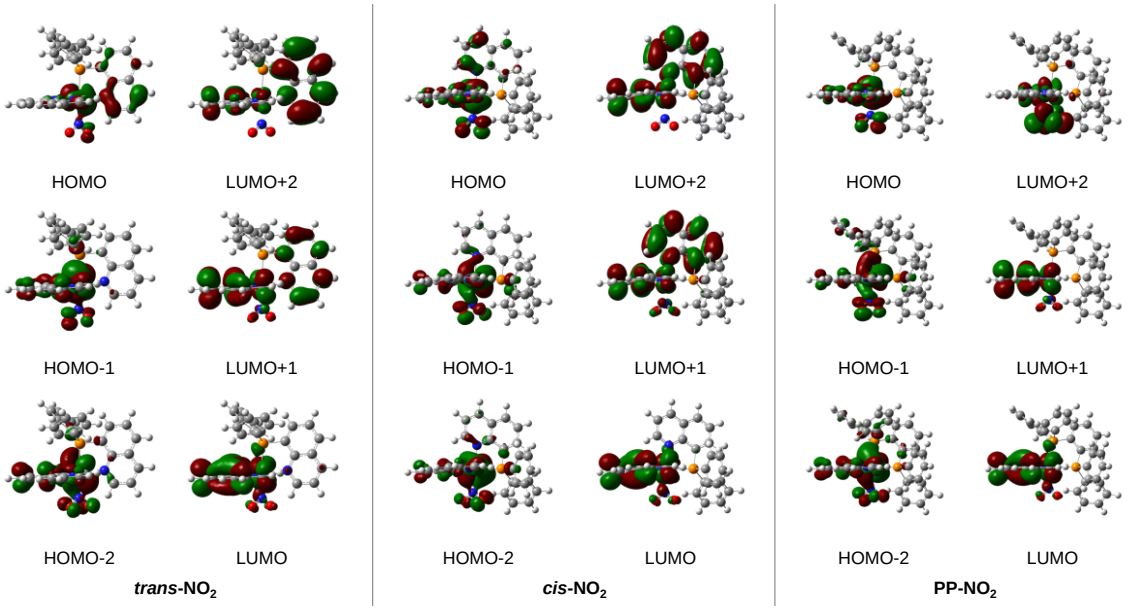

Figure 7. Isodensity surface plots of selected frontier molecular orbitals of ***trans*-NO$_2$**, ***cis*-NO$_2$**, and **PP-NO$_2$** based on the optimized ground-state geometry.

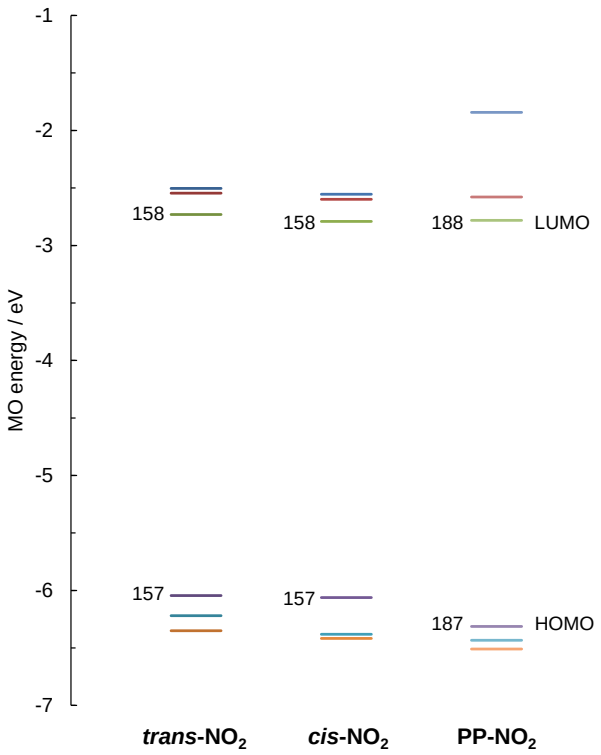

Figure 8. Diagram of DFT-derived molecular orbital energies of ***trans*-NO_2**, ***cis*-NO_2**, and **PP-NO_2**.

Complex	λ / nm	*f*	Transition			|CI coef| (> 0.3)
***trans*-NO_2**	440.86	0.0681	HOMO–2	→	LUMO	0.49267
			HOMO	→	LUMO+2	0.37097
	434.46	0.0589	HOMO–1	→	LUMO+1	0.30404
			HOMO	→	LUMO+2	0.49097
	411.01	0.0260	HOMO–2	→	LUMO+1	0.40021
			HOMO–1	→	LUMO+2	0.31482
	404.06	0.0341	HOMO–2	→	LUMO+1	0.53011
***cis*-NO_2**	436.63	0.0714	HOMO	→	LUMO+2	0.49267
	420.79	0.0489	HOMO–2	→	LUMO	0.30590
			HOMO–2	→	LUMO+1	0.34591
			HOMO–1	→	LUMO	0.32855
			HOMO	→	LUMO+1	0.33384
	415.44	0.0200	HOMO–1	→	LUMO+1	0.63146
	407.86	0.0246	HOMO–2	→	LUMO+1	0.58333
PP-NO_2	413.93	0.0299	HOMO–2	→	LUMO+1	0.32625
			HOMO–1	→	LUMO+1	0.35894
			HOMO	→	LUMO+1	0.37271
	402.79	0.0364	HOMO–1	→	LUMO+1	0.59003
	390.03	0.0317	HOMO–2	→	LUMO+1	0.60400

Table 5. Calculated TD-DFT excitation energies of ***trans*-NO_2**, ***cis*-NO_2**, and **PP-NO_2** in acetonitrile media. *f* denotes the oscillator strength calculated for each transition.

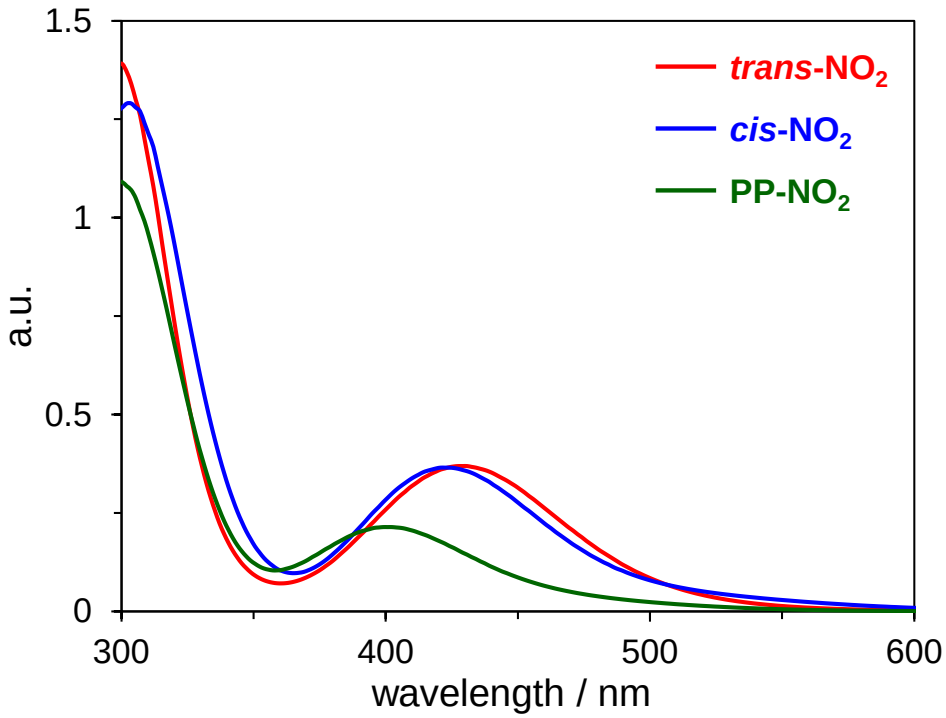

Figure 9. Simulated absorption spectra of ***trans*-NO_2**, ***cis*-NO_2**, and **PP-NO_2** in acetonitrile based on TD-DFT calculations.

Electrochemical Properties.

The cyclic voltammograms (CVs) of ***trans*-NO_2**, ***cis*-NO_2**, and **PP-NO_2** are shown in Figure 10. Electrochemical data of these complexes and related compounds are listed in Table 5. The CVs were measured in 0.1 M tetraethylammonium perchlorate (TEAP)/acetonitrile. ***cis*-NO_2** displayed one reversible oxidation wave in the positive region at $E_{1/2}$ = 0.79 V vs ferrocene/ferrocenium (Fc/Fc^+), which is assigned to a Ru(III)/Ru(II) redox couple. In contrast, ***trans*-NO_2** and **PP-NO_2** exhibited one irreversible (E_{pc} = 0.79 for ***trans*-NO_2** and 0.95 V for **PP-NO_2**) and one reversible ($E_{1/2}$ = 0.97 for ***trans*-NO_2** and 1.05 V for **PP-NO_2**) redox waves in the positive region. The former irreversible oxidation peaks are attributed to the oxidation of Ru centre, and the latter reversible waves were observed exactly at the same potential as the Ru(III)/Ru(II) redox couples of corresponding acetonitrile complexes ($E_{1/2}$ = 0.97 for ***trans*-MeCN** and 1.27 V for **PP-MeCN**, Table 5 and Figure 11).[18] Based on the aforementioned observation, we can describe electrochemical behaviour of these complexes in the positive region as follows. First, upon oxidation of ***trans*-NO_2** and **PP-NO_2**, NO_2, which is one-electron oxidised species of NO_2^-, was released and subsequent coordination of MeCN resulted in the formation of corresponding acetonitrile complexes. Further potential sweep to positive region oxidise the generated acetonitrile complexes and the reversible waves of acetonitrile complexes were obtained.

In the negative potential region, ***cis*-NO_2** displayed two reversible reduction waves at −1.70 and −1.99 V, which are assigned to a trpy/$trpy^-$ and Pqn/Pqn^- redox couples, respectively. ***trans*-NO_2** exhibits two redox waves at $E_{1/2}$ = −1.77 and −2.13 V and these redox potentials are same as the those of ***trans*-MeCN** (Table 3 and Figure S6a-b in the ESI**)**. **PP-NO_2** displays two irreversible (E_{pa} = −1.70 V and E_{pc} = −1.45 V) and one reversible ($E_{1/2}$ = −2.49 V) redox waves in the negative region. The redox potentials of the reversible wave and the second irreversible wave were consistent with **PP-MeCN** (Table 3 and Figure 11**)**. These redox behaviours of ***trans*-NO_2** and **PP-NO_2** revealed that the reduction of these complexes induce the dissociation of NO_2^- and the formation of MeCN coordinated species, and these behaviour is similar to that observed in the positive potential region. The summary of electrochemical behaviours of nitrite complexes is shown in Scheme 3.

***cis*-NO** display one reversible redox peak at $E_{1/2}$ = 0.05 V and one irreversible reduction peal at E_{pa} = −0.61 V (Figure 12). Comparison with related nitrosyl compounds revealed that the former redox wave is attributed to $NO^+/NO^\bullet$ redox couple and the latter peak can be assigned to the reduction of $NO^\bullet$ to NO^-. Note that a Ru(III)/Ru(II) redox couple was not observed in the potential region between −1.6 to

1.5 V due to the low HOMO energy level derived from strong π-back bonding ability of NO^+ ligand.

Cyclic voltammograms of *cis*-isomers with various labile ligands are shown in Figure 13. The redox potentials of a Ru(III)/Ru(II) redox couple for each complexes were observed at 0.49, 0.79, and 1.05 V for *cis(P,Cl)*-$[Ru(trpy)(Pqn)(Cl)]^+$ (***cis*-Cl**),[18] ***cis*-NO_2** and ***cis*-MeCN**, respectively. This result indicates the increase of HOMO energy level by the electron donation from labile ligands and is consistent with the result of UV-vis absorption spectroscopy.

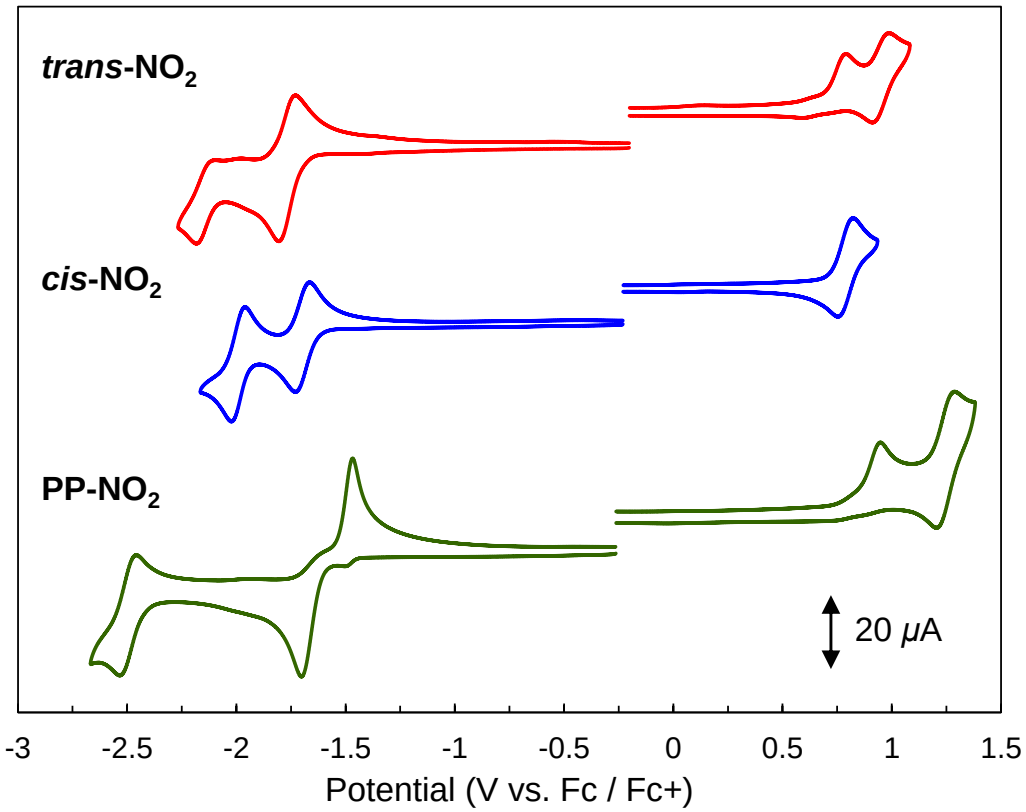

Figure 10. Cyclic voltammograms of ***trans*-NO_2**, ***cis*-NO_2**, and **PP-NO_2** (0.5 mM) in 0.1 M TEAP/acetonitrile under an Ar atmosphere (WE: GC, CE: Pt wire, RE: Ag/Ag^+; Scan rate: 100 mV/s).

Table 5. Redox potentials (V vs Fc/Fc^+) in acetonitrile for ***trans*-NO_2**, ***cis*-NO_2**, **PP-NO_2**, and related compounds at room temperature.

	Ox.			Red.	
complex	*E* (1)	*E* (2)	*E* (3)	*E* (1)	*E* (2)
***trans*-NO_2**	−1.7[b]	[b]	−2.13[b]	0.8[e]	1.05[e]
***cis*-NO_2**	−1.70	−1.99		0.79	
PP-NO_2	−1.7[c]	[c]	−2.49[c]	0.9[f]	1.27[f]
***trans*-MeCN**[a]	−1.70	−1.77	−2.13	0.97	
***cis*-MeCN**[a]	[d]	[d]	[d]	1.05	
PP-MeCN[a]	−1.50	−1.46	−2.49	1.27	

[a] Reference 18. [b] ***trans*-NO_2** exhibits the reduction of these complexes induce the dissociation of NO_2^- and the formation of ***trans*-MeCN**. [c] **PP-NO_2** exhibits the reduction of these complexes induce the dissociation of NO_2^- and the formation of **PP-MeCN**. [d] ***cis*-MeCN** underwent isomerization to ***trans*-MeCN** upon reduction. [e] Upon oxidation of ***trans*-NO_2**, NO_2, which is one-electron oxidised species of NO_2^-, was released and subsequent coordination of MeCN resulted in the formation of ***trans*-MeCN**. [f] Upon oxidation of **PP-NO_2**, NO_2, which is one-electron oxidised species of NO_2^-, was released and subsequent coordination of MeCN resulted in the formation of **PP-MeCN**.

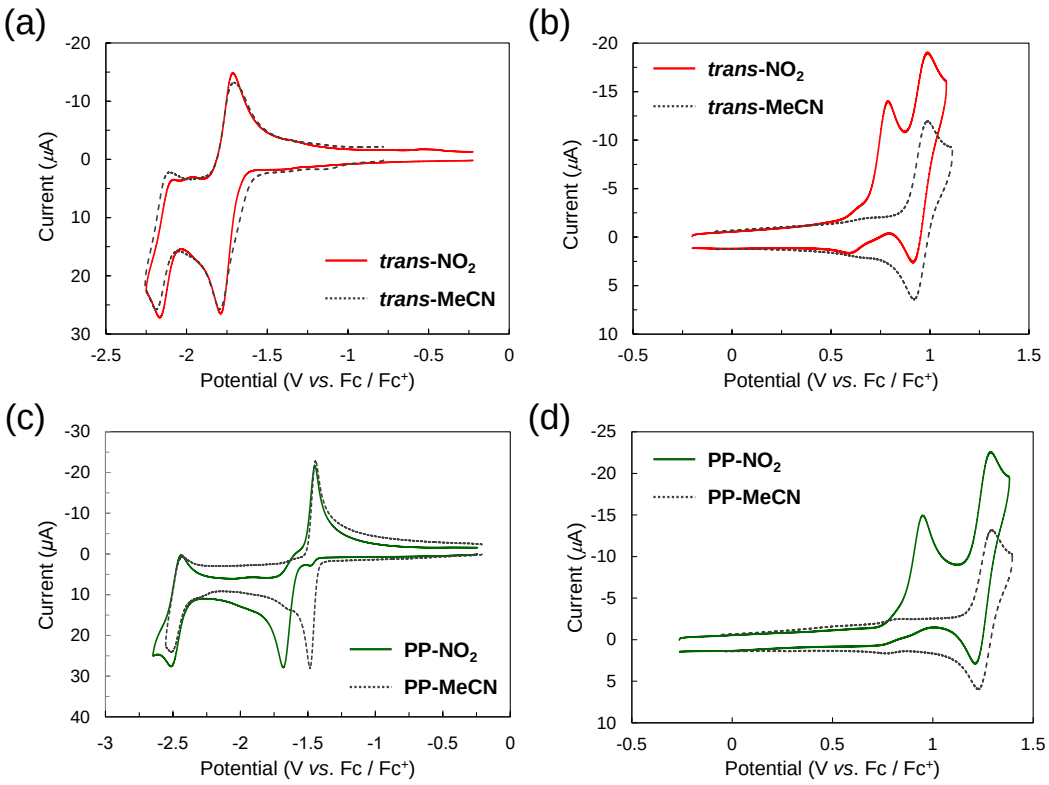

Figure 11. (a), (b) Cyclic voltammograms of ***trans*-NO$_2$** and ***trans*-MeCN** (0.5 mM) in 0.1 M TEAP/acetonitrile under an Ar atmosphere. (c), (d) Cyclic voltammograms of **PP-NO$_2$** and **PP-MeCN** (0.5 mM) in 0.1 M TEAP/acetonitrile under an Ar atmosphere (WE: GC, CE: Pt wire, RE: Ag/Ag$^+$; Scan rate: 100 mV/s).

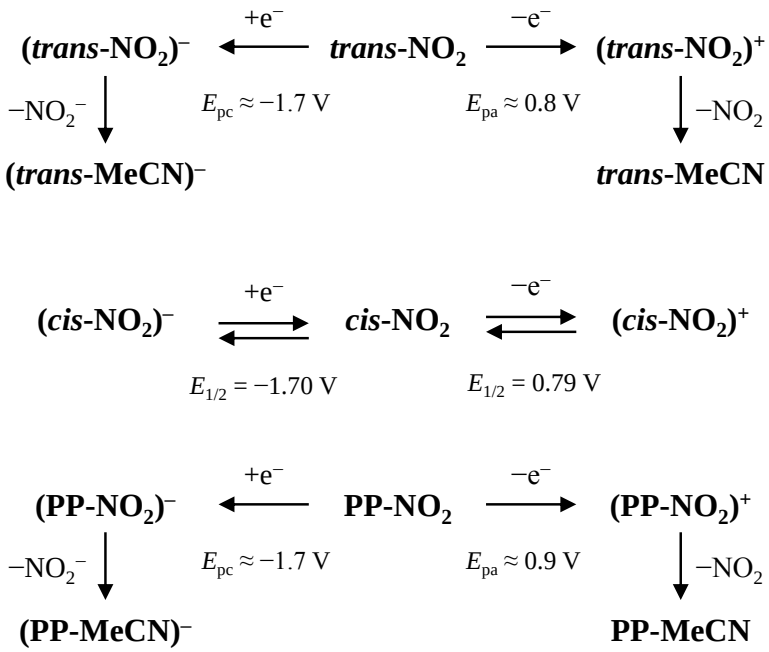

Scheme 3. Electrochemical behaviors of nitrite complexes.

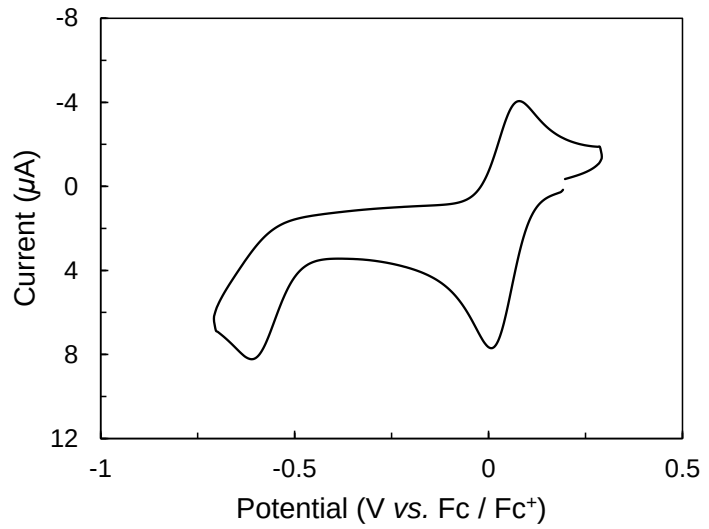

Figure 12. Cyclic voltammogram of ***cis*-NO** (0.5 mM) in 0.1 M TEAP/γ-butyrolactone under an Ar atmosphere (WE: GC, CE: Pt wire, RE: Ag/Ag^+; Scan rate: 100 mV/s).

Table 6. Redox potentials (V vs Fc/Fc^+) in acetonitrile for ***cis*-NO** and related compounds at room temperature.

complex	E ($NO^+/NO^\bullet$)	E ($NO^\bullet/NO^-$)
***cis*-NO**[a]	0.05	–0.61[e]
[Ru(trpy)(bpy)(NO)]$(PF_6)_3$[b]	0.14	–0.51[e]
[Ru(trpy)(bpm)(NO)]$(PF_6)_3$[c]	0.17	–0.47
trans(P,P)-[Ru(trpy)$(PPh_3)_2$(NO)]$(ClO_4)_3$[d]	0.12	*f*

[a] CV data in γ-butyrolactone. [b] Reference 21. [c] Reference 20. [d] Reference 19. [e] E_{pa} values for the irreversible processes. [f] Data not collected.

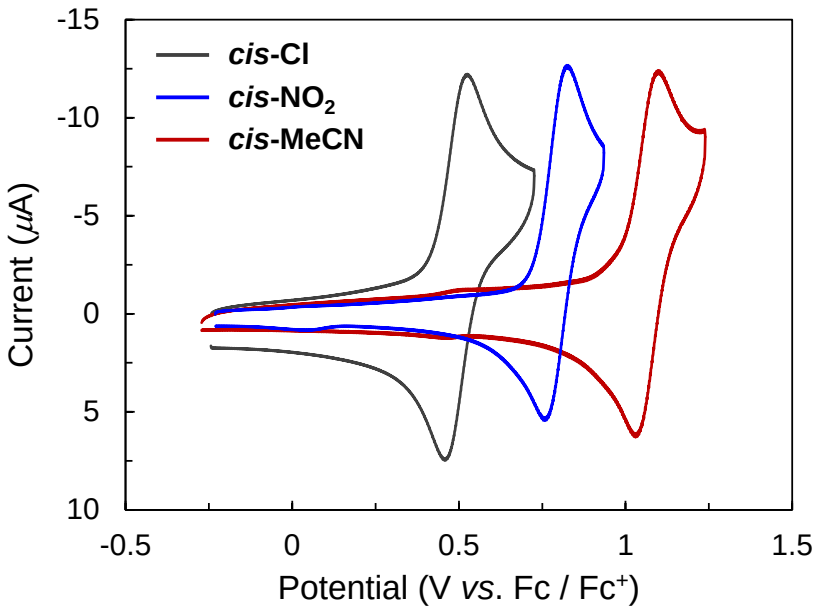

Figure 13. Cyclic voltammograms of ***cis*-Cl**, ***cis*-NO_2**, and ***cis*-MeCN** (0.5 mM) in 0.1 M TEAP/acetonitrile under an Ar atmosphere (WE: GC, CE: Pt wire, RE: Ag/Ag^+; Scan rate: 100 mV/s).

Photochemical Nitric Oxide Release

Nitric oxide (NO) has become one of the most important intercellular signaling molecules identified in the 1980s. Knowledge about its involvement in all kinds of physiological systems continues to expand for vasodilation, bronchodilation, and neurotransmission as shown in Figure 14.[29] Ruthenium(II) polypyridine complexes with NO donors are thermally quite stable but are photochemically active toward NO release. The relative stability of the complexes has also drawn attention to possible applications for NO delivery to biological targets.[13] In 1977, Meyer and co-workers reported that the polypyridine complex, $[Ru(bpy)_2(NO)Cl]^{2+}$, exhibits photochemical release of NO in acetonitrile and then produces $[Ru(bpy)_2(MeCN)Cl]^{2+}$.[30] Moreover, ruthenium compounds containing nitrogen oxide as one of their ligands generally exist as hexacoordinated species like $[Ru(TL)(BL)(NO_x)]^{n+}$ (TL = tridentate ligand, BL = bidentate ligand, NOx = nitrogen oxide ligand, *e.g.* NO^+ and NO_2^-). The $[Ru(TL)(BL)(NO_x)]^{n+}$ mainly contains a trpy ligand as a TL and a N-N polypyridine, as a BL and studies on $[Ru(TL)(BL)(NO_x)]^{n+}$ involve the reactivity of the coordinated nitrogen oxide ligands, which include redox properties, photochemical reactivity, and kinetic aspects.[31] Surprisingly, there are only few studies examining substitution of phosphine for pyridine moiety in such ruthenium(II) polypyridine complexes.[19] Here it is investigated the photostability for the nitrosyl complex.

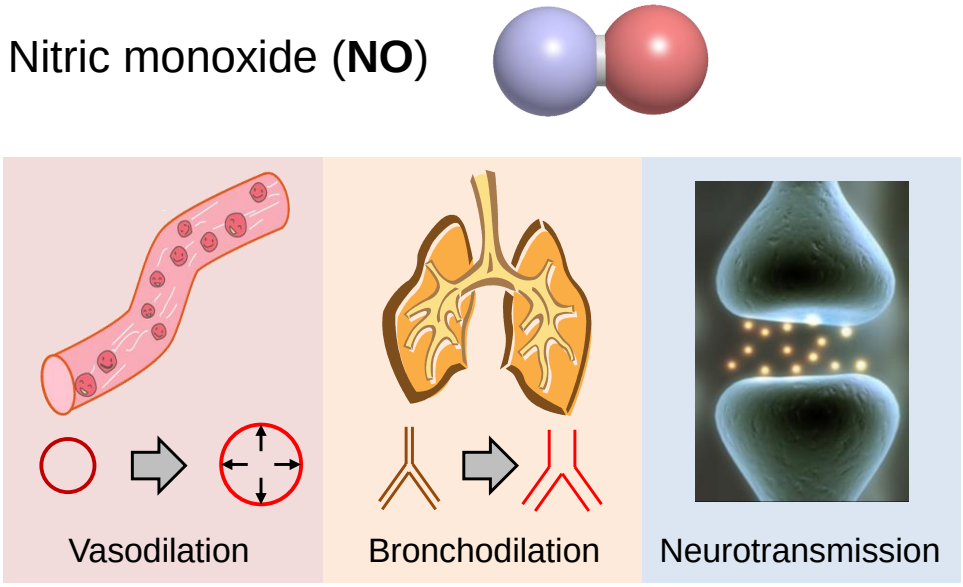

Figure 14. Typical mammalian-biological functions of nitric oxide.

Photostability of a Nitrosyl Complex

Photostability of ***cis*-NO** was investigated by UV-vis absorption spectroscopy. ***cis*-NO** in ethylene glycol (0.05 mM) was irradiated using a laser flash-photolysis (λ = 355 nm). Upon photoirradiation, ***cis*-NO** was almost quantitatively converted to the *trans*-isomer of solvent coordinated complex via the release of a labile ligand and the subsequent isomerization reaction (Figures 15-16). However, the amount of produced NO quantified using Nitric Oxide Analyzer (NOA) was quite low. The estimated quantum yields at 365 nm are 0.0048 under air condition and 0.0025 under helium, respectively (Figure 17). As previously reported,[32] there are two possible pathways in the photo reactions of Ru(II)-based nitrosyl complexes to release labile ligands; one is the release of NO with the formation of oxidised Ru(III) complex and the other is the release of NO^+ to afford Ru(II) complex. In the present case, π-back donation from phosphine stabilises the low-valent Ru(II) state and the labile ligand of ***cis*-NO** might be released not as NO but as NO^+ form.

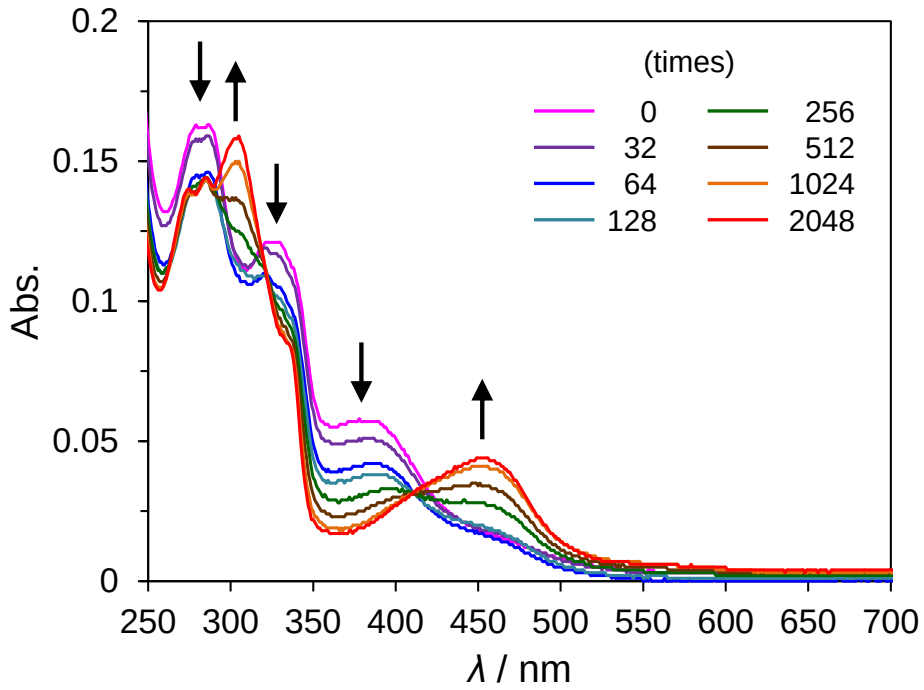

Figure 15. UV-Vis absorption spectra of ***cis*-NO** in ethylene glycol at room temperature during flash-photolysis at 355 nm.

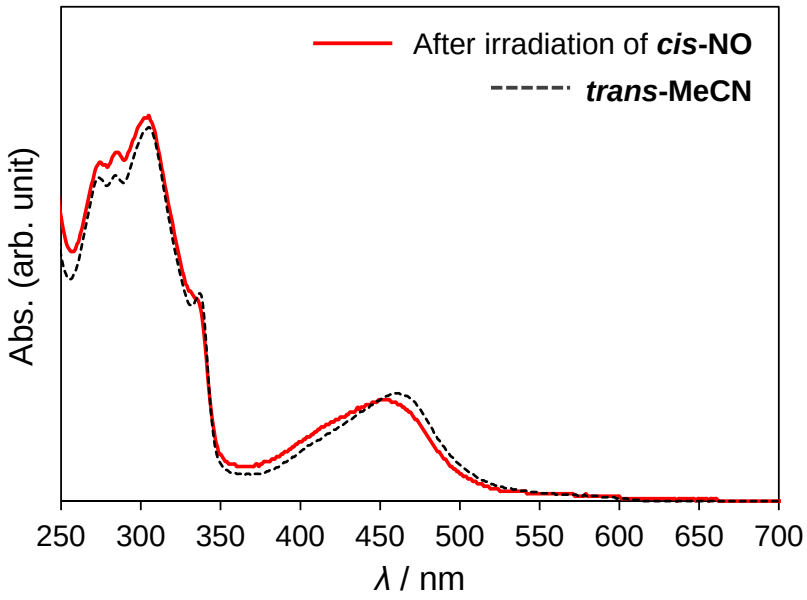

Figure 16. UV-vis absorption spectra of ***cis*-NO** in MeCN after photoirradiation of 355 nm laser for 2048 times (pulse width = 5 ns, beam diameter incident on the sample = 6 mm, repetition rate = 5 Hz) and that of ***trans*-MeCN** in ethylene glycol at room temperature.

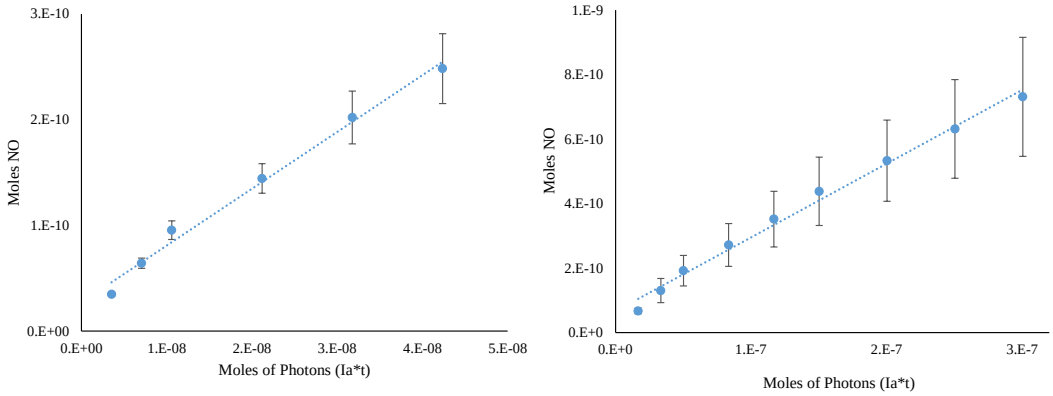

Figure 17. Plots of moles of NO vs photons for the photorelease of ***cis*-NO** when irradiated at 365 nm under air conditions (left) and Ar (right). Error bars reflect one standard deviation of the cumulative moles of NO produced over the duration of the experiment. The slope is equal to quantum yield. From these data, quantum yields of 0.0048 under air conditions and 0.0025 under helium were calculated.

Factors to Determine the Stability of Complexes

Several experimental results described above enabled us to discuss the stability of complexes in detail. First, the reaction of ***cis*-NO_2** with HPF_6 afforded desired ***cis*-NO**. However, the similar reactions of ***trans*-NO_2**, and **PP-NO_2** resulted in the formation of the corresponding solvent coordinated complexes via the dissociation of labile ligands, N(O)OH or NO^+. Second, UV-vis absorption spectroscopy revealed that NO_2^+ ligands of ***trans*-NO_2**, ***cis*-NO_2**, and **PP-NO_2** do not dissociate even in highly coordinative solvent as acetonitrile, whereas ligand exchange reactions of **(*trans*-MeCN)$^+$** and **(PP-MeCN)$^+$** easily undergoes under such a condition (Figure 18). ***cis*-NO** was not stable in coordinating solvent and easily converted to solvent coordinated form (Figure 19).

The stability of these complexes in the oxidised and reduced states can also be clarified by the results of electrochemical measurements. In the one-electron oxidised states, ***trans*-NO_2** and **PP-NO_2** exhibited labile nature and was converted to solvent-coordinated form, ***trans*-MeCN**, and **PP-MeCN**, respectively. In contrast, ***cis*-NO_2** was inert during oxidation process and thus, reversible redox wave was observed in the electrochemical measurement. Similarly, in the reduced states, nitrite ligands of ***trans*-NO_2**, and **PP-NO_2** easily dissociates, although ***cis*-NO_2** was stable during whole electrochemical process. However, this stability of ***cis*-NO_2** was quite different from that of ***cis*-MeCN**: acetonitrile ligand of ***cis*-MeCN** becomes labile upon reduction and the dissociation of the ligand resulted in the isomerization of ***cis*-MeCN** to ***trans*-MeCN**.[18] The stability labile site for each complex is shown in Scheme 4.

The difference in the stability of these complexes can be explained by considering following factors. First, the σ-donor character of phosphine group significantly elongates the bond length between the ruthenium centre and the ligand located at the *trans* position of the phosphine group, called the *trans* influence. This *trans* influence of P atom is clearly observed in X-ray structures of a series of nitrite complexes; the bond distances between the ruthenium atom and nitrogen atom of the nitrite ligand are 2.141(3), 2.124(2) and ca. 2.03 Å for ***trans*-NO_2**, **PP-NO_2**, and ***cis*-NO_2**, respectively. Therefore, *trans*-isomers and PP complexes exhibited more labile properties compared with corresponding *cis*-isomers. Second, the electron donation from labile ligands can stabilize Ru-L bonds. The donating ability of labile ligands were confirmed by the comparison of HOMO energy levels obtained from electrochemical measurements of *cis*-isomers as NO_2^- > MeCN > NO^+ and was in well accordance with the stability of complexes. Third, the oxidation of complexes decrease the electron density of Ru centre, and π back donating ability of Ru centres should be weaken. DFT-calculation of nitrite

complexes revealed that π back donation from Ru to NO_2 ligand exists to stabilise Ru-L bond (Figure 7). Moreover, asymmetric and symmetric vibrations of NO_2 moiety of nitrite complexes were observed in higher energy region compared with that of $NaNO_2$ (Table 3), suggesting the existence of π back donation of Ru centres to strengthen N-O bonds of labile ligands. Therefore, the oxidation of complexes should induce the dissociation of NO_2 ligand when Ru-L is not strong enough. Finally, the reduction of complex stabilise the five-coordinated species as we previously reported.[18] The formation of five-coordinated species in MeCN results in ligand exchange of ***trans*-NO_2**, and **PP-NO_2** or isomerization of ***cis*-MeCN** to ***trans*-MeCN**, whereas no observable chemical process exists in the case of ***trans*-MeCN**, and **PP-MeCN**. These results suggest that (1) number and position of P atom(s), (2) coordinating ability of labile ligand, and (3) oxidation state of complexes are contributed to determine the stability of complexes.

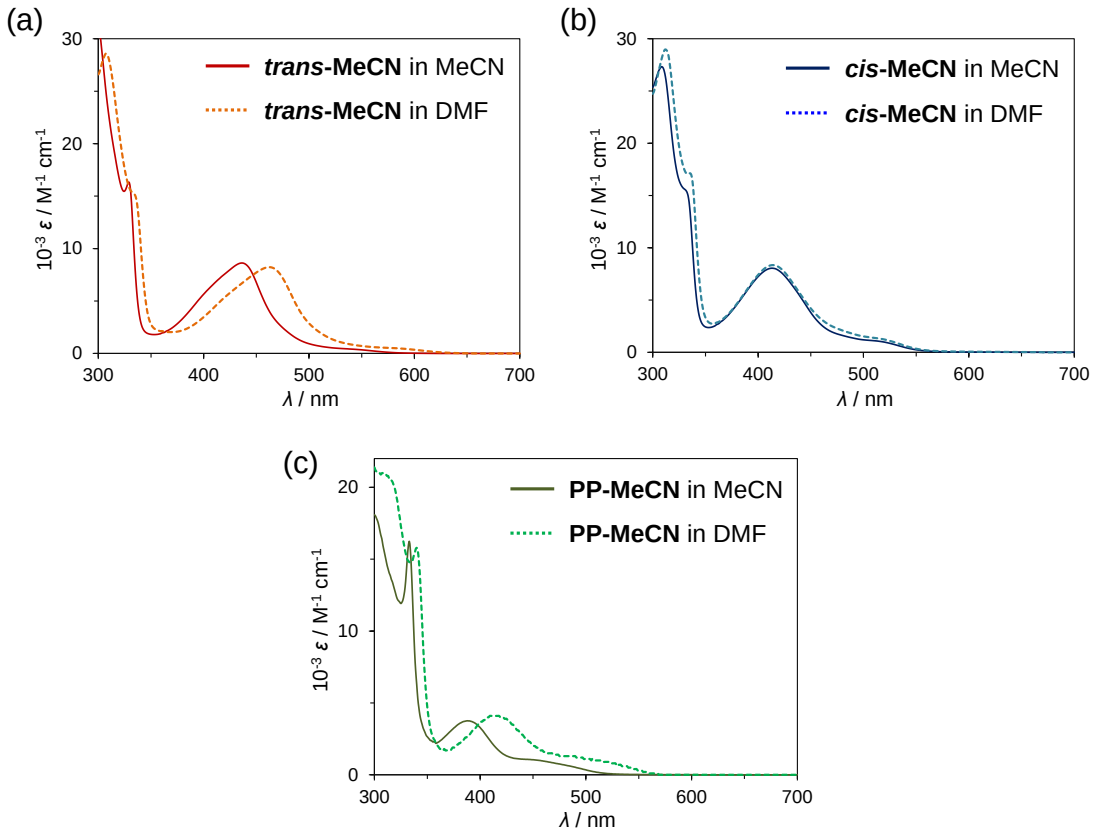

Figure 18 UV-vis absorption spectra of ***trans*-MeCN**, ***cis*-MeCN** and **PP-MeCN** in acetonitrile and DMF at room temperature. The UV-vis spectra indicate that the acetonitrile ligand of ***trans*-MeCN** and **PP-MeCN** can easily undergo a ligand substitution and form *trans(P,DMF)*-[Ru(trpy)(Pqn)(DMF)]$(PF_6)_2$ (***trans*-DMF**) and [Ru(trpy)(dppbz)(DMF)]$(PF_6)_2$ (**PP-DMF**), whereas that of ***cis*-MeCN** is barely substituted.

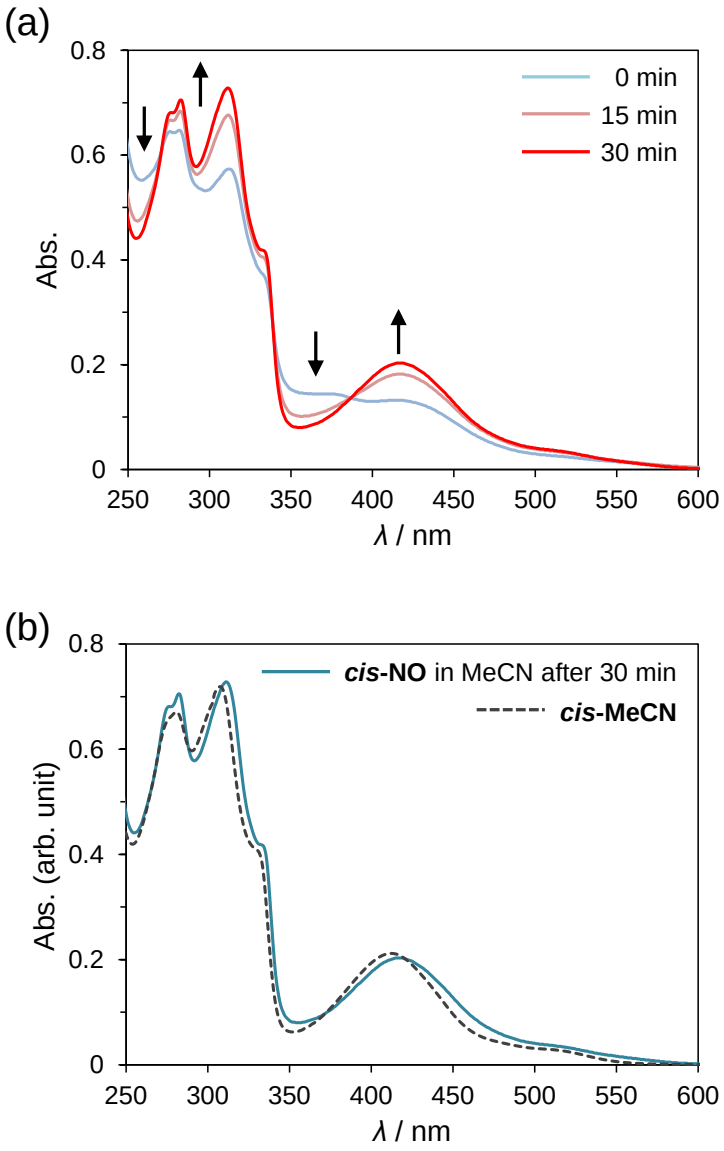

Figure 19. (a) UV-vis absorption spectral changes of ***cis*-NO** in MeCN at room temperature. Dissociation of NO from the complex resulted in the formation of ***cis*-MeCN**. (b) UV-vis absorption spectra of ***cis*-NO** in MeCN after 30 min and that of ***cis*-MeCN** in MeCN.

(a) NO_2 complex

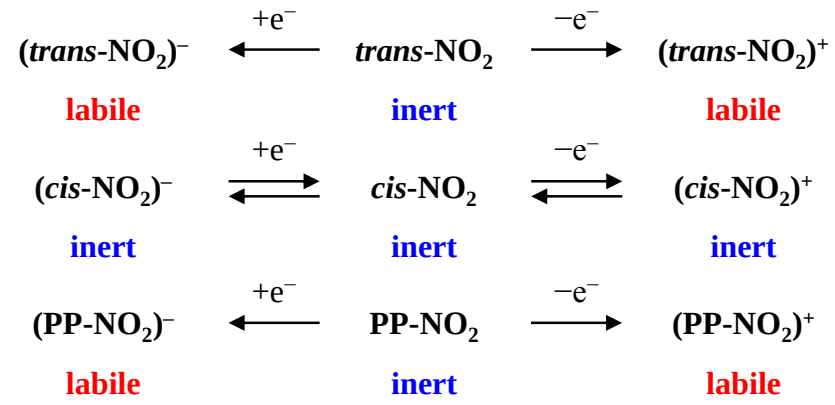

(b) MeCN complex

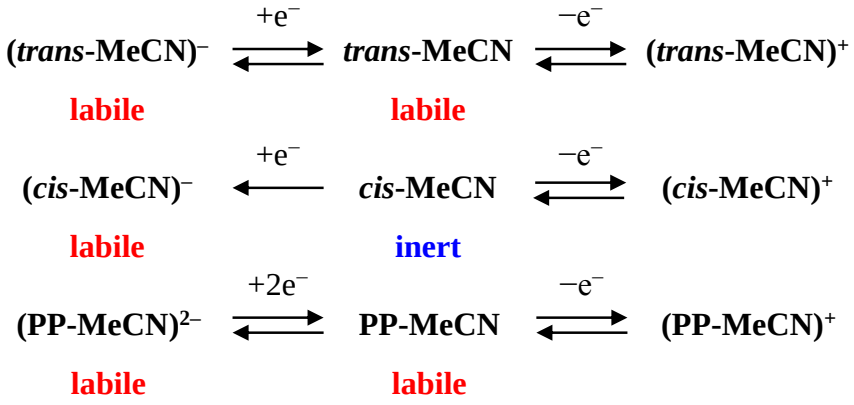

Scheme 4. The stability of labile site for each complex.

Conclusion

In this study, four novel phosphine-substituted Ru(II) based polypyridine complexes with a single labile ligands were synthesised and their structures and electronic properties were investigated. Stability of complexes varies greatly depending on (1) number and position of P atom(s), (2) coordinating ability of labile ligand, and (3) oxidation state of complexes. Experimental and computational study revealed that all factors mentioned above contributed to change the strength of Ru-L bonds.

Experimental Section

Materials

$NaNO_2$ was purchased from Kanto Chemical Co., Inc. NH_4PF_6 and HPF_6 were purchased from Wako Pure Chemical Industries, Ltd. All solvents and reagents were of the highest quality available and were used as received. *trans(P,MeCN)*- and *cis(P,MeCN)*-[Ru(trpy)(Pqn)(MeCN)]$(PF_6)_2$ (***trans*-MeCN** and ***cis*-MeCN**), and [Ru(trpy)(dppbz)(MeCN)]$(PF_6)_2$ (**PP-MeCN**) were prepared by the literature methods.[18]

Measurements

The ^1H and $^{31}P\{^1H\}$ NMR spectra were recorded at room temperature on a JEOL JNM-LA500 spectrometer using tetramethylsilane as an internal reference for ^1H NMR spectra and phosphoric acid as an external reference for $^{31}P\{^1H\}$ NMR spectra. UV−vis absorption spectra were obtained on a Shimadzu UV-2450SIM spectrophotometer at room temperature. Elemental analyses were carried out on a Yanagimoto MT-5 elemental analyser. ESI-TOF mass spectra were recorded on a JEOL JMS-T100LC mass spectrometer. All the ESI-TOF mass spectrometric measurements were recorded in the positive ion mode at a cone voltage of 20 V. Typically, each sample solution was introduced onto the spectrometer at a flow rate of 10 mL/min using a syringe pump. Cyclic voltammograms were measured at room temperature on a BAS ALS Model 650DKMP electrochemical analyser in acetonitrile ([complex] = 0.5 mM; 0.1 M tetraethylammonium perchlorate (TEAP)). A glassy carbon disk, platinum wire, and Ag/Ag^+ electrode (Ag / 0.01 M $AgNO_3$) were used as the working, auxiliary, and reference electrodes, respectively. The redox potentials of samples were calibrated against the redox signal for the ferrocene/ferrocenium (Fc/Fc^+) couple. The photochemical experiments were made using a laser photolysis apparatus consisting of a LS-2134UTF YAG laser (Tokyo Instruments, INC.) with excitation provided by the third harmonic at λ = 355 nm. The YAG lamp energy was 15 J. The pulse width was 5 ns, the beam diameter incident on the sample was 6 mm, and the repetition rate was 5 Hz.

Synthesis of *trans(P,NO$_2$)*-[Ru(trpy)(Pqn)(NO$_2$)]PF$_6$ (*trans*-NO$_2$).

A mixture of ***trans*-MeCN** (26.8 mg, 0.0252 mmol) and $NaNO_2$ (38.8 mg, 0.562 mmol) in ethanol (4 cm^3) / water (4 cm^3) was heated at 100ºC for 3 hours and then cooled to room temperature. Acetonitrile 2 cm^3 and a NH_4PF_6 (188.4 mg, 1.16 mmol) / water (2 cm^3) solution was added to the solution. The resulting red solution was concentrated to

ca. 5 cm^3 under reduced pressure. The red product was collected by filtration and washed with water and diethyl ether. Yield 19.1 mg (0.0216 mmol, 86%). Single red crystals suitable for X-ray crystallography were grown by the slow diffusion of diethyl ether into a mixture of methanol and a few drops of acetonitrile solution of ***trans*-NO_2.** ESI-TOF MS (positive ion, acetonitrile): *m/z* 694 ($[Ru(trpy)(Pqn)(NO_2)]^+$). ^1H NMR (CD_3CN): δ 6.56 (t, 2H, *J* = 9.0 Hz), 6.98 (t, 4H, *J* = 7.0 Hz), 7.14 (t, 2H, *J* = 7.0 Hz), 7.21 (t, 2H, *J* = 8.0 Hz), 7.65 (d, 2H, *J* = 5.0 Hz), 7.80 (t, 2H, *J* = 8.0 Hz), 7.91 (m, 3H), 8.03 (d, 2H, *J* = 8.0 Hz), 8.09 (t, 1H, *J* = 7.5 Hz), 8.23 (d, 2H, *J* = 8.0 Hz), 8.46 (d, 1H, *J* = 7.0 Hz), 8.75 (d, 1H, *J* = 8.0 Hz), 9.93 (d, 1H, *J* = 5.0 Hz). $^{31}P\{^1H\}$ NMR (CD_3CN): δ 53.10 (s). FT-IR: $\nu_s(NO_2)$ 1304, $\nu_{as}(NO_2)$ 1349 cm^{-1}. Anal. Found: C, 51.72; H, 3.56; N, 9.33. Calcd for $C_{38}H_{30}F_6N_6O_2P_2Ru$ (***trans*-NO_2**·MeCN): C, 51.88; H, 3.44; N, 9.55.

Synthesis of *cis(P,NO_2)*-[Ru(trpy)(Pqn)(NO_2)]PF_6 (*cis*-NO_2).

This complex was prepared from ***cis*-MeCN** (26.0 mg, 0.0250 mmol) instead of ***trans*-MeCN** by a method similar to that for ***trans*-NO_2**. Yield 19.5 mg (0.0221 mmol, 88%). ESI-TOF MS (positive ion, acetonitrile): *m/z* 694 ($[Ru(trpy)(Pqn)(NO_2)]^+$). ^1H NMR (CD_3CN): δ 6.81 (t, 2H, *J* = 6.5 Hz), 7.06 (m, 1H), 7.4 1 (d, 2H, *J* = 5.5 Hz), 7.52 (m, 4H), 7.63 (t, 2H, *J* = 7.5 Hz), 7.73 (m, 4H), 7.84 (t, 2H, *J* = 8.0 Hz), 7.92 (d, 1H, *J* = 5.5 Hz), 7.97 (t, 1H, *J* = 7.5 Hz), 8.18 (d, 1H, *J* = 8.0 Hz), 8.23 (d, 1H, *J* = 8.0 Hz), 8.36 (m, 3H), 8.55 (d, 2H, *J* = 8.0 Hz) 8.78 (t, 1H, *J* = 8.0 Hz). $^{31}P\{^1H\}$ NMR (CD_3CN): δ 54.06 (s). FT-IR: $\nu_s(NO_2)$ 1286, $\nu_{as}(NO_2)$ 1339 cm^{-1}. Anal. Found: C, 50.38; H, 3.44; N, 8.19. Calcd for $C_{36}H_{29}F_6N_5O_3P_2Ru$ (***cis*-NO_2**·H_2O): C, 50.47; H, 3.41; N, 8.18.

Synthesis of *cis(P,NO_2)*-[Ru(trpy)(Pqn)(NO_2)]BPh_4 (*cis*-NO_2').

This complex was prepared by a method similar to that for ***cis*-NO_2** with excess $NaBPh_4$ instead of NH_4PF_6. The product was recrystallized from dichloromethane and a small amount of acetonitrile / diethyl ether to afford orange red crystals of ***cis*-NO_2'**. Anal. Found: C, 70.54; H, 4.72; N, 6.92. Calcd for $C_{60}H_{48}BN_5O_{2.5}PRu$ (***cis*-NO_2'**·$0.5H_2O$): C, 70.52; H, 4.73; N, 6.85.

Synthesis of *cis(P,NO)*-[Ru(trpy)(Pqn)(NO)]$(PF_6)_3$ (*cis*-NO).

***cis*-NO_2** (22.4 mg, 0.0261 mmol) was dissolved in 1 cm^3 acetone. An excess of 60% HPF_6 acid solution was added dropwise until the solution changed color from red to yellow with ice water bath. The resulting yellow solution was concentrated under reduced pressure and 10 cm^3 of diethyl ether was added to precipitate the product. Yield 27.4 mg (0.0223 mmol, 85%). ^1H NMR (acetone-d_6): δ 7.47 (t, 2H, *J* = 7.0 Hz), 7.66 (m,

1H), 7.80 (d, 2H, J = 6.0 Hz), 7.86 (m, 4H), 8.01 (t, 2H, J = 7.5 Hz), 8.12 (dd, 4H, J = 7.5, 13.0 Hz), 8.42 (t, 1H, J = 7.5 Hz), 8.49 (m, 2H), 8.55 (m, 1H), 8.80 (d, 1H, J = 8.0 Hz), 9.01 (m, 3H), 9.10 (m, 1H) 9.22 (m, 3H),. $^{31}P\{^{1}H\}$ NMR (acetone-d_6): δ 54.23 (s). FT-IR: ν_s(NO) 1929 cm^{-1}. Anal. Found: C, 35.03; H, 2.95; N, 5.59. Calcd for $C_{36}H_{40}F_{18}N_5O_{7.5}P_4Ru$ (***cis*-NO**·6.5H_2O): C, 35.16; H, 3.28; N, 5.70.

Synthesis of [Ru(trpy)(dppbz)(NO_2)]PF_6 (PP-NO_2).

This complex was prepared from **PP-MeCN** (31.5 mg, 0.0263 mmol) instead of ***trans*-MeCN** by a method similar to that for ***trans*-NO_2**. Yield 22.9 mg (0.0227 mmol, 86%). Single orange crystals suitable for X-ray crystallography were grown by the slow diffusion of diethyl ether into a mixture of methanol and a few drops of acetonitrile solution of **PP-NO_2**. ESI-TOF MS (positive ion, acetonitrile): *m/z* 827 ([Ru(trpy)(dppbz)(NO_2)]$^+$). ^{1}H NMR (CD_3CN): δ 6.50 (m, 4H), 6.78 (m, 2H), 6.88 (m, 4H), 7.08 (d, 2H, J = 5.5 Hz), 7.17 (m, 2H), 7.45 (t, 4H, J = 7.5 Hz), 7.61 (m, 7H), 7.77 (m, 3H), 7.87 (t, 1H, J = 7.5 Hz), 8.03 (d, 2H, J = 8.0 Hz), 8.23 (m, 3H), 8.39 (t, 1H, J = 7.5 Hz). $^{31}P\{^{1}H\}$ NMR (CD_3CN): δ 62.65 (d, $^2J_{P-P}$ = 14.2 Hz), 68.59 (d, $^2J_{P-P}$ = 14.2 Hz). FT-IR: ν_s(NO_2) 1311, ν_{as}(NO_2) 1354 cm^{-1}. Anal. Found: C, 53.62; H, 4.05; N, 5.46. Calcd for $C_{45}H_{39}F_6N_4O_4P_3Ru$ (**PP-NO_2**·2H_2O): C, 53.63; H, 3.90; N, 5.56.

Crystallography.

The X-ray data collection and processing were performed on a Kappa APEX II CCDC diffractometer by using graphite-monochromated Mo-Kα radiation (0.71075 Å) for ***trans*-NO_2** and **PP-NO_2**. Single crystal X-ray diffraction measurement of ***cis*-NO_2'** was performed with a RAXIS-RAPID Imaging Plate diffractometer equipped with confocal monochromated Mo-Kα (0.71075 Å) radiation and data was processed using RAPID-AUTO (Rigaku). All non-hydrogen atoms were refined anisotropically. Molecular graphics were generated using *ORTEP-3* for *Windows*[33] and *POV-RAY*.[34] The summary of crystallographic data and structure refinement parameters is shown in Table 1. Crystallographic data have been deposited with Cambridge Crystallographic Data Center: Deposition numbers CCDC 1040452, 1040453, and 1040454 for ***trans*-NO_2**, ***cis*-NO_2'**, and **PP-NO_2**, respectively. Copies of the data can be obtained free of charge *via* www.ccdc.cam.ac.uk/data_request/cif.

DFT calculations.

Calculations were performed using the DFT method implemented in the Gaussian 09 package of programs.[22] The structures were fully optimized using the B3LYP method, which uses hybrid Becke's three-parameter exchange functional[23] with the correlation energy functional of Lee, Yang, and Parr.[24] All calculations were performed using the standard double-ζ type LanL2DZ basis set[25] implemented in Gaussian 09, without adding any extra polarization or diffuse function. The LanL2DZ basis set also uses relativistic effective core potentials (RECP) for the Ru atom to account for the scalar relativistic effects of the inner 28 core electrons ($[Ar]3d^{10}$) for Ru. All calculations were performed using the polarizable continuum model (PCM)[26] to compute the structures in acetonitrile. All stationary points were characterized by their harmonic vibrational frequencies as minima. The free energies at 298 K and 1 atm were obtained through thermochemical analysis of the frequency calculation, using the thermal correction to Gibbs free energy as reported by Gaussian 09. The excited states were calculated using the TD-DFT[27] method within the Tamm-Dancoff approximation as implemented in Gaussian 09. These calculations employ the hybrid B3LYP functional along with the basis sets described above. At least 100 excited states were computed in each calculation. To obtain the simulated spectrum of each species, transition energies and oscillator strengths have been interpolated by a Gaussian convolution with a common σ value of 0.2 eV.

Quantum Yield Measurements

Nitric oxide was detected and analyzed using a GE Sievers model 280i nitric oxide analyzer (NOA). Known volumes of the gases from the solution headspace were injected into the NOA purge vessel, and these gases were entrained to the detector using helium. The NO present in the sample was quantified using a calibration curve generated from the reaction of $NaNO_2$ with acidic KI. Chemical actinometry was performed with ferric oxalate solutions.[35] The photolysis source was the output from a 200 W high-pressure mercury lamp passed through an IR filter and collimated with lenses. An appropriate interference filter was used to select the desired λ_{irr}. A shutter shielded the sample from the arc lamp. A sample of known volume in a quartz 1 cm square cuvette with a magnetic stirring bar was irradiated for defined time periods. NO quantum yields (Φ_t) were calculated based on plots of NO concentrations obtained by NO meter measurement vs moles of photons ($I_a \cdot t$).

References

1 (a) K. Kalyanasundaram, *Coord. Chem. Rev.* **1982**, *46*, 159–244, (b) A. Juris, V. Balzani, F. Barigelletti, S. Campagna, P. Belser, A. von Zelewsky, *Coord. Chem. Rev.* **1988**, *84*, 85–277, (c) V. Balzani, A. Juris, *Coord. Chem. Rev.* **2001**, 211, 97–115, (d) S. Campagna, F. Puntoriero, F. Nastasi, G. Bergamini, V. Balzani, *Top. Curr. Chem.* **2007** *280*, 117–214, (e) T. P. Yoon, M. A. Ischay, J. Du, *Nat. Chem.* **2010**, *2*, 527–532, (f) Q. Sun, S. Mosquera-Vazquez, Y. Suffren, J. Hankache, N. Amstutz, L. M. L. Daku, E. Vauthey, A. Hauser, *Coord. Chem. Rev.* **2015**, 282–283, 87–99.

2 (a) C. D. Clark, M. Z. Hoffman, *Coord. Chem. Rev.* **1997**, *159*, 359–373, (b) L. De Cola, P. Belser, *Coord. Chem. Rev.* **1998**, *177*, 301–346, (c) M. D. Ward, F. Barigelletti, *Coord. Chem. Rev.* **2001**, *216–217*, 127–154. (d) M. H. V. Huynh, D. M. Dattelbaum, T. J. Meyer, *Coord. Chem. Rev.* **2005,** *249*, 457–483. (d) H. Kon, K. Tsuge, T. Imamura, Y. Sasaki, S. Ishizaka, N. Kitamura, M. Kato, *Dalton Trans.* **2008**, 1541–1543, (e) A. Lavie-Cambot, C. Lincheneau, M. Cantuel, Y. Leydet, N. D. McClenaghan, *Chem. Soc. Rev.* **2010**, *39*, 506–515, (f) O. Filevich, B. García-Acosta, R. Etchenique, *Photochem. Photobiol. Sci.* **2012**, *11*, 843–847.

3 (a) F. G. Gao, A. J. Bard, *J. Am. Chem. Soc.* **2000**, *122*, 7426–7427, (b) J. N. Demas, B. A. DeGraff, *Coord. Chem. Rev.* **2001**, *211*, 317–351, (c) P. D. Beer, E. J. Hayes, *Coord. Chem. Rev.* **2003**, *240*, 167–189, (d) R. Martinez-Máñez, F. Sancenón *Chem. Rev.* **2003**, *103*, 4419−4476, (e) A. S. Polo, M. K. Itokazu, N. Y. M. Iha, *Coord. Chem. Rev.* **2004**, *248*, 1343–1361, (f) M. S. Vickers, K. S. Martindale, P. D. Beer, *J. Mater. Chem.* **2005**, *15*, 2784–2790, (g) N. Haddour, J. Chauvin, C. Gondran, S. Cosnier, *J. Am. Chem. Soc.* **2006**, *128*, 9693–9698, (h) H. Wei, E. Wang, *Trends Anal. Chem.* **2008**, *27*, 447–459, (i) J. L. Delaney, C. F. Hogan, J. Tian, W. Shen, *Anal. Chem.* **2011**, *83*, 1300–1306.

4 (a) G. J. Wilson, A. Launikonis, W. H. F. Sasse, A. W.-H. Mau, *J. Phys. Chem.* A **1997**, *101*, 4860–4866, (b) J. A. Simon, S. L. Curry, R. H. Schmehl, T. R. Schatz, P. Piotrowiak, X. Jin, R. P. Thummel, *J. Am. Chem. Soc.* **1997**, *119*, 11012–11022, (c) D. S. Tyson, C. R. Luman, X. Zhou, F. N. Castellano, *Inorg. Chem.* **2001**, *40*, 4063–4071, (d) A. D. Guerzo, S. Leroy, F. Fages, R. H. Schmehl, *Inorg. Chem.* **2002**, *41*, 359–366, (e) S. Bernhard, J. A. Barron, P. L. Houston, H. D. Abruña, J. L. Ruglovksy, X. Gao, G. G. Malliaras, *J. Am. Chem. Soc.* **2002**, *128*, 9693–9698, (f) S. Welter, K. Brunner, J. W. Hofstraat, L. D. Cola, *Nature* **2003**, *421*, 54–57, (g) H. Shahroosvand, P. Abbasi, A. Faghih, E. Mohajerani, M. Janghouri, M. Mahmoudi,

RSC Adv. **2014**, *4*, 1150–1154.

5 (a) J. K. Barton, *Science* **1986**, *233*, 727–734, (b) C. Turro, S. H. Bossmann, Y. Jenkins, J. K. Barton, N. J. Turro, *J. Am. Chem. Soc.* **1995**, 117, 9026–9032, (c) H. B. Gray, J. R. Winkler, *Ann. Rev. Biochem.* **1996**, *65*, 537–561, (d) A. D. Guerzo, A. K.-D. Mesmaeker, *Inorg. Chem.* **2002**, *41*, 938–945. (e) S. Le Gac, M. Foucart, P. Gerbaux, E. Defrancq, C. Moucheron A. Kirsch-De Mesmaeker, *Dalton Trans.* **2010**, *39*, 9672–9683, (f) H. Song, J. T. Kaiser, J. K. Barton, *Nat. Chem.* **2012**, *4*, 615–620, (g) H. Niyazi, J. P. Hall, K. O'Sullivan, G. Winter, T. Sorensen, J. M. Kelly, C. J. Cardin, *Nat. Chem.* **2012**, *4*, 621–628, (h) A. C. Komor, J. K. Barton, *Chem. Commun.* **2013**, *49*, 3617–3630.

6 (a) T. J. Meyer, M. H. V. Huynh, *Inorg. Chem.* **2003**, *42*, 8140–8160, (b) E. Masllorens, M. Rodriguez, I. Romero, A. Roglans, T. Parella, J. Benet-Buchholz, M. Poyatos, A. Llobet, *J. Am. Chem. Soc.* **2006**, *128*, 5306–5307. (c) Y. Shiota, J. M. Herrera, Gergely Juhász, T. Abe, S. Ohzu, T. Ishizuka, T. Kojima, K. Yoshizawa, *Inorg. Chem.* **2011**, *50*, 6200–6209, (d) T. Kojima, K. Nakayama, K. Ikemura, T. Ogura, S. Fukuzumi, *J. Am. Chem. Soc.* **2011**, *133*, 11692–11700, (e) Z. Hu, H. Du, W.-L. Man, C.-F. Leung, H. Liang, T.-C. Lau, *Chem. Commun.* **2012**, *48*, 1102–1104, (f) Z. Hu, L. Ma, J. Xie, H. Du, W. W. Y. Lam, T.-C. Lau, *New J. Chem.* **2013**, *37*, 1707–1710.

7 (a) J. J. Concepcion, J. W. Jurss, J. L. Templeton, T. J. Meyer, *J. Am. Chem. Soc.* **2008**, *130*, 16462–16463, (b) H.-W. Tseng, R. Zong, J. T. Muckerman, R. P. Thummel, *Inorg. Chem.* **2008**, *47*, 11763–11773, (c) S. Romain, L. Vigara, A. Llobet, *Acc. Chem. Res.* **2009**, *42*, 1944–1953, (d) J. J. Concepcion, J. W. Jurss, M. K. Brennaman, P. G. Hoertz, A. O. T. Patrocinio, N. Y. Murakami Iha, J. L. Templeton, T. J. Meyer, *Acc. Chem. Res.* **2009**, *42*, 1954–1965, (e) L. Duan, L. Tong, Y. Xu, L. Sun, *Energy Environ. Sci.* **2011**, *4*, 3296–3313, (f) D. J. Wasylenko, R. D. Palmer, C. P. Berlinguette, *Chem. Commun.* **2013**, *49*, 218–227. (g) M. D. Kärkäs, O. Verho, E. V. Johnston, B. Åkermark, *Chem. Rev.* **2014**, in press.

8 (a) S. Masaoka, K. Sakai, *Chem. Lett.* **2009**, *38*, 182–183. (b) M. Yoshida, S. Masaoka, K. Sakai, *Chem. Lett.*, **2009**, *38*, 702–703. (c) M. Yoshida, S. Masaoka, J. Abe, K. Sakai, *Chem. Asian J.* **2010**, *5*, 2369–2378. (d) J. Kiyota, J. Yokoyama, M. Yoshida, S. Masaoka,, K. Sakai, *Chem. Lett.*, **2010**, *39*, 1146–1148. (e) A. Kimoto, K. Yamauchi, M. Yoshida, S. Masaoka, K. Sakai, *Chem. Commun.*, **2012**, *48*, 239–241. (f) M. Okamura, M. Yoshida, R. Kuga, K. Sakai, M. Kondo, S. Masaoka, *Dalton Trans.*, **2012**, *41*, 13081–13089. (g) M. Yoshida, S. Masaoka, *Res. Chem. Intermed.* **2014**, *40*, 3169–3182, (h) M. Yoshida, M. Kondo, T. Nakamura, K. Sakai,

S. Masaoka, *Angew. Chem. Int. Ed.* **2014**, *53*, 11519–11523, (i) M. Okamura, S. Masaoka, *Chem. Asian J.* **2014**, in press.

9 (a) H. Yamazaki, T. Hakamata, M. Komi, M. Yagi, *J. Am. Chem. Soc.* **2011**, *133*, 8846–8849, (b) J. L. Boyer, D. E. Polyansky, D. J. Szalda, R. Zong, R. P. Thummel, E. Fujita, *Angew. Chem. Int. Ed.* **2011**, *50*, 12600–12604, (c) S. K. Padhi, R. Fukuda, M. Ehara, K. Tanaka, *Inorg. Chem.* **2012**, *51*, 5386–5392, (d) M. Hirahara, M. Z. Ertem, M. Komi, H. Yamazaki, C. J. Cramer, M. Yagi, *Inorg. Chem.* **2013**, *52*, 6354–6364.

10 (a) K. Tanaka, D. Ooyama, *Coord. Chem. Rev.* **2002**, *226*, 211–218, (b) J.-M. Savéant, *Chem. Rev.* **2008**, *108*, 2348–2378. (c) Y. Tsukahara, T. Wada, K. Tanaka, *Chem. Lett.* **2010**, *39*, 1134–1135, (d) K. Kobayashi, T. Kikuchi, S. Kitagawa, K. Tanaka, *Angew. Chem. Int. Ed.* **2014**, *52*, 1–6.

11 (a) Z. Chen, C. Chen, D. R. Weinberg, P. Kang, J. J. Concepcion, D. P. Harrison, M. S. Brookhart, T. J. Meyer, *Chem. Commun.* **2011**, *47*, 12607–12609. (b) Z. Chen, J. J. Concepcion, M. K. Brennaman, P. Kang, M. R. Norris, P. G. Hoertz, T. J. Meyer, *Proc. Natl. Acad. Sci. USA* **2012**, *109*, 15606–15611, (c) Z. Chen, P. Kang, M.-T. Zhang, T. J. Meyer, *Chem. Commun.* **2014**, *50*, 335–337, (d) P. Kang, Z. Chen, A. Nayak, S. Zhang, T. J. Meyer, *Energy Environ. Sci.* **2014**, *7*, 4007–4012.

12 (a) A. Kobayashi, R. Takatori, I. Kikuchi, H. Konno, K. Sakamoto, O. Ishitani, *Organometallics* **2001**, *20*, 3361–3363, (b) A. Kobayashi, H. Konno, K. Sakamoto, A. Sekine, Y. Ohashi, M. Iida, O. Ishitani, *Chem. Eur. J.* **2005**, *11*, 4219–4226, (c) M. Kimura, K. Tanaka, *Angew. Chem. Int. Ed.* **2008**, *47*, 9768–9771, (d) Y. Matsubara, E. Fujita, M. D. Doherty, J. T. Muckerman, C. Creutz, *J. Am. Chem. Soc.* **2012**, *134*, 15743–15757, (e) Y. Matsubara, T. Kosaka, K. Koga, A. Nagasawa, A. Kobayashi, H. Konno, C. Creutz, K. Sakamoto, O. Ishitani, *Organometallics* **2013**, *32*, 6162–6165, (f) J. Huang, J. Chen, H. Gao, L. Chen, *Inorg. Chem.* **2014**, *53*, 9570−9580.

13 (a) R. W. Callahan, T. J. Meyer, *Inorg. Chem.* **1977**, 574–581, (b) H. Hadadzadeh, M. C. DeRosa, G. P. A. Yap, A. R. Rezvani, R, J. Crutchley, *Inorg. Chem.* **2002**, *41*, 6521−6526, (c) M. G. Sauaia, R. G. de Lima, A. C. Tedesco, R. S. da Silva, *J. Am. Chem. Soc.* **2003**, *125*, 14718–14719, (d) Z. N. da Rocha, M. S. P. Marchesi, J. C. Molin, C. N. Lunardi, K. M. Miranda, L. M. Bendhack, P. C. Ford, R. S. da Silva, *Dalton Trans.* **2008**, 4282–4287, (e) A. C. Pereira, P.C. Ford, R. S. da Silva, L. M. Bendhack, *Nitric Oxide* **2011**, *24*, 192–198, (f) T. A. Heinrich, A. C. Tedesco, J. M. Fukuto, R. S. da Silva, *Dalton Trans.* **2014**, *43*, 4021–4025, (g) R. G. de Lima, B. R. Silva, R. S. da Silva, L. M. Bendhack, *Molecules* **2014**, *19*, 9628–9654.

14 (a) T. Kinoshita, J. T. Dy, S. Uchida, T. Kubo, H. Segawa, *Nat. Photonics* **2013**, *7*, 535–539. (b) R. Katoh, A. Furube, *J. Photochem. Photobiol. C* **2014**, *20*, 1–16.

15 (a) R. Noyori, T. Ohkuma, *Angew. Chem. Int. Ed.* **2001**, *40*, 40–73, (b) R. Noyori, *Angew. Chem. Int. Ed.* **2002**, *41*, 2008–2022. (c) R. Noyori, *Adv. Synth. Catal.* **2003**, *345*, 15–32, (d) S. E. Clapham, A. Hadzovic, R. H. Morris, *Coord. Chem. Rev.* **2004**, *248*, 2201–2237, (e) A. F. Trindade, P. M. P. Gois, C. A. M. Afonso, *Chem. Rev.* **2009**, *109*, 418–514. (f) R. Noyori, *Angew. Chem. Int. Ed.* **2013**, *52*, 79–92.

16 (a) P. Schwab, M. B. France, J. W. Ziller, R. H. Grubbs, *Angew. Chem. Int. Ed.* **1995**, *34*, 2039–2041, (b) H. Clavier, S. P. Nolan, *Chem. Eur. J.* **2007**, *13*, 8029–8036, (c) G. C. Vougioukalakis, R. H. Grubbs, *Chem. Rev.* **2010**, *110*, 1746–1787, (d) J. S. M. Samec, B. K. Keitz, R. H. Grubbs, *J. Organomet. Chem.* **2010**, *695*, 1831–1837, (e) S. P. Nolan, H. Clavier, *Chem. Soc. Rev.* **2010**, *39*, 3305–3316.

17 (a) D. K. Dutta, B. Deb, *Coord. Chem. Rev.* **2011**, *255*, 1686–1712, (b) C. S. Yi, *J. Organomet. Chem.* **2011**, *696*, 76–80, (c) I. Mellone, M. Peruzzini, L. Rosi, D. Mellmann, H. Junge, M. Beller, L. Gonsalvi, *Dalton Trans.* **2013**, *42*, 2495–2501, (d) C. M. Moore, N. K. Szymczak, *Chem. Commun.* **2013**, *49*, 400–402, (e) K.-N. T. Tseng, J. W. Kampf, N. K. Szymczak, *Organometallics* **2013**, *32*, 2046–2049, (f) K.-N. T. Tseng, A. M. Rizzi, N. K. Szymczak, *J. Am. Chem. Soc.* **2013**, *135*, 16352–16355.

18 G. Nakamura, M. Okamura, M. Yoshida, T. Suzuki, H. D. Takagi, M. Kondo, and S. Masaoka, *Inorg. Chem.*, **2014**, *53*, 7214–7226.

19 R. A. Leising, S. A. Kubow, K. J. Takeuchi, *Inorg. Chem.* **1990**, *29*, 4569–4574.

20 P. Singh, J. Fiedler, S. Záliš, C. Duboc, M. Niemeyer, F. Lissner, T. Schleid, W. Kaim, *Inorg. Chem.* **2007**, *46*, 9254–9261.

21 (a) D. W. Pipes, T. J. Meyer, *Inorg. Chem.* **1984**, *23*, 2466–2472, (b) W. R. Murphy, Jr., K. J. Takeuchi, M. H. Barley, T. J. Meyer, *Inorg. Chem.* **1984**, *25*, 1041–1053.

22 Frisch, M. J.; Trucks, G. W.; Schlegel, H. B.; Scuseria, G. E.; Robb, M. A.; Cheeseman, J. R.; Scalmani, G.; Barone, V.; Mennucci, B.; Petersson, G. A.; Nakatsuji, H.; Caricato, M.; Li, X.; Hratchian, H. P.; Izmaylov, A. F.; Bloino, J.; Zheng, G.; Sonnenberg, J. L.; Hada, M.; Ehara, M.; Toyota, K.; Fukuda, R.; Hasegawa, J.; Ishida, M.; Nakajima, T.; Honda, Y.; Kitao, O.; Nakai, H.; Vreven, T.; Montgomery Jr., J. A.; Peralta, J. E.; Ogliaro, F.; Bearpark, M.; Heyd, J. J.; Brothers, E.; Kudin, K. N.; Staroverov, V. N.; Keith, T.; Kobayashi, R.; Normand, J.; Raghavachari, K.; Rendell, A.; Burant, J. C.; Iyengar, S. S.; Tomasi, J.; Cossi, M.; Rega, N.; Millam, J. M.; Klene, M.; Knox, J. E.; Cross, J. B.; Bakken, V.; Adamo, C.; Jaramillo, J.; Gomperts, R.; Stratmann, R. E.; Yazyev, O.; Austin, A.

J.; Cammi, R.; Pomelli, C.; Ochterski, J. W.; Martin, R. L.; Morokuma, K.; Zakrzewski, V. G.; Voth, G. A.; Salvador, P.; Dannenberg, J. J.; Dapprich, S.; Daniels, A. D.; Farkas, O.; Foresman, J. B.; Ortiz, J. V.; Cioslowski, J.; Fox, D. J. *Gaussian 09 (Revision C.01)*, Gaussian, Inc. Wallingford CT, **2010**.

23 A. D. Becke, *J. Chem. Phys.* **1993**, *98*, 5648−5652.

24 C. Lee, W. Yang, R. G. Parr, *Phys. Rev. B* **1988**, *37*, 785−789.

25 (a) T. H. Dunning Jr., P. J. Hay, in *Modern Theoretical Chemistry*, ed. Schaefer III, H. F.; Plenum, New York, **1976**. (b) Hay, P. J.; Wadt, W. R. *J. Chem. Phys*. **1985**, *82*, 270−283. (c) P. J. Hay, W. R. Wadt, *J. Chem. Phys*. **1985**, *82*, 299−310.

26 M. Cossi, G. Scalmani, N. Rega, V. Barone, *J. Chem. Phys.* **2002**, *117*, 43−54.

27 (a) M. E. Casida, C. Jamorski, K. C. Casida, D. R. Salahub, *J. Chem. Phys.* **1998**, *108*, 4439−4449. (b) R. E. Stratmann, G. E. Scuseria, M. J. Frisch, *J. Chem. Phys.* **1998**, *109*, 8218−8224. (c) R. Bauernschmitt, R. Ahlrichs, *Chem. Phys. Lett.* **1996**, *256*, 454−464.

28 K. Nakamoto, Infrared and Raman Spectra of Inorganic and Coordination Compounds, Wiley-Interscience, New York (1986).

29 (a) R. F. Furchgott, J. V. Zawadzki, *Nature* **1980**, *288*, 373–376. (b) M. W. Radomski, R. M. J. Palmer, S. Moncada, *Br. J. Pharmacol.* **1987**, *92*, 639–646. (c) R. M. Palmer, D. S. Ashton, S. Moncada, *Nature* **1988**, *333*, 664–666. (d) D. D. Rees, R. M. Palmer, S. Moncada, *Proc. Nat. Acad. Sci. USA* **1989**, *86*, 3375–3378. (e) D. S. Bredt, P. M. Hwang, S. H. Snyder, *Nature* **1990**, *347*, 768–770. (f) S. Moncada, M. J. Palmer, E. A. Higgs, *Pharmacol. Rev.* **1991**, *43*, 109–142. (g) J. Garthwaite, *Trends Neurosci.* **1995**, *18*, 51–52. (h) D. D. Kline, T. N. Yang, P. L. Huang, N. R. Prabhakar, *J. Physiol.* **1998**, *511*, 273–287. (i) F. Plane, K. E. Wiley, J. Y. Jeremy, R. A. Cohen, C. J. Garland, *Br. J. Pharmacol.* **1998**, *123*, 1351–1358. (j) D. H. Triyoso, T. A. Good, *J. Physiol.* **1999**, *515*, 355–365. (k) B. Akesson, I. Lundquist, *J. Physiol.* **1999**, *515*, 463–473. (l) C. E. Van Hove, C. van der Donckt, A. G. Herman, H. Bult, P. Fransen, *Br. J. Pharmacol.* **2009**, *158*, 920–930.

30 R. W. Callahan, T. J. Meyer, *Inorg. Chem.* **1977**, 574–581.

31 (a) P. A. Adcock, F. R. Keene, R. S. Smythe, M. R. Snow, *Inorg. Chem.* **1984**, *23*, 2336–2343. (b) B. Mondal, H. Paul, V. G. Puranik, G. K. Lahiri, *J. Chem. Soc., Dalton Trans.* **2001**, 481–487. (c) H. Hadadzadeh, M. C. DeRosa, G. P. A. Yap, A. R. Rezvani, R, J. Crutchley, *Inorg. Chem.* **2002**, *41*, 6521−6526. (d) S. Frantz, B. Sarkar, M. Sieger, W. Kaim, F. Roncaroli, J. A. Olabe, S. Záliš, *Eur. J. Inorg. Chem.* **2004**, 2902−2907. (e) N. Chanda, S. M. Mobin, V. G. Puranik, A. Datta, M. Niemeyer, G. K. Lahiri, *Inorg. Chem.* **2004**, *43*, 1056–1064. (f) S. Sarkar, B. Sarkar,

N. Chanda, S. Kar, S. M. Mobin, J. Fiedler, W. Kaim, G. K. Lahiri, *Inorg. Chem.* **2005**, *44*, 6092−6099. (g) R. G. de Lima, M. G. Sauaia, D. Bonaventura, A. C. Tedesco, L. M. Bendhack, R. S. da Silva, *Inorg. Chim. Acta* **2006**, *359*, 2543–2549. (h) K. Karidi, A. Garoufis, N. Hadjiliadis, M. Lutz, A. L. Spek, J. Reedijk, *Inorg. Chem.* **2006**, *45*, 10282−10292. (i) S. Maji, C. Chatterjee, S. M. Mobin, G. K. Lahiri, *Eur. J. Inorg. Chem.* **2007**, 3425–3434. (j) S. Maji, B. Sarkar, M. Patra, A. K. Das, S. M. Mobin, W. Kaim, G. K. Lahiri, *Inorg. Chem.* **2008**, *47*, 3218–3227. (k) K. Christopoulos, K. Karidi, A. Tsipis, A. Garoufis, *Inorg. Chim. Acta* **2008**, *11*, 1341−1346. (l) P. De, T. K. Mondal, S. M. Mobin, B. Sarkar, G. K. Lahiri, *Inorg. Chim. Acta* **2010**, *363*, 2945–2954.

32 R. G. de Lima, M. G. Sauaia, D. Bonaventure, A. C. Tedesco, L. M. Bendhack, R. S. da Silva, *Inorg. Chim. Acta* **2006**, *359*, 2543–2549.

33 L. J. Farrugia, *J. Appl. Crystallogr.* **1997**, *30*, 565.

34 T. D. Fenn, D. Ringe, G. A. Petsko, *J. Appl. Crystallogr.* **2003**, *36*, 944−947.

35 (a) J. G. Calvert, J. N. Pitts, Photochemistry, J. Wiley & Sons: New York, 1967; pp 783–786, (b) G. Malouf, P. C. Ford, *J. Am. Chem. Soc.* **1977**, *99*, 7213–7221, (c) Carmen F. Works, C. J. Jocher, G. D. Bart, X. Bu, P. C. Ford, *Inorg. Chem.* **2002**, *41*, 3728−3739.

Chapter 3

A Phosphine-Substituted Ruthenium(II) Polypyridine Complex as a Catalyst for CO_2 Reduction

Introduction

The catalytic reduction of carbon dioxide (CO_2) is a challenging target that is of interest not only as a means of counteracting unsustainable emissions of CO_2 but also as a method for the development of renewable fuels and essential chemicals.[1] A variety of transition metal complexes have been shown to be active as catalyst precursors but typically at relatively negative potentials or with slow rates.[2–4] Examples include polypyridine complexes of ruthenium(II), notably from the results of Tanaka *et al.* on $[Ru(trpy)(bpy)(CO)]^{2+}$ (trpy = 2,2':6',2"-terpyridine, bpy = 2,2'-bipyridine) and *cis*-$[Ru(bpy)_2(CO)_2]^{2+}$ [5] and Meyer *et al.* on *cis*-$[Ru(bpy)_2(CO)H]^{+}$.[6]

In previous report,[7] we have succeeded in the syntheses and structural determination of a series of phosphine containing ruthienium(II) polypyridine complexes. However, there are a few studies about CO_2 reduction by using the complexes with phosphine moiety. We have succeeded for the first time in the syntheses and structural determination of a phosphine containing ruthenium(II) polypyridine complex with $[Ru(trpy)(Pqn)(MeCN)]^{2+}$ (***trans*-MeCN**, Pqn = 8-(diphenylphosphanyl)quinolone, Scheme 1) were selected as phosphine containing ligand, and the effects of the *trans*-position of a phosphine donor on the structure and electronic property were investigated. Phosphine ligands have σ-donating and π-accepting abilities, and the substitution of coordinating N atom to P atom in ruthenium(II) polypyridine complexes should be one of the key strategies to develop CO_2 reduction. Here we show theoretical study and electrochemical research under Ar and CO_2.

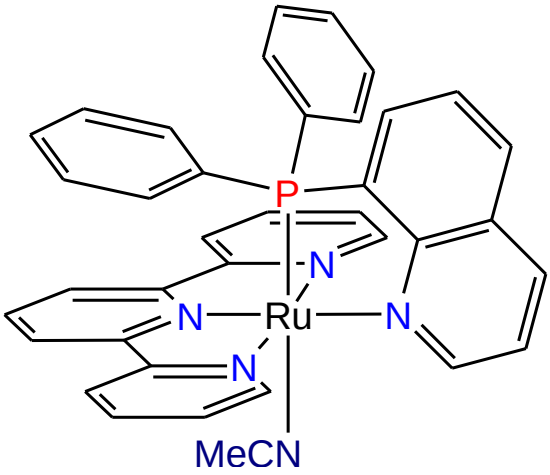

Scheme 1. Structure of ***trans*-MeCN**.

Results and Discussion

Electrochemistry under Ar

Synthesis and characterization of *trans(P,MeCN)*-[Ru(trpy)(Pqn)(MeCN)]$(PF_6)_2$ (***trans*-MeCN**) as the acetonitrile complexes have been reported.[7] Figure 1 shows cyclic voltammograms (CVs) of a solution 0.5 mM in ***trans*-MeCN** in 0.1 M TEAP/MeCN (TEAP = tetrabutylammonium perchlorate) at a glassy carbon electrode with the solutions purged by Ar streams for 15 min. The potentials were measured vs. an $Ag/AgNO_3$ reference electrode and are converted to ferrocene/ferrocenium (Fc/Fc^+). Density functional theory (DFT) calculations were obtained at B3LYP/LANL2DZ level with the Gaussian 09 (G09) program package. Table 1 summarizes the sums of electronic and thermal free energies.

Three $1e^-$ reversible waves appeared for ***trans*-MeCN** at $E_{1/2}$ = −1.70, −1.77, and −2.13 V vs Fc/Fc^+, respectively (Figure 1).[7] Based on DFT calculations, Figure 2 shows singly occupied molecular orbital (SOMO) and total spin density (TSD) for $1e^-$ reduced species, $[Ru(trpy)(Pqn)(MeCN)]^+$ (***trans*-MeCN$^-$**). Both SOMO and TSD are mainly spread over the trpy ring, indicating that the first reduction occurs at the trpy ligand. There are two possibilities $1e^-$ reduced spices; one is $[Ru(trpy^-)(Pqn)(MeCN)]^+$, the other is $[Ru(trpy^-)(Pqn)]^+$ which is a five-coordinated complex and dissociated an acetonitrile ligand from $[Ru(trpy^-)(Pqn)(MeCN)]^+$. Although a bond dissociation free energy (BDFE, shown in Table 2) upon liberation of the acetonitrile ligand was estimated, the positive $\Delta G°$ value (2.5 kj/mol) for ***trans*-MeCN$^-$** as BDFE insists that dissociation of the acetonitrile ligand to form $[Ru(trpy)(Pqn)]^+$ is not favored. Therefore, the first wave at −1.70 V in the CV under Ar is a $1e^-$ trpy-based reduction (eq. 1, assignments of configuration are omitted in all equations).

$$[Ru(trpy)(Pqn)(MeCN)]^{2+} + e^- \rightarrow [Ru(trpy^-)(Pqn)(MeCN)]^+ \qquad (1)$$

The $2e^-$ reduced complex, $[Ru(trpy)(Pqn)(MeCN)]^0$ (***trans*-MeCN^{2-}**), has two possible electronic configurations: (I) The two added electrons are paired and both are distributed over the trpy ring, i.e., the complex is in the closed singlet state, $^1[Ru(tpy)(bpy)(MeCN)]^0$. (II) The second electron is added to the Pqn ligand, i.e., the complex is in the triplet state, $^3[Ru(trpy)(Pqn)(MeCN)]^0$. The calculated energy for the closed singlet complex is 41.3 kj/mol higher than the triplet complex. Therefore the behavior of reduction to ***trans*-MeCN^{2-}** is shown as eq. 2. The electronic structures indicate that the electrons enter π^* orbitals of the trpy ring and quinoline ring of Pqn

upon $2e^-$ reduction. The spin density of $^3[Ru(trpy)(Pqn)(MeCN)]^0$ is distributed on both trpy and Pqn ligands. On the other hand, in the case of $2e^-$ reduced five-coordinated complexes, $[Ru(trpy)(Pqn)]^0$, the calculated energy for the closed singlet complex is 22.9 kj/mol lower than the triplet complex. Moreover, the negative $\Delta G°$ value (−23.0 kj/mol) for ***trans*-MeCN**$^{2-}$ as BDFE suggests that dissociation of the acetonitrile ligand to form $^1[Ru(trpy)(Pqn)]^0$ is favored. Therefore, liberation of the acetonitrile ligand is shown as eq. 3. Conclusively, eq. 4 indicates the total reduction reaction for the second wave at −1.77 V. σ-donor character of phosphine group elongates the bond length between the ruthenium center and the ligand located at the *trans* position of the phosphine group, called the *trans* influence, caused this lability. The third wave a $1e^-$ is not successful to be characterized.

$$[Ru(trpy^-)(Pqn)(MeCN)]^+ + e^- \rightarrow {}^3[Ru(trpy^-)(Pqn^-)(MeCN)]^0 \quad (2)$$

$$^3[Ru(trpy^-)(Pqn^-)(MeCN)]^0 \rightarrow {}^1[Ru(trpy)(Pqn)]^0 + MeCN \quad (3)$$

$$[Ru(trpy^-)(Pqn)(MeCN)]^+ + e^- \rightarrow {}^1[Ru(trpy)(Pqn)]^0 + MeCN \quad (4)$$

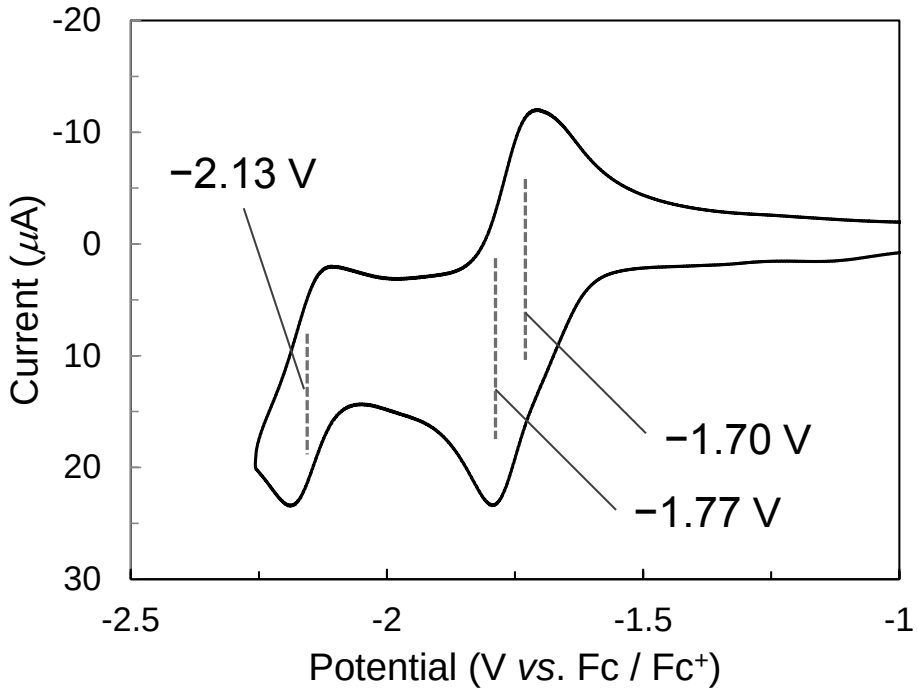

Figure 1. A cyclic voltammogram of ***trans*-MeCN** (0.5 mM) in 0.1 M TEAP/acetonitrile under an Ar atmosphere scanned in the negative region (WE: GC, CE: Pt wire, RE: Ag/Ag^+; Scan rate: 100 mV/s).

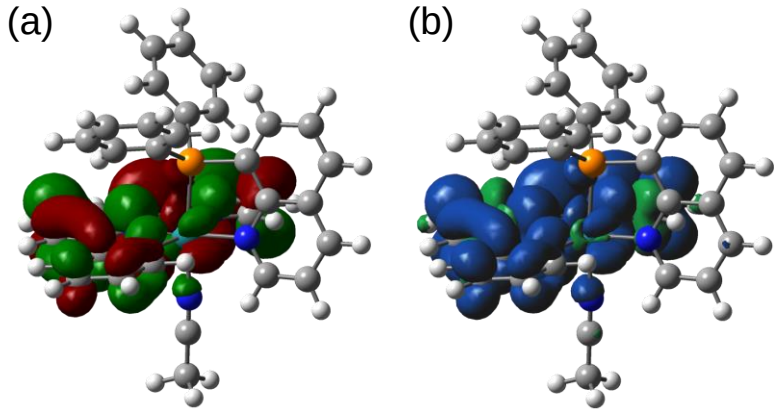

Figure 2. (a) SOMO and (b) TSD for $[Ru(trpy)(Pqn)(MeCN)]^+$.

Table 1. Sums of electronic and thermal free energies for the $1e^-$ and $2e^-$ reduced species of $[Ru(trpy)(Pqn)(L)]^{2+}$ (L = MeCN or CO_2), and MeCN and CO_2 molecule in acetonitrile media (in Hartree). All assignments of configuration are omitted.

Species	Sum of Free Energy
MeCN species	
$[Ru(trpy)(Pqn)(MeCN)]^+$	–1839.433623
$^1[Ru(trpy)(Pqn)(MeCN)]^0$	–1839.521941
$^3[Ru(trpy)(Pqn)(MeCN)]^0$	–1839.537686
MeCN	–132.715120
CO_2 species	
$[Ru(trpy)(Pqn)(CO_2)]^+$	–1895.259416
$^1[Ru(trpy)(Pqn)(CO_2)]^0$	–1895.407359
$^3[Ru(trpy)(Pqn)(CO_2)]^0$	–1895.374468
CO_2	–188.553863
Five-coordinated species	
$[Ru(trpy)(Pqn)]^+$	–1706.717557
$^1[Ru(trpy)(Pqn)]^0$	–1706.831321
$^3[Ru(trpy)(Pqn)]^0$	–1706.822581

Table 2. Bond dissociation free energies (BDFEs) for the $1e^-$ and $2e^-$ reduced reduced species of ***trans*-MeCN** and ***trans*-CO_2** estimated by DFT calculations.

reaction	$\Delta G°$ (kJ / mol)
MeCN complex	
$[Ru(trpy)(Pqn)(MeCN)]^+ \rightarrow [Ru(trpy)(Pqn)]^+ + MeCN$	2.5
$^3[Ru(trpy)(Pqn)(MeCN)]^0 \rightarrow {}^1[Ru(trpy)(Pqn)]^0 + MeCN$	–23.0
CO_2 complex	
$^1[Ru(trpy)(Pqn)(CO_2)]^0 \rightarrow {}^1[Ru(trpy)(Pqn)]^0 + CO_2$	58.2

Electrochemistry under CO_2

In solutions saturated in CO_2 = 0.36 M,[8] a CV of ***trans*-MeCN** shows loss of reversibility and the first reduction (wave (a) in Figure 3) is shifted at −1.68 V from −1.70 and −1.77 V under Ar but reduction at the second wave triggers the appearance of new reduction waves at E_{pc} = −1.94 V (wave (b)) and −2.18 V (wave (c)). There is a significant current enhancement for the wave at E_{pc} = −2.18 V corresponding to electrocatalytic CO_2 reduction as is the case in $[Ru(trpy)(bpy)(MeCN)]^{2+}$.[9]

The $2e^-$ reduction of ***trans*-MeCN** at E_{pc} = −1.68 V with CO_2 gives an intermediate shown as the metallocarboxylate, $[Ru(trpy)(Pqn)(CO_2^{2-})]^0$ (***trans*-CO_2**).[10] Similar electrochemical behavior which involves the positive E_{pc} shift was reported for a manganese complex, $[Mn(dmbpy)(CO)_3(MeCN)]^+$ (dmbpy = 4,4'-dimethyl-2,2'-bipyridine), for which the acetonitrile ligand was lost and a C(O)OH adducts to the metal center upon electrochemical reduction of $[Mn(dmbpy)(CO)_3(MeCN)]^+$ with only the addition of an external proton (H^+) source. $[Mn(dmbpy)(CO)_3(C(O)OH)]^0$ was assumed to be the dominant form of the doubly reduced species.[11] The bulky dmbpy ligand stabilizes five-coordinated species and followed by coordination of CO_2 and H^+. Based on comparisons with the manganese complex, the ***trans*-MeCN** might transform the doubly-reduced species, ***trans*-CO_2**, with CO_2 without H^+ source.

DFT studies also support the formation of ***trans*-CO_2** with $2e^-$ reduction from ***trans*-MeCN** on the assumption that the calculated energy for the closed singlet ***trans*-CO_2** is 86.4 kj/mol lower than the triplet one and the HOMO for ***trans*-CO_2** is located at the coordinated CO_2 molecule as shown in Figure 4. As described earlier, ***trans*-$MeCN^{2-}$** easily changes to five-coordinated species, $^1[Ru(trpy)(Pqn)]^0$, but it is continuously able to form ***trans*-CO_2** in the presence of CO_2 because the BDFE (58.2 kj/mol) for ***trans*-CO_2** is quite high. Therefore, the formation of ***trans*-CO_2** (eq. 5) can be occurred after liberation as shown in eq. 3. From these results, the at $2e^-$ reduction E_{pc} = −1.68 V under CO_2 is expressed as eq. 6.

$$^1[Ru(trpy)(Pqn)]^0 + CO_2 \rightarrow {}^1[Ru(trpy)(Pqn)(CO_2^{2-})]^0 \quad (5)$$

$$[Ru(trpy)(Pqn)(MeCN)]^{2+} + CO_2 + 2e^- \rightarrow {}^1[Ru(trpy)(Pqn)(CO_2^{2-})]^0 + MeCN \quad (6)$$

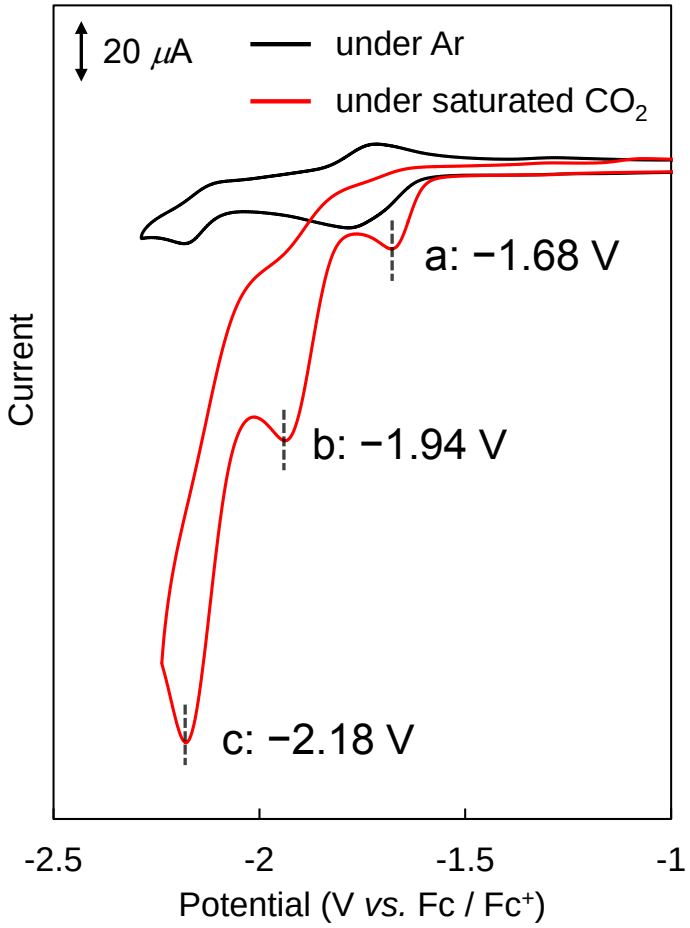

Figure 3. CVs of 0.5 mM ***trans*-MeCN** in 0.1 M TEAP/MeCN under Ar (black line) and CO_2 (red line) at 100 $mV \cdot s^{-1}$ scan rates. The waves relevant to the mechanism in the text are labeled in the Figure.

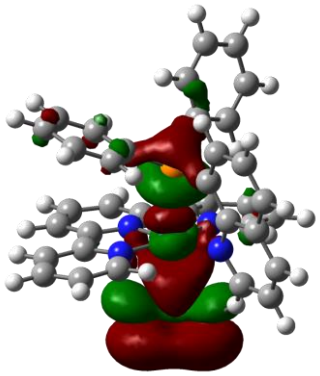

Figure 4. HOMO for $[Ru(trpy)(Pqn)(CO_2)]^0$.

Once formed, the metallocarboxylate complex undergoes further trpy- and Pqn-based $1e^-$ reductions at −1.94 V (eq. 7) and −2.18 V (eq. 8). With added CO_2, the latter triggers catalytic reduction of CO_2 to CO. Meyer and co-workers reported overall CO_2 reduction based on $[Ru(trpy)(bpy)(MeCN)]^{2+}$ was rate limited by substitution of MeCN by CO_2.[9] In contrast, the results for ***trans*-MeCN** including Pqn suggests that the phosphine moiety resolve this rate determining step and attract to form CO_2 complexes with $1e^-$ and further electrons reduction.

$$[Ru(trpy)(Pqn)(CO_2^{2-})]^0 + e^- \rightarrow [Ru(trpy^-)(Pqn)(CO_2^{2-})]^- \quad (7)$$
$$[Ru(trpy^-)(Pqn)(CO_2^{2-})]^- + e^- \rightarrow [Ru(trpy^-)(Pqn^-)(CO_2^{2-})]^{2-} \quad (8)$$

Based on the results of the CV and reported study, CO_2 reduction occurs following substitution of MeCN by CO_2 to give $[Ru(trpy)(Pqn)(CO_2^{2-})]^0$ followed by further $2e^-$ reduction, eq. 9.[9,12] There is no kinetic information about the step that follows but it might occur by O^{2-} transfer to CO_2 to give CO_3^{2-} and the CO complex as an intermediate as shown in eq. 10.[2] The $2e^-$ reduced CO intermediate, $[Ru(trpy)(Pqn)(CO)]^0$, is known to undergo rapid loss of CO at room temperature, eq. 11.[2]

$$[Ru(trpy^-)(Pqn^-)(CO_2^{2-})]^{2-} + 2CO_2 \rightarrow [Ru(trpy)(Pqn)(CO_2^{2-})]^0 + CO + CO_3^{2-} \quad (9)$$
$$[Ru(trpy^-)(Pqn^-)(CO_2^{2-})]^{2-} + CO_2 \rightarrow [Ru(trpy^-)(Pqn^-)(CO)]^0 + CO_3^{2-} \quad (10)$$
$$[Ru(trpy^-)(Pqn^-)(CO)]^0 + CO_2 \rightarrow [Ru(trpy)(Pqn)(CO_2^{2-})]^0 + CO \quad (11)$$

Reaction mechanism of electrocatalytic CO_2 reduction

From CV data and DFT calculation, the proposed mechanism was produced in Scheme 2a and described below in detail. The first step (i) is electrochemical reduction of ***trans*-MeCN** to form $[Ru(trpy^{-})(Pqn)(MeCN)]^{+}$ at E_{pc} = −1.68 V (eq. 1). This reduction reaction under CO_2 is same as that under Ar. The second step (ii) is reduction of $[Ru(trpy^{-})(Pqn)(MeCN)]^{+}$ to form $[Ru(trpy)(Pqn)(CO_2^{2-})]^{0}$ (***trans*-CO_2**) at E_{pc} = −1.68 V (eq. 6). This reduction proceed through five-coordinated species, $[Ru(trpy)(Pqn)]^{0}$ (eq. 5). In this reaction, internal electron transfer occurs to give the metallocarboxylate intermediate with $1e^{-}$ reduction, $[Ru(trpy^{-})(Pqn)(MeCN)]^{+} + CO_2 + e^{-} \rightarrow$ ***trans*-CO_2** + MeCN. The third and fourth steps are stepwise reduction to form $[Ru(trpy^{-})(Pqn)(CO_2^{2-})]^{-}$ and $[Ru(trpy^{-})(Pqn^{-})(CO_2^{2-})]^{2-}$ at −1.94 V (eq. 7) and −2.18 V (eq. 8), respectively. Briefly, ***trans*-CO_2** undergoes further $2e^{-}$ reduction, eq. 9. The fifth step (v) includes O^{2-} transfer to CO_2 to give CO_3^{2-} and the CO complex as an intermediate as shown in eq. 10. In the sixth step (vi), the twice reduced CO intermediate, $[Ru(trpy)(Pqn)(CO)]^{0}$ undergoes rapid loss of CO at room temperature, eq. 11, The $2e^{-}$ reduced species, ***trans*-CO_2**, gives CO and CO_3^{2-} as final products with further ligand-based reduction continuously.

In contrast, as shown in Scheme 2b, $[Ru(trpy)(bpy)(MeCN)]^{2+}$ with polypyridine undergoes sequential $1e^{-}$ ligand-based reductions at E_{pc} = −1.59 V and −1.89 V vs Fc/Fc^{+}, to give $[Ru(trpy^{-})(bpy^{-})(MeCN)]^{0}$ followed by rate limiting substitution of CO_2 for MeCN. The phosphine moiety resolve the rate determining step and attract to form CO_2 complexes with $1e^{-}$ and further electrons reduction.

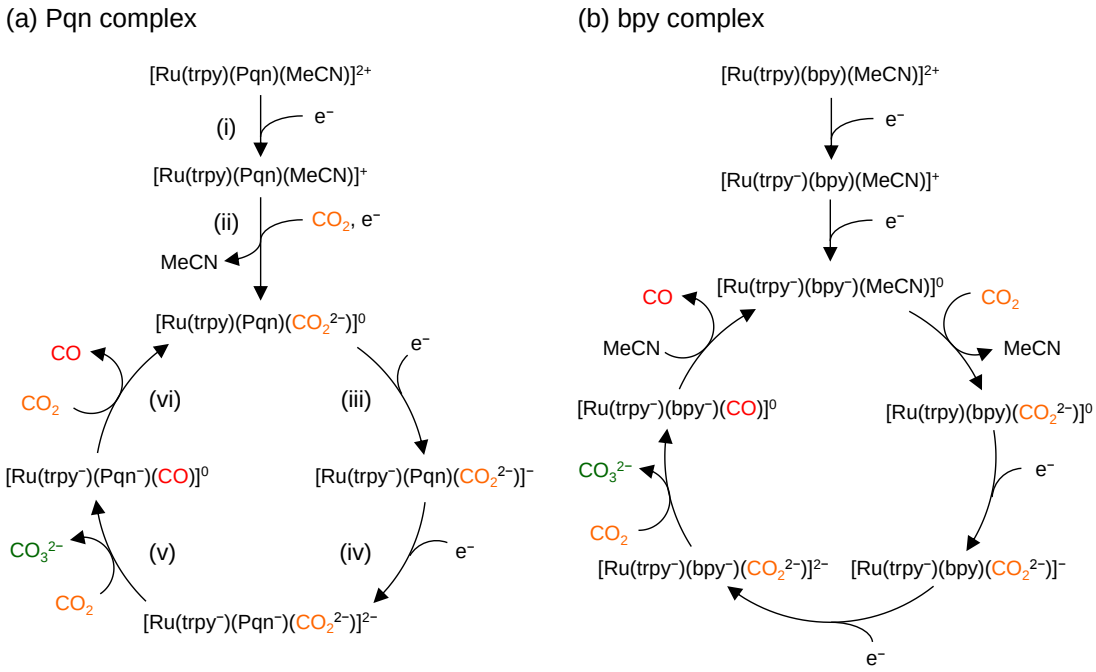

Scheme 2. Comparison of reaction cycles of electrocatalytic CO_2 reduction between (a) Pqn and (b) bpy complexes.

Conclusion

The results reported here are important in providing detailed mechanistic insight into a class of catalysts for sustained electrocatalytic reduction of CO_2 to CO with key prior reductions at the polypyridine and phosphine ligands. The mechanism of electrochemical CO_2 reduction was elucidated by considering $2e^-$ reduced five-coordinated species formed *via* liberation of acetonitrile ligand. The findings reported in this study provide new mechanistic and synthetic insights for improving catalysts in the future, with the ultimate goal of attaining a catalytic system capable of implementation on a large scale.

Experimental Section

General Methods.

Cyclic voltammograms were measured at room temperature on a BAS ALS Model 650DKMP electrochemical analyzer in acetonitrile ([complex] = 0.5 mM; 0.1 M tetraethylammonium perchlorate (TEAP)). A glassy carbon disk, platinum wire, and Ag/Ag^+ electrode (Ag/0.01 M $AgNO_3$) were used as the working, auxiliary, and reference electrodes, respectively. The redox potentials of samples were calibrated against the redox signal for the ferrocene/ferrocenium (Fc/Fc^+) couple.

Materials.

trans(P,MeCN)-[Ru(trpy)(Pqn)(MeCN)]$(PF_6)_2$ (***trans*-MeCN**) was prepared by methods described previously.[7] Tetraethylammonium perchlorate (TEAP) and ferrocene were purchased from Wako Pure Chemical Industries, Ltd. All solvents and reagents were of the highest quality available and were used as received.

DFT calculations.

Calculations were performed using the DFT method implemented in the Gaussian 09 package of programs.[13] The structures were fully optimized using the B3LYP method, which uses hybrid Becke's three-parameter exchange functional[14] with the correlation energy functional of Lee, Yang, and Parr.[15] All calculations were performed using the standard double-ζ type LanL2DZ basis set[16] implemented in Gaussian 09, without adding any extra polarization or diffuse function. The LanL2DZ basis set also uses relativistic effective core potentials (RECP) for the Ru atom to account for the scalar relativistic effects of the inner 28 core electrons ($[Ar]3d^{10}$) for Ru. All calculations were performed using the polarizable continuum model (PCM)[17] to compute the structures in acetonitrile. All stationary points were characterized by their harmonic vibrational frequencies as minima. The free energies at 298 K and 1 atm were obtained through thermochemical analysis of the frequency calculation, using the thermal correction to Gibbs free energy as reported by Gaussian 09. The excited states were calculated using the TD-DFT[18] method within the Tamm-Dancoff approximation as implemented in Gaussian 09. These calculations employ the hybrid B3LYP functional along with the basis sets described above. At least 100 excited states were computed in each calculation. To obtain the simulated spectrum of each species, transition energies and oscillator strengths have been interpolated by a Gaussian convolution with a common σ value of 0.2 eV.

References

1 Benson, E. E.; Kubiak, C. P.; Sathrum, A. J.; Smieja, J. M. *Chem. Soc. Rev.* **2009**, *38*, 89−99.

2 Concepcion, J. J.; House, R. L.; Papanikolas, J. M.; Meyer, T. J. *Proc. Natl. Acad. Sci. U.S.A.* **2012**, *109*, 15560−15564.

3 Appel, A. M.; Bercaw, J. E.; Bocarsly, A. B.; Dobbek, H.; DuBois, D. L.; Dupuis, M.; Ferry, J. G.; Fujita, E.; Hille, R.; Kenis, P. J. A.; Kerfeld, C. A.; Morris, R. H.; Peden, C. H. F.; Portis, A. R.; Ragsdale, S. W.; Rauchfuss, T. B.; Reek, J. N. H.; Seefeldt, L. C.; Thauer, R. K.; Waldrop, G. L. *Chem. Rev.* **2013**, *113*, 6621−6658.

4 (a) C. Costentin, S. Drouet, M. Robert, J.-M. Savéant, *Science* **2012**, *338*, 90−94. (b) C. Costentin, M. Robert, J.-M. Savéant, *Chem. Soc. Rev.* **2013**, *42*, 2423−2436.

5 H. Nagao, T. Mizukawa, K. Tanaka, *Inorg. Chem.* **1994**, *33*, 3415–3420.

6 (a) J. R. Pugh, M. R. M. Bruce, B. P. Sullivan, T. J. Meyer, *Inorg. Chem.* **1991**, *30*, 86. (b) M. R. M. Bruce, E. Megehee, B. P. Sullivan, H. H. Thorp, T. R. O'Toole, A. Downard, J. R. Pugh, T. J. Meyer, *Inorg. Chem.* **1992**, *31*, 4864.

7 G. Nakamura, M. Okamura, M. Yoshida, T. Suzuki, H. D. Takagi, M. Kondo, S. Masaoka, *Inorg. Chem.* **2014**, ***53***, 7214–7226.

8 A. Gennaro, A. A. Isse, E. Vianello, *J. Electroanal. Chem.* **1990**, *289*, 203.

9 (a) Z. Chen, C. Chen, D. R. Weinberg, P. Kang, J. J. Concepcion, D. P. Harrison, M. S. Brookhart, T. J. Meyer, *Chem. Commun.* **2011**, *47*, 12607–12609. (b) Z. Chen, J. J. Concepcion, M. K. Brennaman, P. Kang, M. R. Norris, P. G. Hoertz, T. J. Meyer, *Proc. Natl. Acad. Sci. USA* **2012**, *109*, 15606–15611, (c) Z. Chen, P. Kang, M.-T. Zhang, T. J. Meyer, *Chem. Commun.* **2014**, *50*, 335–337, (d) P. Kang, Z. Chen, A. Nayak, S. Zhang, T. J. Meyer, *Energy Environ. Sci.* **2014**, *7*, 4007–4012.

10 R. S. Nicholson, I. Shain, *Anal. Chem.* **1964**, *36*, 706.

11 M. D. Sampson, A. D. Nguyen, K. A. Grice, C. E. Moore, A. L. Rheingold, C. P. Kubiak, *J. Am. Chem. Soc.* **2014**, *136*, 5460–5471.

12 K. Tanaka, D. Ooyama, *Coord. Chem. Rev.* **2002**, *226*, 211–218.

13 Frisch, M. J.; Trucks, G. W.; Schlegel, H. B.; Scuseria, G. E.; Robb, M. A.; Cheeseman, J. R.; Scalmani, G.; Barone, V.; Mennucci, B.; Petersson, G. A.; Nakatsuji, H.; Caricato, M.; Li, X.; Hratchian, H. P.; Izmaylov, A. F.; Bloino, J.; Zheng, G.; Sonnenberg, J. L.; Hada, M.; Ehara, M.; Toyota, K.; Fukuda, R.; Hasegawa, J.; Ishida, M.; Nakajima, T.; Honda, Y.; Kitao, O.; Nakai, H.; Vreven, T.; Montgomery Jr., J. A.; Peralta, J. E.; Ogliaro, F.; Bearpark, M.; Heyd, J. J.; Brothers, E.; Kudin, K. N.; Staroverov, V. N.; Keith, T.; Kobayashi, R.; Normand,

J.; Raghavachari, K.; Rendell, A.; Burant, J. C.; Iyengar, S. S.; Tomasi, J.; Cossi, M.; Rega, N.; Millam, J. M.; Klene, M.; Knox, J. E.; Cross, J. B.; Bakken, V.; Adamo, C.; Jaramillo, J.; Gomperts, R.; Stratmann, R. E.; Yazyev, O.; Austin, A. J.; Cammi, R.; Pomelli, C.; Ochterski, J. W.; Martin, R. L.; Morokuma, K.; Zakrzewski, V. G.; Voth, G. A.; Salvador, P.; Dannenberg, J. J.; Dapprich, S.; Daniels, A. D.; Farkas, O.; Foresman, J. B.; Ortiz, J. V.; Cioslowski, J.; Fox, D. J. *Gaussian 09 (Revision C.01)*, Gaussian, Inc. Wallingford CT, **2010**.

14 A. D. Becke, *J. Chem. Phys.* **1993**, *98*, 5648−5652.

15 C. Lee, W. Yang, R. G. Parr, *Phys. Rev. B* **1988**, *37*, 785−789.

16 (a) T. H. Dunning Jr., P. J. Hay, in *Modern Theoretical Chemistry*, ed. Schaefer III, H. F.; Plenum, New York, **1976**. (b) Hay, P. J.; Wadt, W. R. *J. Chem. Phys*. **1985**, *82*, 270−283. (c) P. J. Hay, W. R. Wadt, *J. Chem. Phys*. **1985**, *82*, 299−310.

17 M. Cossi, G. Scalmani, N. Rega, V. Barone, *J. Chem. Phys.* **2002**, *117*, 43−54.

18 (a) M. E. Casida, C. Jamorski, K. C. Casida, D. R. Salahub, *J. Chem. Phys.* **1998**, *108*, 4439−4449. (b) R. E. Stratmann, G. E. Scuseria, M. J. Frisch, *J. Chem. Phys.* **1998**, *109*, 8218−8224. (c) R. Bauernschmitt, R. Ahlrichs, *Chem. Phys. Lett.* **1996**, *256*, 454−464.

Acknowledgements

I would like to express my gratitude to many people who have helped me to complete this thesis.

I have been studied from April 2012 to March 2015 under the direction of Associate Professor Dr. Shigeyuki Masaoka in the Graduate University for Advanced Studies (SOKENDAI) and I would like to acknowledgement him for his valuable guidance, warm encouragement, and helpful discussions. I appreciate Assistant Professor Dr. Mio Kondo for her incisive suggestion and giving me useful advices. I am much grateful to Associate Professor Dr. Takayoshi Suzuki in Okayama University for thoughtful teaching. I thank to Associate Professor Dr. Hideo D. Takagi in Nagoya University for his precise comments. I express my thanks to Assistant Professor Dr. Masaki Yoshida in Hokkaido University for his kind supports.

I gratefully acknowledge the collaborative work with Professor Dr. Peter C. Ford and his group in University of California, Santa Barbara. I was able to gain invaluable experiences through the internship for four months.

I am deeply express appreciation to our members in Institute for Molecular Science (IMS), Dr. Praneeth Vijayendran, Mr. Masaya Okamura, Mr. Masakazu Murase who is currently a researcher in Toyota Central R&D Lab, Mr. Takahiro Itoh, Mr. Yuki Okabe, Ms. Pondchanok Chinapang, Mr. Ke Liu, Ms. Arisa Fukatsu, Ms. Yukino Fukahori, Mr. Hitoshi Izu, Mr. Takafumi Enomoto, Ms. Akane Shibata, Ms. Reiko Kuga, Ms. Mari Kanaike, and Ms. Kaori Wakabayashi for many advices, valuable discussions, heartfelt encouragement, and steady friendship. I also wish to express sincere thanks to the visiting researchers from Malaya University, Dr. Woi Pei Meng and Mr. Sze Koon Lee.

I am indebted to the financial assistance provided by the Okazaki Shinkin Bank.

Finally, I would like to thank my family for giving me the opportunity to research and supporting my life as a researcher.

Go Nakamura
March, 2015

List of Publications

Chapter 1

"Electrochemical Behavior of Phosphine-Substituted Ruthenium(II) Polypyridine Complexes with a Single Labile Ligand"

Go Nakamura, Masaya Okamura, Masaki Yoshida, Takayoshi Suzuki, Hideo D. Takagi, Mio Kondo, and Shigeyuki Masaoka

Inorganic Chemistry, **2014**, *53*, 7214-7226.

Chapter 2

"Synthesis and Properties of Phosphine-Substituted Ruthenium(II) Polypyridine Complexes with Nitrogen Oxide"

Go Nakamura, Mio Kondo, Meredith Crisalli, Lee Sze Koon, Akane Shibata, Peter C. Ford, and Shigeyuki Masaoka

To be submitted.

Chapter 3

"A Phosphine-Substituted Ruthenium(II) Polypyridine Complex as a Catalyst for CO_2 Reduction"

Go Nakamura, Mio Kondo, and Shigeyuki Masaoka

Manuscript in preparation.

Other Publications

"Crystal Structure and Spectroscopic Properties of Cyclic Dipeptide: A Racemic Mixture of *cyclo*(D-Prolyl-L-Tyrosyl) and *cyclo*(L-Prolyl-D-Tyrosyl)"
Yong Pyo Hong, Sung-Hong Lee, Jong-Ha Choi, Ayana Kashima, **Go Nakamura**, and Takayoshi Suzuki
Bulletin of the Korean Chemical Society, **2014**, *35*, 2299–2303.